The Pennsylvania State University

The Graduate School

Department of Architectural Engineering

INDOOR AEROSOL SENSING AND RESUSPENSION DYNAMICS

A Dissertation in

Architectural Engineering

by

Parichehr Salimifard

Submitted in Partial Fulfillment
of the Requirements
for the Degree of

Doctor of Philosophy

May 2018

The dissertation of Parichehr Salimifard was reviewed and approved* by the following:

Donghyun Rim
Assistant Professor of Architectural Engineering
Dissertation Advisor
Chair of Committee

James D. Freihaut
Professor of Architectural Engineering

William P. Bahnfleth
Professor of Architectural Engineering

Rui Ni
Assistant Professor of Mechanical Engineering

Richard Mistrick
Associate Professor of Architectural Engineering
Graduate Program Officer of the Architectural Engineering Department

*Signatures are on file in the Graduate School

ABSTRACT

Exposure to indoor particulate matter (PM) is associated with adverse health effects. Controlling the indoor PM exposure relies on an accurate understanding of aerosol transport, as well as accurate real-time monitoring of PM concentration level in the indoor environment.

Indoor aerosol transport is a cycle involving continuous repetitions of deposition and resuspension of particles from indoor surfaces. Occupants' activities such as walking, and indoor environmental conditions such as relative humidity (RH), influence the resuspension rate of particles. The first objective of this dissertation was to investigate the effects of RH and turbulent air swirls on the resuspension rate of allergen carrier particles from indoor surfaces. This study shows that increasing RH can reduce the resuspension and spread of hydrophilic particles such as dust mites and that the presence of carpet significantly increased resuspension rates compared to linoleum flooring surfaces.

This study also analyzes the efficacy of indoor PM sensing with current technologies. Effective PM removal strategies depend on continuous monitoring of indoor aerosols. Although PM monitoring in buildings has not been feasible due to high PM sensor cost, the recent advent of low-cost optical PM sensors has enabled real-time PM monitoring with high spatiotemporal resolution. Since biological particles such as dust mites, pollen, and pet dander are linked to respiratory and allergic symptoms among building occupants, PM sensors can be utilized to accurately measure bioaerosols. However, the performance of low-cost particle sensors in monitoring bioaerosols is under-investigated. Thus, the second objective of this dissertation was to evaluate the performance of low-cost optical particle counters (OPC) in monitoring the common indoor bioaerosols. Controlled chamber experiment results showed that low-cost OPCs performance is strongly influenced by particle concentrations being measured. Low-cost OPCs did not show a linear response compared to the reference sensor in the concentration range less

than 5/cm^3 for measuring $PM_{2.5}$ bioaerosol concentrations, while the tested sensors exhibited more linear responses in the range greater than 5/cm^3. For each low-cost OPC, particle-specific, as well as average linear calibration equations that work well for the aggregate of tested bioaerosols, were developed.

One of the challenges in particle monitoring is size characterization due to the variable and irregular shapes. Usually, for application purposes, particles are assumed to be perfect spheres with corresponding spherical physical behaviors and properties. The general process typically defines a sphere with similar physical properties and assigns it an equivalent diameter size. Aerodynamic equivalent diameter is the most commonly used particle size. While aerodynamic size characterization is required for PM transport and exposure studies, optical-based sensors are used in place of aerodynamic-based sensing in most field applications. The validity of such practice has been called into question by previous studies and further investigation of the relationship between aerodynamic and optical size measurement is necessary. Consequently, the third objective of this dissertation was to experimentally compare the size-resolved concentration measurements of an aerodynamic particle sizer with an optical particle counter. Comparison of multiple tests with sixteen -monodisperse and polydisperse, biological and non-biological- particles showed that the particle type, size, and the measurement size fraction affect the relationship between the two PM sensing techniques. Accordingly, particle type and size-resolved specific empirical linear calibration curves between the two sensors for size fractions of smaller than 10 µm, smaller than 2.5 µm, and total number counts were provided. These calibrations provide an opportunity for real-world application of current technologies to reduce the PM exposure health risks for the public.

TABLE OF CONTENTS

List of Figures in Research Summary

List of Tables in Research Summary

ACKNOWLEDGEMENTS

This research was financially supported by various individuals and institutions. I am grateful to Dr. Donghyun Rim for supporting me with graduate research assistantship. Dr. James Freihaut generously provided funding for purchasing monodisperse particles used in my experiments. I would like to thank American Society of Heating, Refrigeration, and Air-Conditioning Engineers (ASHRAE) for supporting this research through ASHRAE Graduate Grant-in-Aid Fellowship. In addition, generous support of various institutions helped with presenting this research at various conferences; American Association for Aerosol Research (AAAR) Travel Grant in 2017, Sloan Foundation Travel Fellowship in 2015, Engineering Diversity Travel Scholarship in 2015 and 2016, and Penn State College of Engineering Travel Grant-in-Aid in 2015, 2016, and 2017. I would like to also thank the Leonhard Center for honoring me with the College of Engineering Distinguished Teaching Fellowship.

This dissertation was made possible with the support of several people. I am grateful and appreciative of my adviser, Dr. Donghyun Rim, for his guidance and support throughout this research study. His continuous advice and feedback gave me motivation to become a better researcher and a stronger person. I am also thankful to my committee members, Dr. James Freihaut, Dr. William Bahnfleth, and Dr. Rui Ni, whose advice and feedback helped to better shape and improve this dissertation. Dr. Freiahut was closely involved in my research projects and was always willing in sharing his insightful advice. I consider myself a lucky person to start my graduate school with Dr. Freiahut as my M.Sc. adviser and be able to continue working with him in my Ph.D. as well. I will always be grateful to him for supporting me throughout my graduate studies. I had the privilege of not only being Dr. Bahnfleth's student and having him in my Ph.D. committee but also working with him during my service as vice president of the Penn

State ASHRAE student branch. Dr. Bahnfleth's passion and care for ASHRAE and his leadership set an example of what it means to have a meaningful involvement in a professional organization.

I spent the majority of my Ph.D. time working in the lab, designing, fabricating, and setting up my experimental chamber set-up. I would like to thank several people who helped me in the lab in setting up and conducting the experiments; former lab manager of Penn State Architectural Engineering Department, Mr. Paul Kremer, lab assistants, and students who worked with me through Research Experience for Undergraduate (REU) program. Working with REU students was a fulfilling and inspiring experience and made my lab time more fun and memorable. Among the REU students who worked with me, Mr. Sean Michael Eagan, and Ms. Camilla Victoria McCrary's assistance was particularly helpful to this research.

I thank all the faculty members, staff, and fellow graduate students at the Architectural Engineering Department for providing a friendly environment that felt like a family.

I would like to express my sincere gratitude to my friend, mentor, and adviser, Dr. Mohammad Heidarinejad. I was very fortunate to get to know him from the beginning of my graduate studies at Penn State and have had the privilege of his friendship and counsel in ups and downs of my journey ever since.

Last but not least, I wish to extend my deepest gratitude to my all dear family and friends for their unconditional love and support throughout my life. They are the power and motivation that keeps me going forward in life. I am beholden to my husband, Mahdad; without his unwavering support and encouragement completing this dissertation was not possible.

DEDICATION

To my great, strong, and loving role model, my mom, and all the great women throughout history whom I am grateful to, for all their efforts and sacrifices that made the opportunities I received possible.

Chapter 1

Introduction

Health ramifications of exposure to airborne particulate matter (PM) have been revealed by various studies (Clancy et al., 2002; Davidson et al., 2005; Dockery et al., 1993; Pope III and Dockery, 2006). Respirable particles can result in allergic responses such as wheezing and nasal drip (Bardana Jr, 2001; Ormstad, 2000), as well as asthmatic responses that can potentially develop chronic respiratory diseases (Goldsmith, 1999). Previous studies have confirmed that indoor dust frequently contains protein allergens from biologically derived materials (Barnes et al., 2001; Ormstad, 2000; Raja et al., 2010; Roberts et al., 1999). Indoor dust is also one of the main concerns related to patient and employee safety in healthcare facilities (Mohammadpour, 2014). Prolonged exposure to indoor PM can lead to respiratory, cardiovascular, and neurological diseases (Bardana Jr, 2001; Bernstein et al., 2008; Perez-Padilla et al., 2010) especially as people in developed countries spend the majority of their time indoors (Klepeis et al., 2001). Therefore, understanding the transport and monitoring of airborne particles in occupied spaces are important for elucidating human exposure to hazardous biological particles.

1.1. Objectives of this dissertation

The first objective of this dissertation is to examine indoor biological particle resuspension and elucidate the effects of building operating conditions on the resuspension dynamics. Indoor aerosols have both indoor and outdoor origins. They are generated from indoor activities such as cooking or penetrate into buildings from outside via ventilation or infiltration. Regardless of their origin, once aerosols are present in indoor spaces they go through a chain of

deposition-resuspension cycles before transport to different indoor spaces where occupants might be exposed to them. Particle resuspension is a complex phenomenon influenced by various factors; surface characteristics such as roughness, particle properties such as size, shape, and hydrophobicity, and ambient environment conditions such as airflow velocity and turbulence intensity, and relative humidity. The degree to which and how factors such as relative humidity and air swirl velocity influence the particle resuspension are not fully understood. Therefore, this dissertation investigates the effects of relative humidity and air swirl velocity on resuspension of bioaerosols from indoor surfaces.

The second objective is to evaluate the performance of low-cost aerosol sensing technology for monitoring biological and non-biological particles indoors. Accurate sensing and monitoring of indoor aerosols are necessary for understanding aerosol transport and the effective control of indoor air contaminants in occupied buildings. Usually mechanical or natural ventilation is used to reduce the PM concentration in the indoor environment, however, bringing in higher amounts of outside air doesn't always translate into higher indoor air quality (IAQ). Measurement data shows that in polluted cities such as Beijing, PM concentrations are higher outdoors than indoors. Therefore, using unfiltered outdoor air actually exacerbates the IAQ condition. This is a risk even for cities with good outdoor air quality because there could be spikes of outdoor PM concentration due to natural or anthropogenic incidents. Besides ensuring a more resilient IAQ condition, integrating PM sensors into a building management system can save energy by using a demand-response ventilation control strategy, which is more efficient than following a fixed prescriptive ventilation rate. However, PM sensor application in the built environment has been hindered due to the high cost of PM sensors. With recent advances in sensing technology, low-cost optical PM sensors have become available in the market at much more affordable prices. The emergence of low-cost PM sensors has opened new horizons in air quality research, with various applications in PM exposure monitoring and control.

Several studies have examined the performance of low-cost optical PM sensors and found that the performance of these sensors varies between the microenvironments (Kelly et al., 2017; Steinle et al., 2015). Besides microenvironment dependence, low-cost optical sensor responses are influenced by particle properties such as the refractive index. For example, biological particles differ in light diffraction properties from non-biological particles, so optical PM sensors may produce a different reading when monitoring bioaerosols. Given that little information is available in the literature for the evaluation of low-cost PM sensors in monitoring bioaerosols, this dissertation examines the performance of low-cost optical PM sensors for sensing common indoor bioaerosols in a controlled laboratory environment.

The third objective is to compare two major aerosol sensing technologies (*i.e.*, aerodynamic based vs. optical based) in characterizing particle concentrations and sizes. One of the complications in characterizing particle size and concentration is the fact that particles often have irregular rather than spherical shapes. In order to address this issue, equivalent diameters have been defined based on specific properties of the particles for different applications, such as volume-equivalent diameter, or aerodynamic equivalent diameter. Impacts of particle size on indoor particle transport (Nazaroff, 2016), PM removal efficiency (Kasper et al., 2009; Stafford and Ettinger, 1972), or PM exposure (Heyder, 2004) are attributed to the aerodynamic size of the particle. Yet, it is common practice in the field to measure the particles with optical particle counters that provide volume equivalent diameter. The main reason for using optical sensing is convenience and lower cost of optical particle counters compared to aerodynamic sensing. The predominant use of optical particle counters in field applications has led to current low-cost PM sensing technology. Given the fundamental differences between these two measurement techniques, this dissertation elucidates the relationship between the aerodynamic sensing and optical sensing in characterizing the particle size and concentration.

1.2. Structure of this dissertation

This Ph.D. dissertation is outlined in two parts. The first part (chapters 1 to 5) presents the executive summary of this dissertation; background, literature review, research objectives, major findings, and conclusions. The second part presents the research papers that address each research objective in more detail (appendices A to C).

The intent behind writing this dissertation with this structure was to make it easier and more time-efficient for the reader to find the information they are interested in without having to read the whole document. Each paper is written as an independent document. Therefore, should the reader be interested in only one of this dissertations' objectives, one can skip the other chapters of this document and only read the paper addressing that specific objective.

Chapter 2

Literature Review

This chapter presents the study background and the literature review that led to specific research questions of this dissertation. The following section summarizes state-of-the-art findings on indoor aerosol transport and current status of indoor aerosol sensing including low-cost sensor technologies.

2.1. Indoor aerosol transport

Particle transport in buildings involves deposition and resuspension processes. Indoor particles are either directly generated from indoor sources or introduced from outdoors into the building via ventilation and infiltration (Nazaroff, 2016). These particles can deposit on indoor surfaces such as floors, ventilation ducts, and filters. The settled particles can resuspend from floors and become airborne by occupant activities such as walking and vacuuming (Thatcher and Layton, 1995; Ferro et al., 2004). The resuspended airborne particles can transport to the occupants' breathing zones or to building mechanical system via air recirculation. Airborne particles from the recirculated air and outdoor air intake can deposit onto duct surfaces by various mechanisms including gravitational settling, diffusion, and turbulent transport. Particles deposited on duct surfaces can later resuspend by airflow disturbances (Sippola and Nazaroff, 2002). The resuspended particles in the duct can be transported to the occupied zones by the air distribution

systems. Such deposition and resuspension processes repeat and form the particle transport cycle in the building.

Field studies have shown that resuspension rate of particles from indoor surfaces is affected by the occupants' activities (Clayton et al., 1992; Ferro et al., 2004; Sippola and Nazaroff, 2002). Even light occupants' activities such as walking were shown to increase the mass concentration of airborne super-micron particles by 100% (Thatcher and Layton, 1995).

Several experimental studies have attempted to characterize the indoor aerosol resuspension under different indoor activities (Luoma and Batterman, 2001; Cheng et al., 2010; Qian et al., 2014). Gomes (2004) studied the occupant walking kinematics and characterized the walking-induced aerodynamic forces, comprised of air swirl velocities and vibrational forces, which cause the re-aerosolization of the particles deposited on the floor. Gomes et al. (2007) then experimentally investigated the particle resuspension from floor surface samples in a controlled chamber, as they mimicked the swirl air velocities and vibrational forces that represented the characterized walking-induced aerodynamic forces. Their results revealed air swirl velocity level to have the highest impact on particle resuspension while that of walking-induced vibration was minimal. Mukai et al. (2009) reported the impact of airflow characteristics on the particle resuspension from indoor surfaces based on controlled experiments. They measured the relative resuspension of 1-20 μm particles from three indoor surface materials (linoleum, carpet, and galvanized sheet metal) at five bulk air velocity rates (5 to 25 m/s). Their results showed that airflow velocity, turbulence intensity, and particle size had the largest effect on particle relative resuspension respectively.

Ibrahim et al. (2003) conducted an experimental study on the detachment of monolayer deposited stainless steel, glass, and Lycopodium spore micro-particles on a glass substrate under turbulent air. The factors that were controlled in their experiment were airflow acceleration, the final free-stream velocity, relative humidity, initial number density of deposited microparticles,

microparticle counting technique, material, and size. They found that surface energy of adhesion and particle size have the most influence on the airflow threshold velocity for particle detachment. The other important finding was the effect of RH on particle resuspension that is generally ignored in most resuspension studies. Their results showed that resuspension rate is decreased at high RH due to adsorption of water vapor at the particle-substrate interface and which consequently increased the threshold velocity for higher RH levels.

Besides Ibrahim et al. (2003), review of resuspension studies has also identified RH to be an influential factor in particle resuspension (Sehmel, 1980). Multiple studies have looked into the effect of relative humidity on particle resuspension and the mechanism of its effect. Empirical data has shown that particle to surface adhesion force becomes stronger as relative humidity (RH) increases. Hinds' adhesion empirical equation as a function of particle diameter and RH is an example (Hinds, 2012). However, due to the confounding relationship of relative humidity and electrostatic effects on the particle to particle and particle to substrate adhesion forces, the result of these experimental studies on the effect of RH on particle resuspension have not been very clear. Moreover, some of these investigations show conflicting results indicating that resuspension may increase or decrease with indoor humidity. Corn (1961) and Corn and Stein (1965) found adhesion forces were relatively insensitive to increasing RH values up to 30%; after which adhesion forces rapidly increased. A study by Rosati et al. (2008) showed both increasing and decreasing particle resuspension phenomena with humidity changes depending on the surface material composition. Qian and Ferro's full-scale chamber experimental study (2008) reported that walking-induced resuspension rate of Arizona test dust (ATD) in the size range of 0.1-10 μm was not significantly influenced by variation of RH in the range of 30-50%. They concluded that the effect of RH should be investigated in a wider range as their experiment did not allow for such conditions. They also suggested the investigation of RH effect on both organic and inorganic particles as they would have a different particle-humidity interplay. A recent study by Tian et al.

(2014) conducted a similar walking-induced house dust resuspension with higher levels of RH, 40% and 70%, from five different flooring types. Their results showed opposite effects of RH on particle resuspension for different surface types. These study results imply that the particle and substrate surface interaction changes the particle detachment behavior for various RH levels. As the role of RH level has become clear through the previous studies, the need for more extensive information on its effect for both organic and inorganic particle types and various substrate surfaces has been emphasized.

Overall, previous studies reveal that regardless of whether it is a floor surface or a ventilation duct surface, the resuspension of particles depends on three categories: 1) particle properties, 2) surface properties, and 3) airflow conditions (see Figure 2-1s). Particle properties include size, density, composition, and shape. Surface characteristics involve roughness and electrostatic properties. Airflow conditions include velocity, turbulent intensity, aerodynamic and mechanical disturbances, and relative humidity. Based on the literature, characterizing particle resuspension as a function of these factors is essential for developing accurate particle transport models.

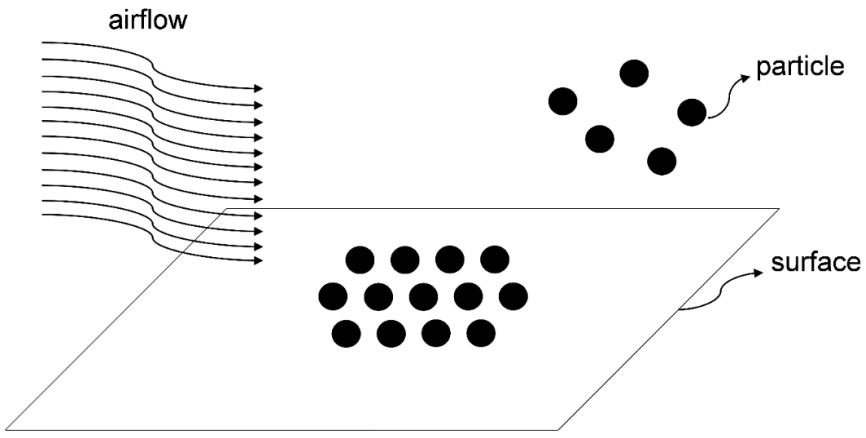

Figure 2-1. Deposition and resuspension of particles depends on various factors that can be divided into three categories: particle properties, surface properties, and airflow conditions.

2.2. Aerosol sensing

2.2.1. Low-cost optical PM sensing

To control the PM concentration in indoor environments, two different strategies can be used. The first strategy comprises the use of a code-prescriptive ventilation rate based on the type of building space, as is suggested within established standards, in order to mitigate PM concentration levels (ASHRAE, 2004). This strategy has two drawbacks. Outdoor air PM concentration itself varies and could be lower or higher than that of indoor air (Rim et al., 2013). Consequently, using unfiltered outdoor air to ventilate the building might even exacerbate the indoor air quality. The other drawback is the high energy consumption associated with building ventilation. Building ventilation accounts for a significant portion of total energy used in buildings (Salimifard, 2014; Salimifard et al., 2014). Moreover, increased outdoor air ventilation rates translate into not only air distribution energy consumption but also higher cooling and heating energy uses (Rim et al., 2014). To control the PM concentration level in a more energy efficient fashion, the demand-response ventilation control strategy can be pursued (Persily, 2015). Achieving acceptable indoor air quality using demand-response ventilation control requires real-time monitoring of pollutant levels in occupied spaces with sufficient measurement nodes across the building zones (Kumar et al., 2016).

There are various established PM sensing techniques that can provide real-time PM size-resolved number concentration measurements. However, these sensors are mostly used in laboratories and their relatively high cost has been a barrier to PM monitoring in indoor occupied spaces (Kumar et al., 2016). Addressing this gap in PM monitoring was made possible by the recent development of low-cost PM sensors (Rai et al., 2017). Most of these low-cost PM sensors

are optical particle counters which characterize the PM size and concentration based on their light diffraction properties (Sousan et al., 2016).

The advent of low-cost PM sensing has not only made indoor PM monitoring affordable but has also caused a paradigm shift in PM exposure research in general (Snyder et al., 2013). Low-cost PM sensors are being used to establish outdoor PM monitoring networks with high spatiotemporal resolutions (Jiao et al., 2016). Portability and affordability of these sensors have enabled initiation of novel areas in PM exposure monitoring; Low-cost sensors are used in projects such as Citizen Scientists (Aoki et al., 2008; Jovašević-Stojanović et al., 2015) to raise social awareness and attention toward air quality issue. In spite of the opportunities that low-cost sensing brings, using them, in any of the aforementioned PM monitoring applications, prior to performance evaluation and calibration can lead to detrimental consequences (Snyder et al., 2013).

To evaluate the performance of low-cost sensors, researchers have conducted experimental and observational studies in lab and field environments. Several researchers have conducted indoor (Patel et al., 2017; Steinle et al., 2015; Weekly et al., 2013) and outdoor (Holstius et al., 2014; Piedrahita et al., 2014; Gao et al., 2015; Steinle et al., 2015; Kelly et al., 2017; Mukherjee et al., 2017; Zikova et al., 2017) field campaign measurement studies which investigated the performance of these sensors in various real-world microenvironment conditions. To further investigate the effect of various factors on sensor performance, controlled laboratory experimental studies (Northcross et al., 2013; Wang et al., 2015; Manikonda et al., 2016; Sousan et al., 2016) examined the response of low-cost PM sensors compared to lab-grade reference sensors under varying conditions. The controlled chamber experimental studies showed that the counting efficiency of the low-cost OPC was influenced by the size, type, and concentration of the tested particles. These findings demonstrated the necessity of the sensor calibration tailored to particle type, size, and concentration specific to each monitoring application.

What research attributes to particle type involves several particle properties influencing light-scattering, such as shape, refractive index, and composition. Research has shown that biological and non-biological particle have different light-scattering properties (Bohren and Huffman, 2004). Testing low-cost OPC sensors with organic and inorganic particles resulted in markedly different responses (Wang et al., 2015). Despite the evidence for the probable different response of low-cost PM sensors under exposure to biological particles, the performance of these sensors in monitoring bioaerosols has not been studied.

Given the significance of bioaerosols in PM exposure-related health effects in building occupants, taken together with the particle type dependence of PM sensor performance, it is essential to evaluate and calibrate the performance of cost sensors in monitoring bioaerosols before using them in indoor spaces. Therefore, the second objective of this study is to examine the performance of low-cost PM sensors under exposure to varying concentrations of several common indoor bioaerosols.

2.2.2. Relationship between optical and aerodynamic diameter size measurements

Any successful attempt at controlling PM exposure strongly relies on accurate particle size characterization, as particle size is the one of the most influential parameters not only in particle transport dynamics but also in its filtration efficiency (Hinds 2012). With regard to indoor particle transport, the particle size is one of the most significant factors (Heidarinejad, 2011; Nazaroff, 2016). The size distribution of indoor particles significantly impacts their dispersion, deposition and resuspension characteristics (Salimifard et al., 2015). Particle size characteristics determine the PM deposition rate as well as removal efficiency (Kasper et al., 2009; Stafford and Ettinger, 1972). Hence, appropriate particle removal and deactivation of indoor dust depend on the accurate characterization of size distribution.

Particle size is characterized based on diameter size of particles, assuming that they are perfect spheres. However, since most particles are not spherical in shape, several diameter equivalent size terms have been defined and used based on the size measurement techniques. Amongst all particle size definitions, optical diameter size and aerodynamic diameter size are the most commonly used terms. Optical diameter size refers to the diameter size of the particle when measured with an optical particle counter. Optical diameter size measured by OPC is usually assumed to be equal to volume equivalent diameter (Bohren and Huffman, 2004). Volume equivalent diameter is the diameter of a sphere which has the same volume as the actual particle. Aerodynamic equivalent diameter (Dae) – or simply aerodynamic diameter- is the diameter of a spherical particle with unit density (density of water 1000 kg/m^3) that has the same settling velocity as the actual particle. Aerodynamic diameter is the more useful and relevant measure that is used aerosol filtration characterization and particle transport models since it standardizes the shape and density of the particle.

Although aerodynamic size is the particle size measure used in deposition and resuspension models, it is not the size measure that is sensed and monitored in particle transport studies. It is common practice in most lab and field studies to use optical particle counters to measure the particle size distribution. As an example, the resuspension experimental study conducted to address the first research objective of this study used optical particle counters to calculate the size-resolved resuspension rate of the particle. Similarly, low-cost PM sensors, discussed in the second objective of this research, are all optical particle counter sensors. So any conclusion drawn from these studies is bound to the inherent difference between optical and aerodynamic particle sizing techniques and cannot be extended for use in particle transport and exposure models unless the relationship between optical and aerodynamic sizing for different particles is well defined.

A number of studies have looked into the relationship between aerodynamic particle size –commonly measured by time-of-flight devices- and optical particle size –measured by optical particle counters. Reponen et al. (2001) compared different methods of size measurement for four fungal species (Penicillium brevicompactum, Penicillium melinii, Cladosporium cladosporioides, and Aspergillus versicolor) and two actinomycete species (Streptomyces albus and Thermoactinomyces vulgaris). They used three microscopic methods to measure the spore sizes: using optical microscope from stained (wet) slides, optical microscope from unstained (dry) slides, and environmental scanning electron microscope (SEM) directly from microbial culture. An aerodynamic particle sizer (Aerosizer, API Match II) was used to measure the spore's aerodynamic diameter. Their study showed that there was no clear trend in the relationship between aerodynamic and physical diameter that was measured with any of the three microscopic methods. A more recent study by Peters et al. (2006) compared size measurement response of two OPCs (Grimm 1.108 and 1.109) and an APS (TSI 3321). They tested three sizes of monodisperse (polystyrene latex spheres in 0.83, 1.0, and 3.0 μm) particles and polydisperse Arizona test dust. They found that that the number counts measured by OPC were higher than that measured by APS for monodisperse PSL spheres, while the number and mass concentrations of polydisperse Arizona test dust were different depending on the particle size. APS particle detection efficiency was lower than both OPCs for Arizona test dust smaller than 0.7 μm, the opposite case was true for 0.7-2 μm size range. Finally, they concluded that further experiment was required to explain the observed discrepancies.

The need for further information on the relationship between aerodynamic and optical diameter size measurement of indoor aerosols has set the motivation for the third objective of this thesis study. It is to investigate and compare the relationship between aerodynamic and optical size measurement of the particle samples resulting from the aerodynamic particle sizer (APS) and optical particle counter (OPC). Size distribution of several biological and non-biological particles

are examined using simultaneous optical and aerodynamic sampling and measurements of particle samples from a bench-scale dispersion chamber.

Chapter 3

Dissertation Aim and Objectives

The broad goal of this dissertation is to advance the current understanding of indoor particle resuspension and aerosol sensing with a focus on biological particles that are commonly found in buildings. Based on the literature review, this dissertation addresses three research questions as follows:

3.1. Specific research questions

1. What are the effects of aerodynamic disturbances and relative humidity on resuspension of indoor biological particles?
2. Can low-cost OPCs be reliably used for monitoring common indoor bioaerosols compared to the lab-grade OPC sensor?
3. Can optical particle sensing be used to characterize the aerodynamic sizes and concentrations of biological and non-biological particles?

3.2. Research objectives

To answer the three specific research questions described above, three research objectives have been achieved as follows.

I. Investigate the effects of relative humidity and aerodynamic disturbances on resuspension rate of the indoor allergen carrier particles in a controlled laboratory setting.

II. Examine the performance of low-cost PM sensors compared to a lab-grade OPC sensor in a controlled chamber experimental study.

III. Investigate the relationship between optical and aerodynamic diameter size measurements in a controlled chamber experimental study.

The first objective is addressed and presented in Paper 1 (Appendix A) (Salimifard et al., 2017). To address this objective, first, the effect of relative humidity on particle resuspension rate is investigated, considering four types of indoor particles (quartz, dust mite, dog fur, and cat fur) and two floor surface types (carpet and linoleum). Secondly, particle resuspension from a duct surface is studied and characterized as a function of duct vibration frequency and swirl flow velocity. The resuspension study results were published in 2015 Healthy Buildings conference (Salimifard et al., 2015) and presented in 2016 American Association for Aerosol Research (AAAR) conference (Salimifard at al., 2016). The second objective is addressed and presented in Paper 2 (Appendix B). To address this objective, the response of four low-cost optical particle counters are compared with that of the reference sensor under exposure to varying concentrations of several biological and non-biological aerosols. This study results will be presented at Indoor Air 2018 conference, and 10th International Aerosol Conference (IAC). The third objective is addressed and presented in Paper 3 (Appendix C). To address this objective, simultaneous size-resolved number concentration measurements by an aerodynamic particle sizer and an optical particle counter when exposed to varying concentrations of several particles with various size, shape, density, and optical properties are compared. The results of this study were presented at 2017 AAAR conference (Salimifard et al., 2017).

Chapter 4

Methods

This chapter presents the research methods used to address the specific research questions and objectives of this dissertation study.

4.1. Particle resuspension study (Objective I)

Previous experimental studies in Indoor Aerosol Lab have investigated the effects of substrate and ambient airflow conditions on particle resuspension. Since the inception of this dissertation, the author has been involved in the in-depth analysis of chamber measurement data and disseminating the experimental results. One set of these experiments was designed to examine the resuspension rates of indoor dust from the duct surfaces as a result of variation in duct vibration and swirl flow velocities.

Another set of these experiments investigated the effect of relative humidity on the resuspension of three common indoor allergen particles (dust mite, dog fur, and cat fur), and bacterial spore (*Bacillus thuringiensis*) from two floor surface types (carpet and linoleum). Each particle was first deposited on the substrate using a particle dispersion chamber. Then, the particle-laden surface sample was placed in the resuspension chamber where it was subjected to various air swirl velocities.

Figure 4-1 shows the schematic diagram of the resuspension chamber system that was employed to perform the experiments. A mechanical shaker was used to transmit the vibration force patterns representing those existing in mechanical ventilation ducts, or on floor surfaces caused by occupants' walking (Figure 4-2). The mechanical vibration, airflow, and air swirl

disturbances prompt the deposited particles on the surface to resuspend into the air. An optical particle counter at the outlet of the resuspension chamber measured the size-resolved number concentration of the reuspended particles. This experiment with each particle-substrate combination was repeated for different air swirl velocities and relative humidity levels. An environmental chamber was used to provide airflow at 10%, 45%, and 80% RH at 25 °C.

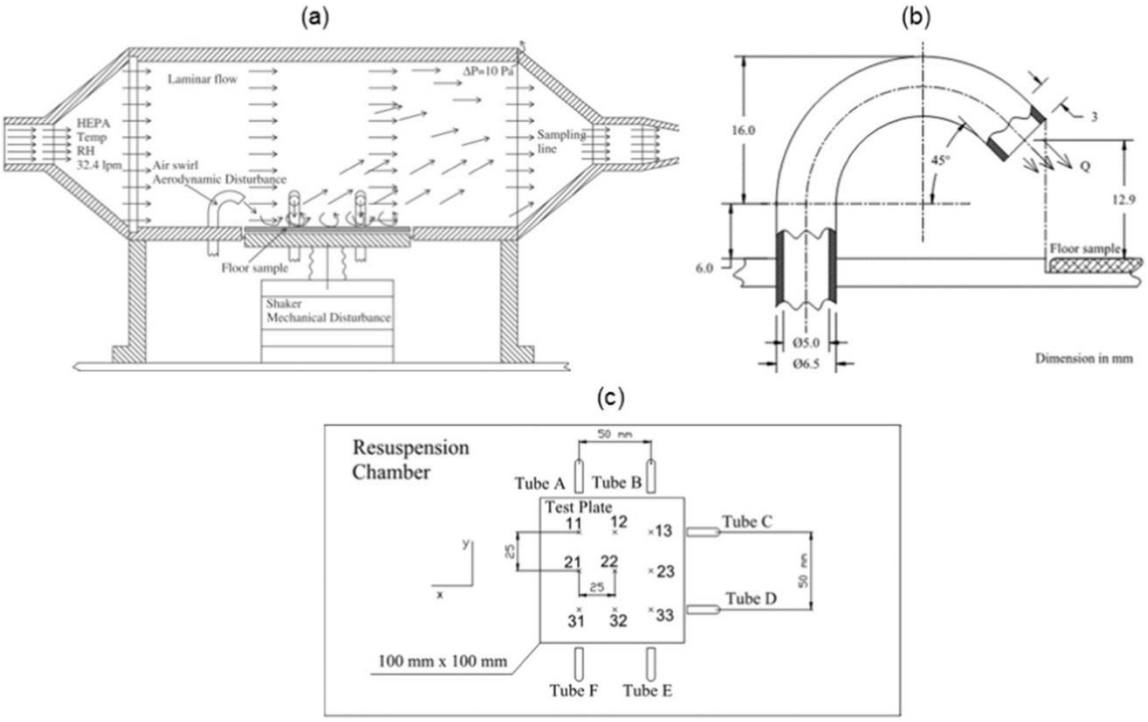

Figure 4-1. Schematic diagram of experiment set-up: (a) resuspension chamber system; (b) air swirl jet tubes; (c) top view of the air velocity measurements at nine locations 2.5 mm above the test surface (Gomes et al., 2007).

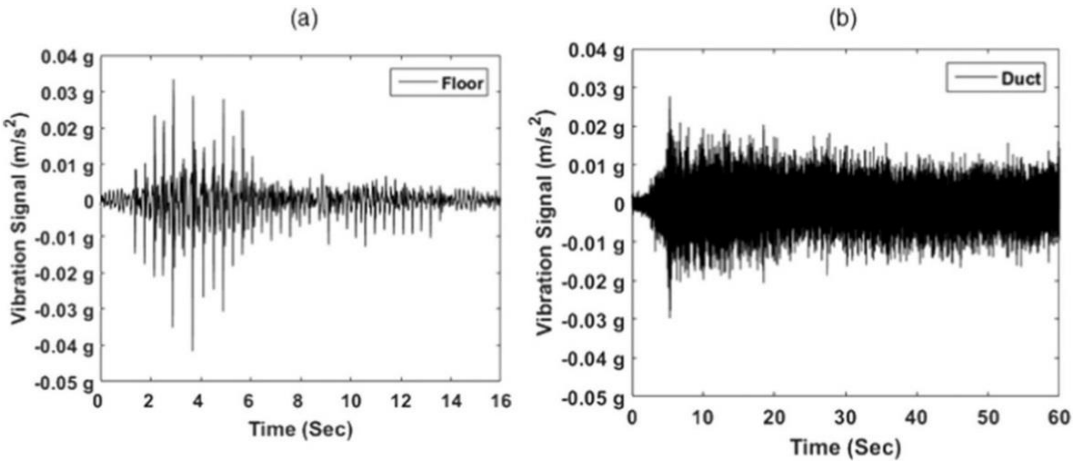

Figure 4-2 Vibration wave forms applied to the resuspension chamber via a mechanical shaker: (a) floor vibration; (b) duct vibration.

To calculate the particle resuspension rate the following equations were used.

$$RR_d = \frac{G_d}{C_{surface,d}} \quad (1)$$

Where, RR_d is resuspension rate for particles of size d (min^{-1}), $C_{surface,d}$ is surface concentration for particles of size d ($\frac{\#}{m^2}$), and G_d is surface removal rate for particles of size d ($\frac{\#}{m^2.min}$), which is defined as follows.

$$G_d = \frac{\int_t \ Q_{sweep,flow} \cdot \ C_{air,d}\, dt}{A_{surface} \cdot \left(\frac{1\ min}{60\ s}\right) \cdot \int_t \ dt} \quad (2)$$

Where, $Q_{sweep,flow}$, flow is the air cross-flow over the floor sample ($\frac{m^3}{s}$), $C_{air,d}$, d is air dust concentration for particles of size d ($\frac{\#}{m^3}$), $A_{surface}$ is the sample surface area (m^2), and dt is time interval (s).

Further details about the experimental set-up, sample preparation, and data analysis methods used in this experimental study are provided in Appendix A.

4.2. Aerosol sensing study (Objectives II & III)

4.2.1. Experimental set-up

Both objectives II and III are pursued using the same experimental set-up and process. Figure 4-3 shows the schematic of the experimental set-up used for the particle sensing study. In order to test the sensor responses under varying concentrations of different aerosols, a particle dispersion chamber (0.76 × 0.76 × 0.42 m) with a controlled particle injection system was used. There are two lines of pressurized filtered air delivering air to the chamber. Line 1 is particle-free air supplied into the chamber from the top center inlet. Line 2 is particle-free air going through a syringe with particles, pushing the particles injected into the chamber from the bottom middle inlet of the chamber. The collision of the two air jets (from lines 1 and 2) facilitates an optimum dispersion of the particles inside the chamber. There are four fans at four corners of the chamber running to create a well-mixed environment with relatively homogenous particle concentration inside the chamber.

Since one of the objectives of this study is to investigate the effect of particle concentration on the sensors' performance, it was intended to collect the sensors responses over a range of particle concentration. To achieve such conditions in each test, particle concentration decay was simulated inside the chamber as follows. Each test starts with five minutes of background sampling. Then line 2 is opened and particles are dispersed into the chamber for two minutes. At minute seven, particles injection is stopped (line 2 is closed) and particle decay sampling continues for the rest of the test. Each test runs for 2.5 hours. The amount of particle mass placed inside the syringe in each test is calculated based on the peak particle number concentration limit needed inside the chamber, assuming a constant density and average particle size.

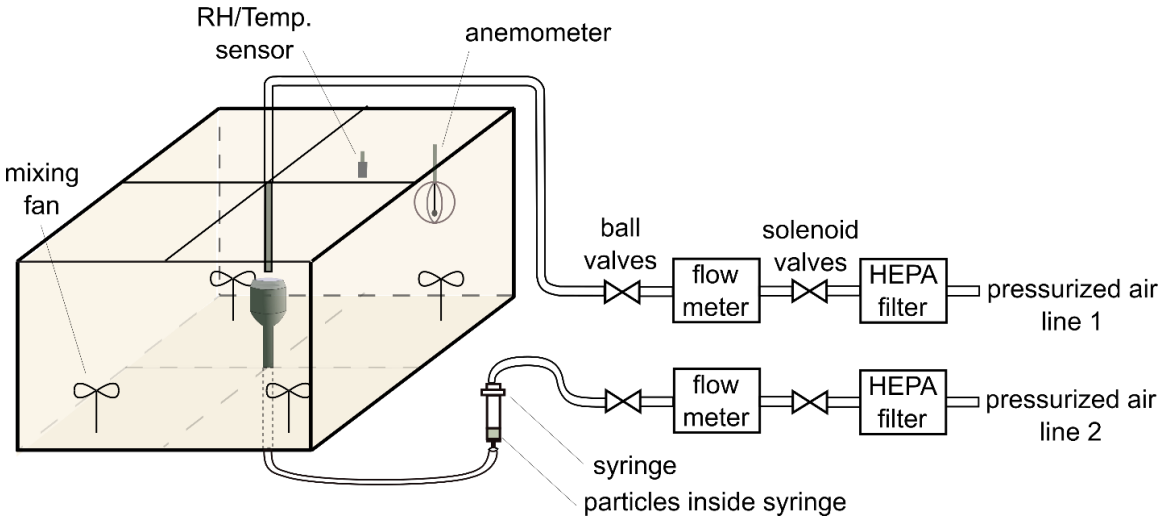

Figure 4-3. Schematic of the chamber experiment set-up.

4.2.2. Tested sensors

All sensors tested in the low-cost sensing study (objective II) and aerodynamic versus optical sensing study (objective III) are set up to measure the particle number concentration simultaneously throughout each test. Specifications and characteristics of the sensors used in the low-cost sensing (shown in Figure 4-4) and aerodynamic vs. optical sensing (shown in Figure 4-5) studies are summarized in Table 4-1 and Table 4-2, respectively.

Figure 4-4. Sensors examined in this study.
a) OPC N2 (Alphasense Ltd., Essex, United Kingdom),
b) IC Sentinel (Oberon Inc., State College, PA),
c) Speck (Airviz Inc., Pittsburgh, PA),
d) Dylos (Dylos, Riverside, CA), and
e) Handheld AeroTrak (TSI, Inc., Shoreview, MN), reference sensor.

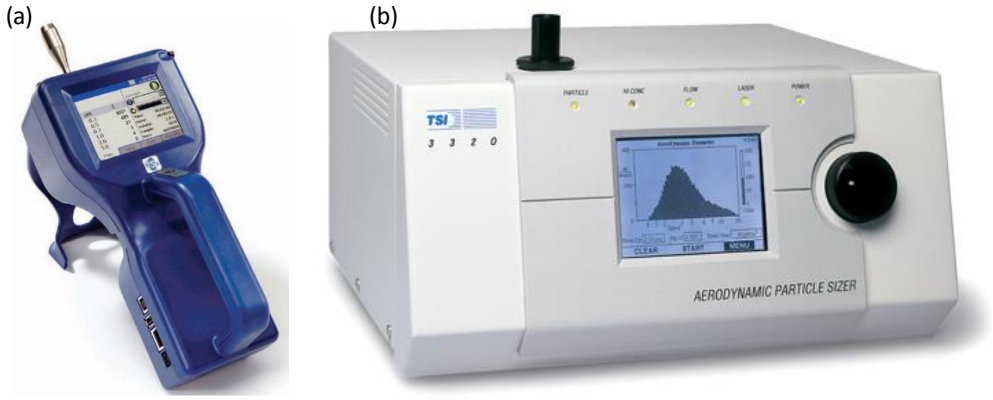

Figure 4-5. Sensors used in this study: (a) Handheld AeroTrak (TSI), (b) APS3321 (TSI).

Table 4-1. Low-cost and reference OPC sensors' specifications as reported by the manufacturer

Low-cost & reference sensors	OPC N2 (Alphasense)	IC Sentinel	Speck[1]	Dylos (DC1100)	AeroTrak (TSI 9306)
Light source wavelength (nm)	658 [2]	650 [3]	850[4]	650	785 [5]
Detection size range (µm)	0.38-17	1, 5	0.5–3	>1	0.3-25
# of bins	16	4	1	2	6
Bin size cuts (µm)	0.46, 0.66, 0.92, 1.20, 1.47, 1.83, 2.54, 3.50, 4.50, 5.75, 7.25, 9.00, 11.00, 13.00, 15.00, 16.75	0.5, 1, 5, 10	2	1, 5	0.3, 0.5, 1.0, 3.0, 5.0, 10.0
Flow rate (L/min)	sampling: 0.22, total:1.2	1.5	not specified	not specified	2.83
Measurement time resolution (sec)	1	120	30	60	1
Detection concentration range	10,000 particles/sec	3×10^6 particles/ft^3	not specified	not specified	3×10^6 particles/ft^3 at 5% coincidence loss

1: uses DSM501A (Syhitech DSM501, Syhitech Co., Ltd) sensor, 2: laser diode, 3: laser diode (10 mW), 4: LED, 5: enhanced active cavity HeNe laser.

Table 4-2. Sensors' specifications as reported by the manufacturer

Sensor	Measurement type	Light source wavelength (nm)	Detection size range (µm)	# of bins	Bin size cuts (µm)	Flow rate (L/min)	Time resolution (sec)	Detection concentration range
AeroTrak (TSI 9306)	optical – particle count	785 [1]	0.3-14	6	0.3, 0.5, 1.0, 3.0, 5.0, 10.0	2.83	1	3×10^6 particles/ft^3 at 5% coincidence loss
APS (TSI 3321)	aerodynamic – particle count	658	0.5-20	52	0.523, 0.542, 0.583, 0.626, 0.673, 0.723, 0.777, 0.835, 0.898, 0.965, 1.037, 1.114, 1.197, 1.286, 1.382, 1.486, 1.596, 1.715, 1.843, 1.981, 2.129, 2.288, 2.458, 2.642, 2.839, 3.051, 3.278, 3.523, 3.786, 4.068, 4.371, 4.698, 5.048, 5.425, 5.829, 6.264, 6.732, 7.234, 7.774, 8.354, 8.977, 9.647, 10.37, 11.14, 11.97, 12.86, 13.82, 14.86, 15.96, 17.15, 18.43, 19.81	sample flow rate: 1, total flow rate: 5	1	0.001 - 1000 particles/cm^3

1: enhanced active cavity HeNe laser.

4.2.3. Tested particles

Sixteen different particle batches were used to test the sensors. These particles include eight monodisperse and eight polydisperse batches. Monodisperse particles are poly methyl methacrylate (PMMA-R) in 5.1 and 9.9 µm, melamine resin (MF-R) in 1.041, 2.81, and 10.55 µm, and silicon dioxide –also known as silica or quartz- (SiO_2-R) in 0.977, 2.81, and 5.04 µm. the eight polydisperse particle batches include both non-biological and biological particles. The polydisperse non-biological particles are quartz (crushed quartz #10 bt#4339, Particle Technology Limited, UK), and aluminum oxide (Al_2O_3). The biological particles are pollen, dust mite (Indoor Biotechnologies Inc., Charlottesville, VA, USA), dog fur, cat fur, *Bacillus thuringiensis* (BT) spore, and NIST indoor dust. Table 4-3 provides a summary of all the tested particles and their properties.

The APS and OPC (TSI) responses for all the sixteen particles are analyzed in the aerodynamic versus optical sensing study. For the low-cost sensors study, since the focus is on indoor biological particles, the following nine particle batches are tested; dust mite, pollen, cat, and dog fur as four common indoor bioaerosols; plus monodisperse melamine resin (MF-R) in 1.041, and 2.81 µm, monodisperse silicon dioxide (SiO_2-R) in 0.977, and 2.81 µm, and polydisperse quartz.

Table 4-3. Tested particles' characteristics

Particle type	Size distribution type	Size range (µm)	Biological / Non-biological	Density (kg/m^3)	Shape	Roughness	Refractive Index	Hydrophobicity
poly (methyl methacrylate) (PMMA-R)	monodisperse	5.1 ± 0.13[1], 9.9 ± 0.22[1]	non-biological	1190	spherical	smooth	1.48[h,i]	hydrophobic
melamine resin (MF-R)	monodisperse	1.041 ± 0.03[1], 2.81 ± 0.06[1], 10.55 ± 0.14[1]	non-biological	1510	spherical	smooth	1.68[i]	hydrophilic
silicon dioxide (SiO2-R)	monodisperse	0.977 ± 0.026[1], 2.81 ± 0.1[1], 5.04 ± 0.2[1]	non-biological	1850	spherical	smooth	1.42[i]	hydrophilic
crushed quartz (>95% of SiO_2)	polydisperse	0.58-22.5	non-biological	2650	varied[3]	smooth	1.544[g]	hydrophilic
aluminum oxide (Al_2O_3)	polydisperse	-	non-biological	3950	-	-	1.768[a]	-
pollen	polydisperse	-	biological	1000	near spherical[l]	-	1.5[b]	hydrophilic
dust mite	polydisperse	0.58-48	biological	1140	rounded[2]	smooth	-	hydrophilic
dog fur	polydisperse	0.58-351	biological	1000	fibers	rough	1.37-1.55[d]	hydrophobic
cat fur	polydisperse	0.58-409	biological	1000	fibers	rough	1.35-1.43[d]	hydrophobic
Bacillus thuringiensis (BT) spore	polydisperse	0.58-56.2	biological	1000	round	smooth	1.84[e]	hydrophobic[k]
NIST indoor dust	polydisperse	-	-	-	-	-	-	-

1: size ± standard deviation, 2: with prismatic edges resulted from the ball mill crushing effect, 3: varied from squares to rectangles (5/1 ratios maximum).
a: (Weber, 1986), b: (Gullvåg, 1964), d: (Yan et al., 2015), e: (Fromentin et al., 2008), g: (Hinds, 2012), h: (Sultanova et al., 2009), i: as provided by the manufacturer, j: (Radhakrishnan, 1947), k: (Koshikawa et al., 1989; Tufts et al., 2014), l: (Hinds, 2012).

4.2.4. Data Analysis

In sensor calibration studies, linear regression analysis is widely used to analyze the systematic biases of the tested sensor response (as dependent variable) against that of the reference sensor response (as independent variable) (Holstius et al., 2014; Manikonda et al., 2016; Miller et al., 1991; Patel et al., 2017; Sousan et al., 2017, 2016b; Wang et al., 2015; Yanosky et al., 2002). Assuming the reference sensor will provide true measurements, if the tested sensor measurements match that of the reference sensor, ideally the slope of the linear regression result should be 1 and the intercept should be 0 (schematics shown in Figure 4-6). Deviation of the slope and intercept from 1 and 0 can be attributed to the presence of proportional (PB) and fixed (FB) biases respectively, in the tested sensor. The linearity of the tested response with the reference sensor is judged by R^2 value. If the tested sensor exhibits a linear response with respect to the reference sensor (high R^2), the fixed and proportional biases in the measurement can be corrected with the developed linear calibration equation (Equation 4). The precision of the linear calibration equation is reflected by the root mean squared error (RMSE) value.

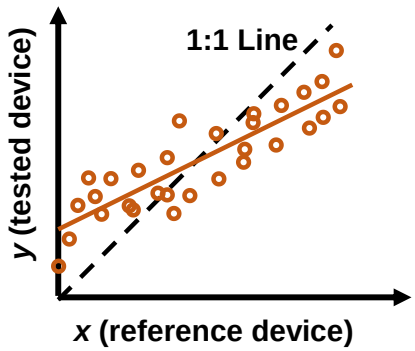

Figure 4-6. Linear regression analysis is used to evaluate the performance of the low-cost sensors. The tested sensors' measurements are considered as the dependent variable while the reference device measurements as the independent variable. The intercept and slope values different from 0 and 1 represent the fixed and proportional biases of the tested sensors with respect to the reference sensor.

$$y = FB + PB \times x \quad \text{(Equation 3)}$$

$$x = -\frac{FB}{PB} + \left(\frac{1}{PB}\right) y \quad \text{(Equation 4)}$$

Where,

- *x* (independent variable) is the number concentration measured by the reference sensor ($\#/cm^3$),
- *y* (dependent variable) is the number concentration measurement of the low-cost sensor estimated by the linear regression model ($\#/cm^3$),
- *FB* is the fixed bias (intercept of the regression model) ($\#/cm^3$),
- *PB* is the proportional bias (slope of the regression model).

To compare the performance of low-cost sensors against the reference sensor, low-cost sensor responses were considered as the dependent (y) and the lab-grade OPC was considered as the independent (x) variables in the linear regression analysis. The focus of the analysis for low-cost sensor performance evaluation was on particles smaller than 2.5 µm for two reasons; first, the significance of PM2.5 monitoring due to its exposure health effects, second, particles smaller than 2.5 µm is size range covered by all the tested low-cost sensors. Since the tested sensors have different measurement time resolutions varying from 1 second to 2 minutes, all the measurements for the low-cost sensing study analysis were time-averaged at over 2-minute time intervals.

Similarly, to investigate the relationship between the aerodynamic and optical sensing, OPC measurements were considered as the dependent (y) while APS measurements were considered as the independent variables (x) in the linear regression analysis.

Further details about the experimental set-up, tested sensors and particles, and data analysis methods used in the aerosol sensing study are provided in Appendices B (low-cost sensing) and C (aerodynamic and optical sensing).

Chapter 5

Main Findings

This chapter presents the major findings for the three main objectives of this dissertation.

5.1. Research Objective I: particle resuspension study

5.1.1. Relative humidity effect on resuspension rate from floor surfaces

Figure 5-1.a-h show the size-resolved resuspension rates of quartz, dust mite, cat fur, and dog fur particles from carpet and linoleum surfaces. These results represent the tests with 1.5 m/s air swirl velocity for both 10% and 80% RH.

A clear trend of resuspension rate variation as a function of size is observed for all test cases and conditions. Resuspension rate first decreases with an increase in size up to a certain point after which the reverse occurs. This trend of increased resuspension rate with the particle size in the range of 0.5-10 μm agrees well with previous empirical findings (Gomes et al., 2007; Qian and Ferro, 2008; Qian et al., 2014). The relationship between the particle size and resuspension rate can be explained by analyzing the particle dynamics and balance of forces acting on a particle at the detachment moment. The motion of submicron particles smaller than 0.5 μm is influenced more by the Brownian diffusion than by Stokes drag force (Soltani and Ahmadi, 1995). As the particle size decreases, Brownian diffusivity increases and becomes the dominant force influencing the particle transport (Hinds, 2012). However, for relatively large particles, Stokes drag force is the driving force in the particle detachment and transport. The dip in the resuspension curve represents the region where neither Brownian diffusion nor Stokes drag

force is large enough to resuspend the particles from the substrate. It should be noted that resuspension rate reaches a peak and follows a downward trend when the particle size is large enough that the gravitational force overcomes the drag force. This study does not focus on those size ranges in the design of its experiment.

Besides particle size, Figure 5-1 shows RH to be an influential factor on resuspension rate, but not to the same degree for all test cases. RH variation influences the resuspension rate of quartz and dust mite particles, while not affecting cat fur and dog fur resuspension rates. The difference between the test cases where RH variation was influential or not is particle hydrophilicity property. Quartz and dust mite particles are hydrophilic, while cat fur and dog fur particles are hydrophobic. Increase in humidity causes a decrease in particle resuspension only for hydrophilic particles via a capillary condensation film adhesion layer forming between the particle and reservoir surfaces (Qian et al., 2014). The water film decreases the resuspension of hydrophilic particles by increasing the adhesion of the particle to the reservoir surface and also by decreasing the potential for electrostatic field strength.

Amongst the test cases with hydrophilic particles, RH variation seems to be more influential on the resuspension of particles from linoleum surfaces than for carpets. Increase in RH reduces the resuspension rate of hydrophilic particles from linoleum further than carpet. This can be due to the fact that carpet fibers absorb part of the moisture content, leaving less moisture to form the water film around the particles. The other observed impact of substrates on the resuspension is higher resuspension from carpet surface when other conditions and factors are kept the same. The higher resuspension rate from the carpet can be explained by the lower adhesion force between the carpet surface and particles, as compared with that of the linoleum surface.

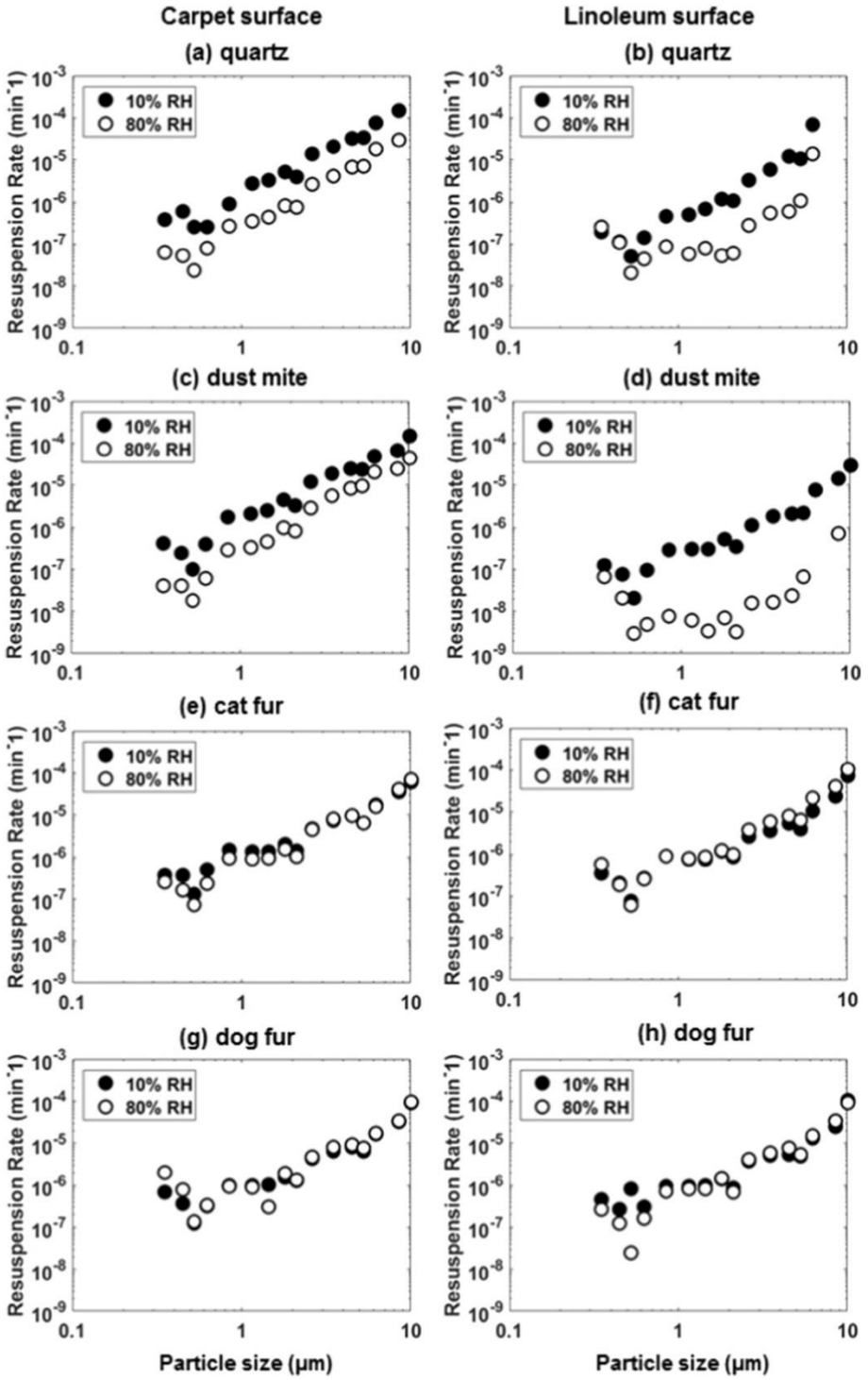

Figure 5-1. Size-resolved resuspension rates of four types of particles (quartz: a–b; dust mite: c–d; cat fur: e–f; dog fur: g–h) under 10% and 80% relative humidity levels for carpet (a, c, e, g) and linoleum (b, d, f, h) surfaces. The average swirl velocity was 1.5 m/s with a dust loading of the substrate sample of 3 g/m^2.

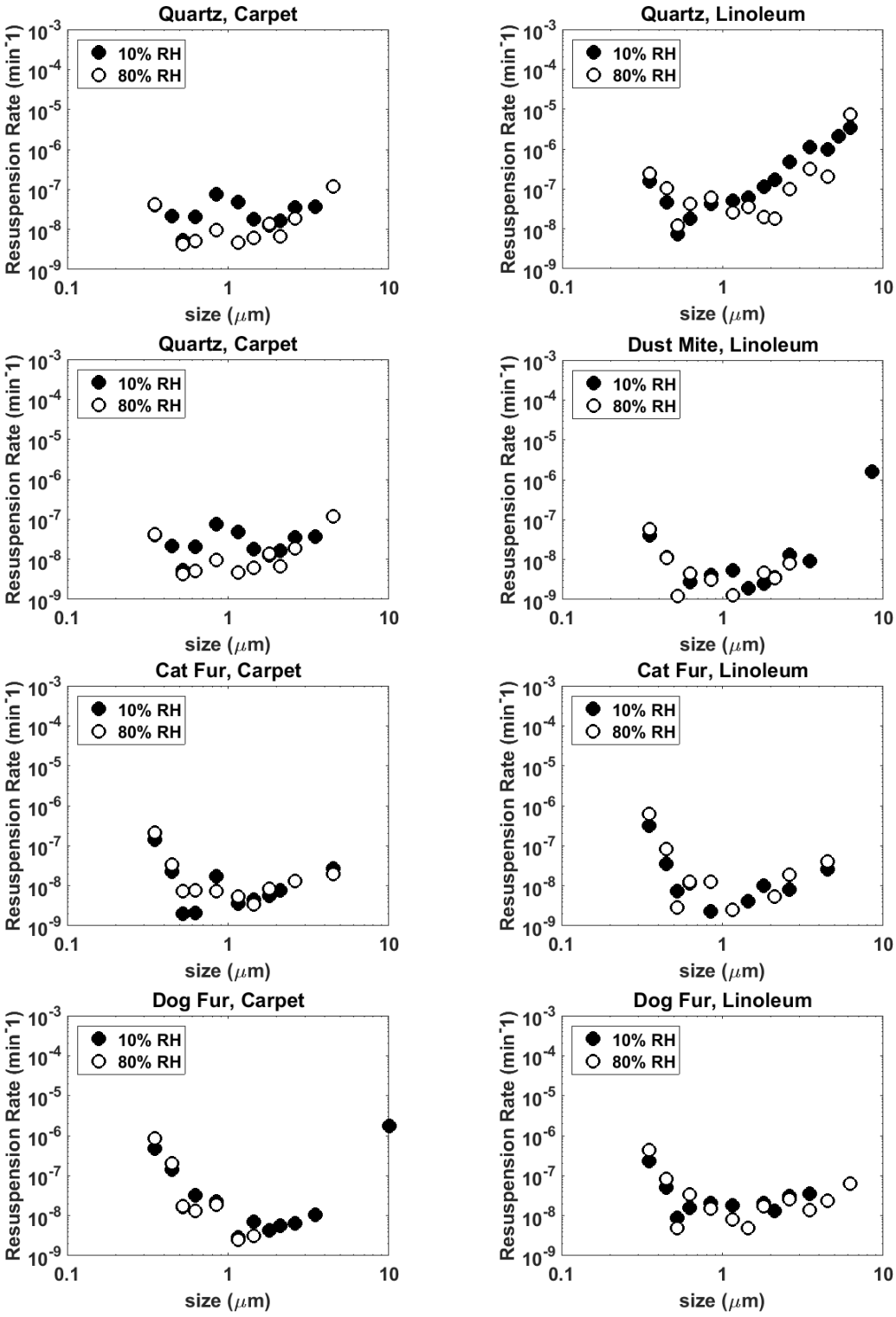

Figure 5-2. Size-resolved resuspension rates of four types of particles (quartz, dust mite, cat fur, and dog fur) under 10% and 80% relative humidity levels for carpet and linoleum surfaces. The average swirl velocity was 0.3 m/s with a dust loading of the substrate sample of 3 g/m^2.

Comparing the results of the test cases with 1.5 m/s air swirl velocity (Figure 5-1) and those with 0.3 m/s air swirl velocity (Figure 5-2) shows the impact of the air swirl velocity and how it intertwines with other factors. At the higher air swirl velocity, resuspension rate at the larger size range -where drag force is dominant- is increased within several orders of magnitude. Whereas, the resuspension rate at the lower size range -where Brownian diffusion is dominant- doesn't seem to be much affected. Also, at the lower air swirl velocity of 0.3 m/s, the effect of RH variation influence on resuspension rate is not as significant as the higher air swirl velocity of 1.5 m/s.

5.1.2. Resuspension rate from duct surface

Figure 5-3 shows the resuspension rate of bacterial spore (*Bacillus thuringiensis*) particles from the duct surface sample made of galvanized sheet metal. In all presented test cases, the substrate is subjected to vibration representing vibration forces present in mechanical ventilation ducts, while the air swirl velocity applied varied from 0 to 2.5 m/s amongst test cases.

Similar to resuspension of particles from the floor surface, the resuspension of particles from the duct surface is a function of particle size. Resuspension rate increases with particle size due to the increase in drag force, until it reaches a point where, with further increase in particle size, the weight force surpasses the drag force.

When the deposited particles are subjected to vibration and laminar flow fields alone (air swirl velocity of 0 m/s), the resuspension rate is relatively low. By adding even a low air swirl velocity of 0.3 m/s, a clear rise in resuspension rate is observed. With further increase of air swirl velocity, the resuspension rate increases. However, the degree of increase from 0 to 0.3 m/s is significantly higher than the rest of step increases in air swirl velocity.

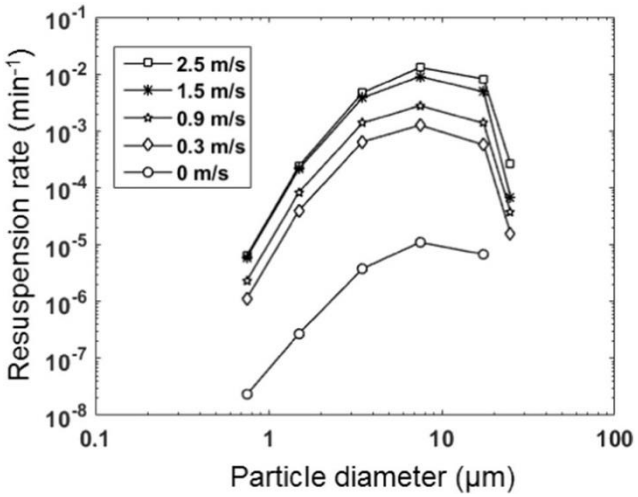

Figure 5-3. Resuspension rates of *Bacillus thuringiensis* spore particles from a galvanized sheet metal duct surface observed at varying air swirl velocities between 0 and 2.5 m/s.

5.2. Research Objective II: performance evaluation of low-cost sensors

As shown in the time-series profile (Figure 5-4), number concentration measurements of the tested low-cost sensors follow the general pattern of the reference sensors measurements. However, the reported particle concentration by the low-cost sensors differs from the reference sensor with varying degrees amongst the tested sensors. While OPC N2 and IC Sentinel are in closer agreement with the reference sensor, Speck and Dylos underestimate the particle concentration by several orders of magnitude. The discrepancies between the reference and low-cost sensor measurements indicate the presence of fixed and/or proportional biases in the low-cost sensors. Besides, the varying decay rates exhibited by the tested sensors with respect to concentration denotes different rates of proportional and fixed biases within different concentration ranges.

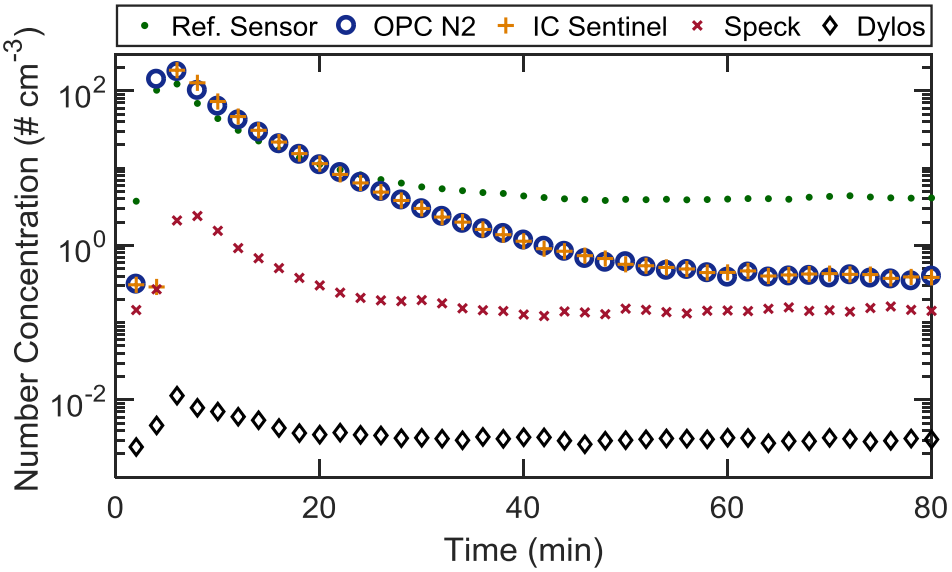

Figure 5-4. Time-series profile of the 2-minute-averaged particle number concentration of tested particles smaller than 2.5 µm measured by low-cost sensors as well as reference sensor throughout one test duration. Each test runs for 2.5 hours which consists of three phases; 1) background level (minutes 0-5), 2) particle injection (minutes 5-7), and 3) particle concentration decay (minutes 7-150). All test cases with different particle types and sizes had similar temporal concentration profile trends. This figure presents the test case results with the polydisperse particle of dust mite.

Testing the low-cost sensors with different particles showed that the linearity of low-cost sensor response with respect to the reference sensor is strongly influenced by particle number concentration. In general, tested low-cost sensors showed non-linear responses in lower concentration ranges and linear responses in higher concentration ranges. The particle type (refractive index) and size also affected the linearity of sensors response. Comparing biological and non-biological test cases revealed a marked difference between the response of low-cost sensors to the non-biological (Figure 5-5-a) and biological particles (Figure 5-5-b). Sensor responses to bioaerosols seem to converge to one linear line as concentration increases. The convergence of responses to biological particles occurs in the concentration range of above ~ 5/cm^3, while such convergence occurs at a higher concentration for non-biological particles.

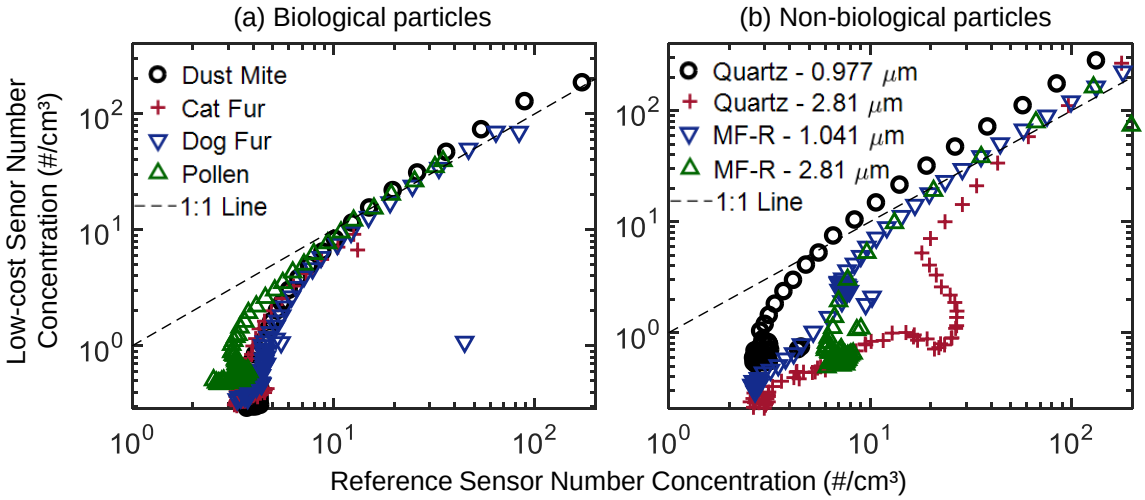

Figure 5-5. Response of IC sentinel sensor under exposure to non-biological (a) and biological (b) aerosols with respect to the reference sensor.

Analysis of the low-cost sensor measurement versus the reference sensor revealed a clear distinction between their linear relationship in low and high concentrations. Figure 5-6-a shows the response of the IC Sentinel versus the reference sensor that varies with the tested aerosol. The results suggest that low-cost sensors have different linear relationships, PB and FB depending on the particle type and concentration. Nevertheless, the linearity of response of these sensors in the high concentration range (Figure 5-6-b) reflects that correcting the observed biases using the developed linear calibration curves could increase the accuracy of the low-cost sensors.

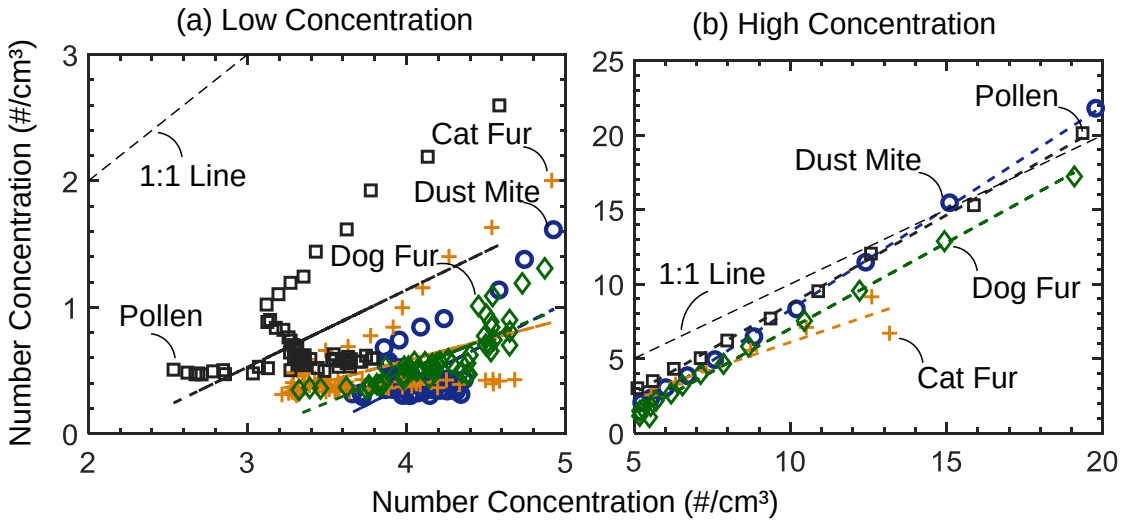

Figure 5-6. Particle number concentrations measured by IC Sentinel sensors versus those of the reference sensor under exposure to varying concentration levels of different bioaerosols. Subplot (a) represents the low number concentration range (0-5/cm^3) within which low-cost sensors don't show a linear response in lower concentration levels (a, c, e, and g). Subplots in the right column represent the concentration range where all tested sensors demonstrate a linear response (b, d, f, and h). The particle number concentration of 5 #/cm^3 seems to be the cut-off point of linearity that can be applied to all tested sensors for all tested bioaerosols. OPC N2 did not record data during dog fur test.

Figure 5-7 shows the distribution of linear regression analysis results of all the low-cost tested sensors under exposure to common indoor bioaerosols. The slope and intercept show the proportional and fixed biases in the tested sensors. According to the linear regression result, OPC N2 and IC Sentinel demonstrate a lower proportional bias, as they are closer to 1, whilst Speck and Dylos displayed higher proportional biases. Combining PB and FB reveals whether the sensor underestimates or overestimates the PM concentration. For the OPC N2 and IC sentinel sensors, the slope is above 1 and the intercept is below 0. Therefore, it can be concluded that at low concentrations they underestimate, whereas, at higher concentrations, they overestimate the PM concentration. For Speck and Dylos sensors, the intercept is negative and the slope is below 1, suggesting that they underestimate the PM concentration.

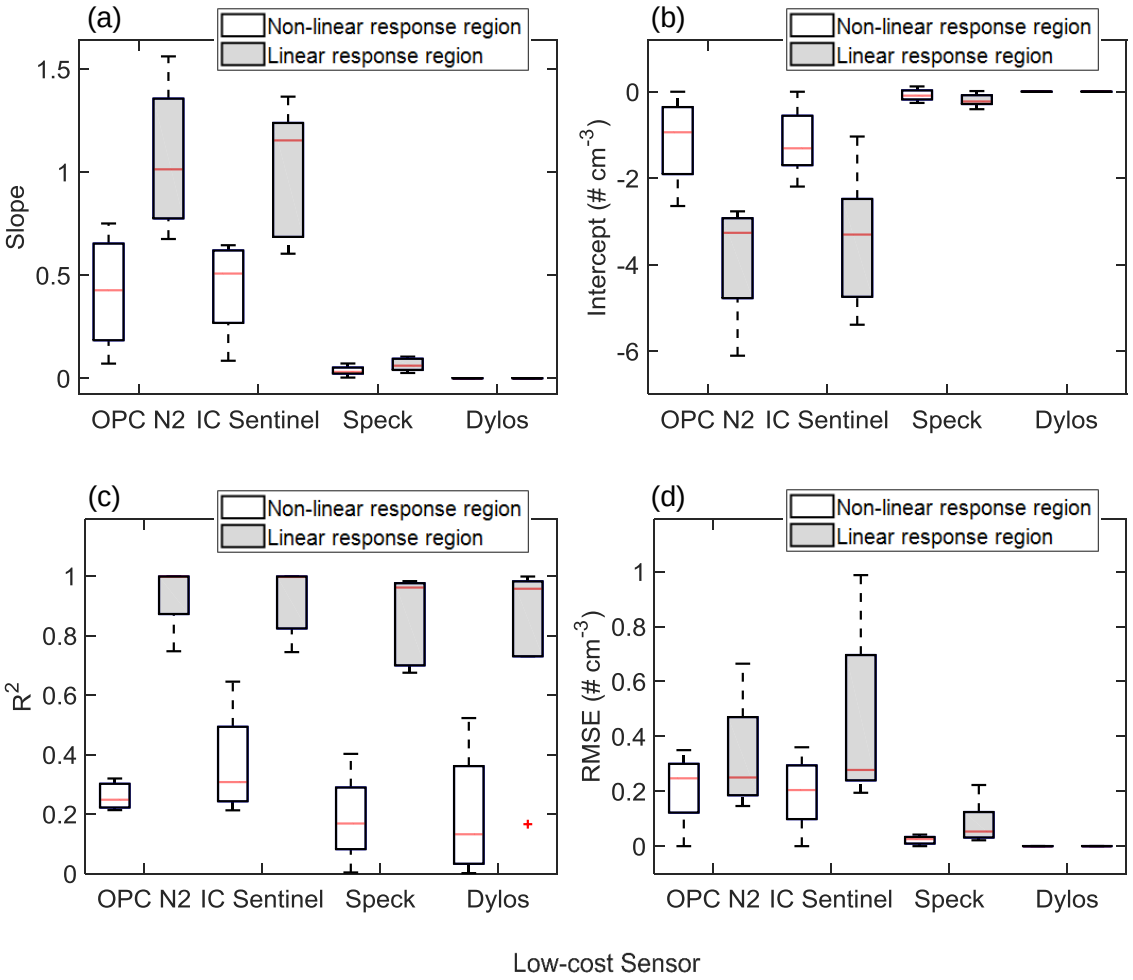

Figure 5-7. Distribution of linear regression analysis results of low-cost sensors with respect to the reference sensor under exposure to low and high concentration levels of various common indoor bioaerosols. (a): slope (proportional bias), (b): intercept (proportional bias), (c) R^2 (linearity), and (d): RMSE (calibration precision).

Despite the presence of systematic biases in the tested low-cost sensors, the high linearity (R^2, Figure 5-7-c) of their response at a high concentration range (above 5/cm^3) signifies the possibility of using developed linear calibration curves to correct the measurement biases with precision rates represented by RMSE values (Figure 5-7-d).

Further details about the tested low-cost sensor responses in different test cases, analysis of the results in the context of previous literature findings, and linear regression coefficients estimates for calibration curves are provided in Appendix B.

5.3. Research Objective III: comparison of aerodynamic and optical sensing

Figure 5-8 shows the time-series of the normalized particle number concentration profile of 2.81 µm particles simultaneously measured by APS and OPC throughout one test duration. It can be seen that OPC measures a higher number concentration compared to APS at all concentrations during the decay test. However, the gap between the two sensors' measurements widens at lower concentrations. The measurements presented in Figure 5-8 represent the total number concentration measured by the two sensors across all their size bins. However, in PM exposure studies and monitoring applications, measurement of particles in specific size fractions (e.g. PM10 or PM2.5) is pursued.

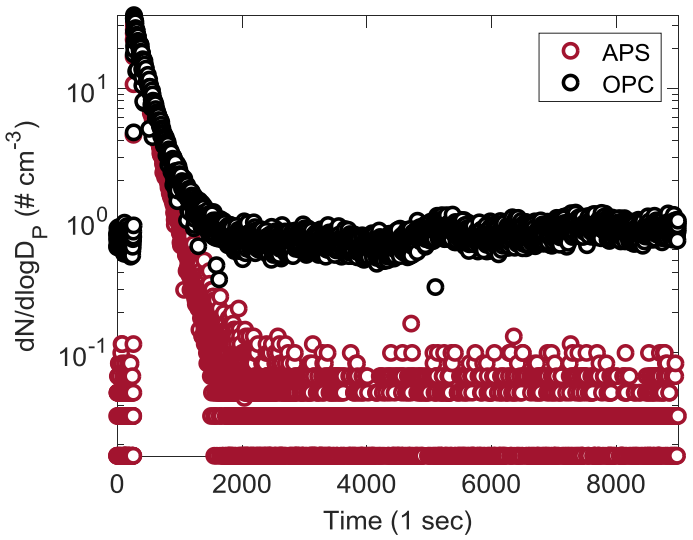

Figure 5-8. Time-series profile of the total normalized particle number concentration of tested particles measured by APS and OPC sensors across all of their size bins throughout one test duration. Each test runs for 2.5 hours which consists of three phases; 1) background level (minutes 0-5), 2) particle injection (minutes 5-7), and 3) particle concentration decay (minutes 7-150). All test cases with different particle types and sizes had similar temporal concentration profile trends. This figure presents the test case results with the monodisperse particle of MF-R in 2.81 µm.

Figure 5-9 shows the normalized particle number concentration of the APS and OPC sensors for the same test case presented in Figure 5-8, across various size fractions. OPC has a higher number concentration measurements for particles bigger than 0.5 µm (Figure 5-9-a) as well as particles bigger than 1 µm (Figure 5-9-b), but to a less degree. Whereas, for particles larger than 3 µm (Figure 5-9-c) and 5 µm (Figure 5-9-d) size fractions, APS number concentration measurements surpass those of OPC.

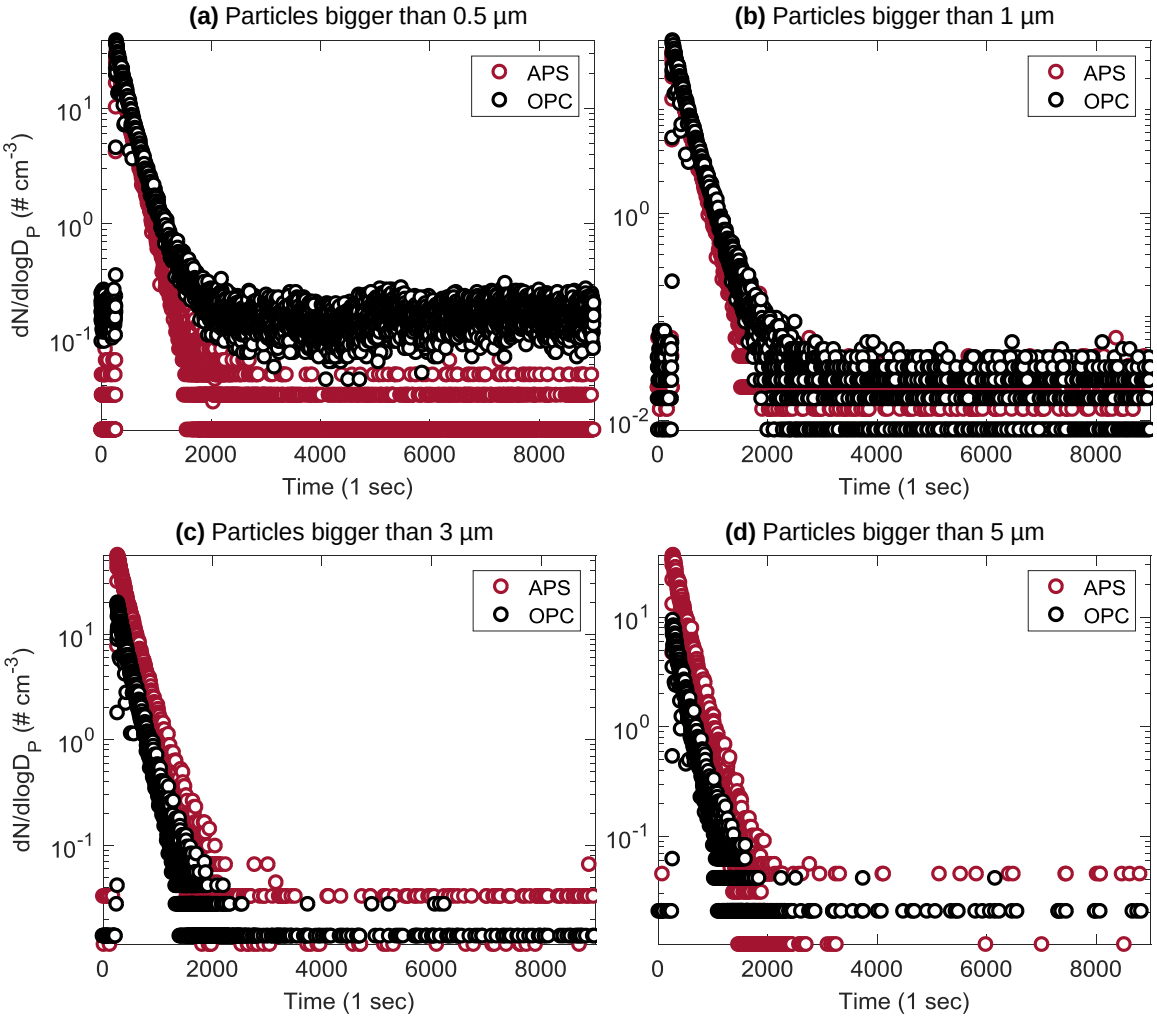

Figure 5-9. The normalized particle number concentration time-series profile measured by APS and OPC across various particle size fractions.

The distribution of the normalized number counts proportion of OPC to APS across each of the discussed size fractions (presented in Figure 5-9) is shown in Figure 5-10. The variation in the number counts proportion across different size bins implies possible size-dependency of the relationship between APS and OPC measurements. This effect of size particle size range intended for monitoring on the calibration is more clearly disclosed and quantified by comparing the linear regression analysis results between the two sensors measurement across different size ranges. An example of such dissimilarity is presented in Figure 5-11. While the OPC measurements of the total counted particles (Figure 5-11-a) follow a linear line close to the 1:1 line with respect to APS measurements, for particles smaller than 2.5 (representing PM2.5) it deviates significantly from the 1:1 line.

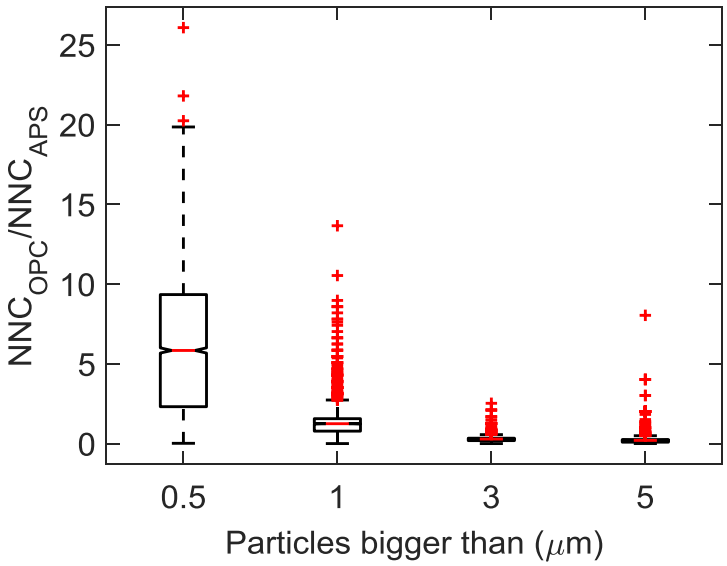

Figure 5-10. OPC to APS measurement proportion of normalized number concentration distribution across different size bins.

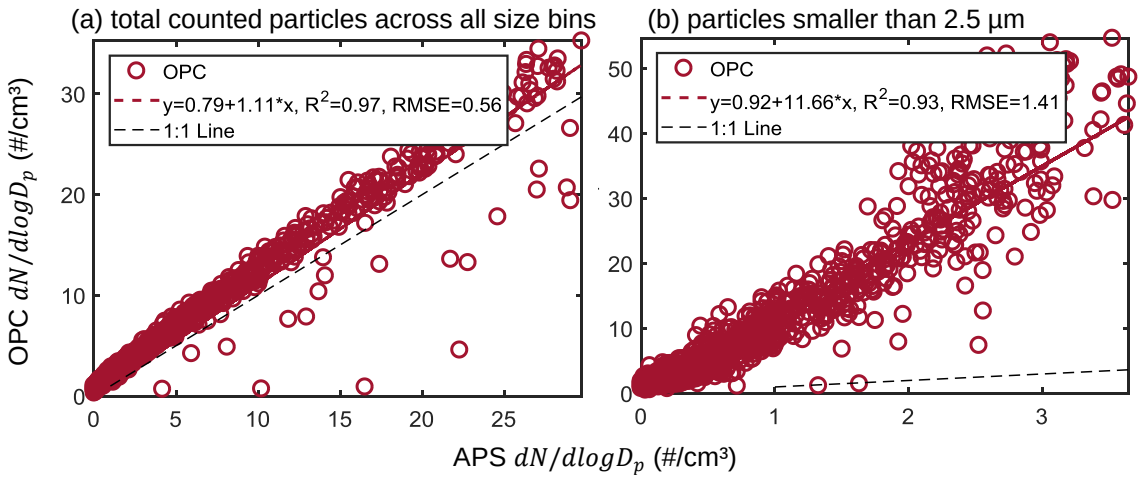

Figure 5-11. Linear relationship between APS and OPC measurements of 2.81 µm MF-R particles.

The linear regression analysis results of OPC versus APS measurements across three different size fractions for all sixteen tested particles are provided in Table 3 of Appendix C. Using the provided linear regression coefficients estimates, corresponding calibration curves can be developed. Also, size-resolved normalized number concentration profiles measured by APS and OPC for various tested particles are discussed in Appendix C.

.

Chapter 6

Conclusions

This dissertation studied the resuspension and sensing of indoor aerosols. The resuspension of particles from indoor surfaces under various RH and air swirl velocities typical of indoor ambient conditions was examined in a simulated chamber experiment. Floor (carpet and linoleum) and duct (galvanized sheet metal) surfaces as two surfaces where aerosols and allergen carrier particles deposit and act as reservoirs for future resuspension were used as substrate samples. The tested particles were dust mite, cat fur, dog fur, bacterial spores (*Bacillus thuringiensis*), and quartz. Study results showed that particle resuspension rate is a strong function of particle size. Three distinct patterns of resuspension rate variation with an increase in particle size were observed in the conducted experiment results. For small particles (~ < 0.5 µm) where Brownian diffusion is dominant in particle motion, the particle resuspension rate decreases with an increase in particle size. For particles in 0.5 µm to ~ 10 µm, the particle resuspension rate increases with particle size. This pattern is explained by the dominance of drag force in this region. The increase in resuspension rate with particle size continues until the drag force equals the weight force. Further increase in particle size reduces the resuspension rate as particle weight surpasses the lifting forces.

Experimental results also confirmed the effect of RH on particle resuspension. Relative humidity variation significantly influences the particle resuspension rate. Increasing relative humidity reduces the resuspension rate of hydrophilic particles, as hydrophilic particles readily adsorb the moisture, which forms a capillary condensation layer between the particle and substrate. The practical implication of this finding is that resuspension, and therefore the transport of hydrophilic allergen carrier particles, such as dust mites, can be controlled by changing the

relative humidity in indoor spaces. In spaces (such as healthcare facilities and buildings with occupants prone to asthma) where transport and spread of allergen carriers is a concern, increasing the relative humidity can be used as a control strategy. Such a control strategy could be applied in HVAC operating modes such as winter season where it fits the indoor air quality and comfort design boundaries. Also, based on these study results, linoleum seems to be a better flooring surface option than carpet in terms of indoor air quality. Resuspension rate and spread of particles from carpet surfaces are higher than with linoleum. Overall, the results of this study showed that if the RH is to be used as a PM transport control strategy, it works more effectively with a linoleum surface than a carpet.

This dissertation also evaluated the performance of low-cost sensors in monitoring indoor bioaerosols in a controlled lab experimental study. Four low-cost optical particle counters were compared and calibrated against a lab-grade sensor of the same type. Results showed that low-cost sensors might under- or overestimate actual particle concentration depending on its type and concentration. Linear relationships between low-cost sensors and the reference sensor occurred in concentrations higher than 5/cm^3, for common indoor bioaerosols tested in this study. This result implies that particle-specific calibration curves can be developed and applied before deploying them in a building.

In field PM exposure monitoring applications, sensors are exposed to a combination of PM, and not to isolated batches of specific particle type and size. Subsequently, although the highest precision would be provided by using particle-specific and size-specific calibration curves, using such calibration curves is not actually practical when it comes to field applications. Experimental results show that bioaerosols draw a fairly similar linear response from the tested sensors in the analyzed linear response region, reflecting the opportunity to use an average linear calibration that would be suitable for all the four analyzed bioaerosols. The findings of this study

show promising results in terms of using linear calibration curves that work well for monitoring common indoor bioaerosols in particle number concentration range of $5/cm^3$ - $20/cm^3$.

The third objective of this dissertation was focused on investigating the relationship between aerodynamic and optical sensing. APS and OPC measurements for sixteen different particles including monodisperse and polydisperse, biological and non-biological particles were tested in a controlled chamber environment. Results showed that the relationship between the two sensors depends on particle type, concentration, and size range being monitored. These findings imply that a generalized conversion equation between the volume-equivalent diameter and aerodynamic diameter does not yield reliable results. Similarly, the calibration curves provided for OPC sensors based on aerodynamic sensors is size fraction specific and cannot be used for other size fractions. Accordingly, empirical linear calibration equations for three size fractions were provided; total counted particles across all size bins of the two sensors, particles smaller than 10 µm, and particles smaller than 2.5 µm.

Appendix A

Paper 1. Resuspension of biological particles from indoor surfaces: effects of humidity and air swirl

(Published in *Science of the Total Environment 583(2017)241–247*)

Graphical Abstract

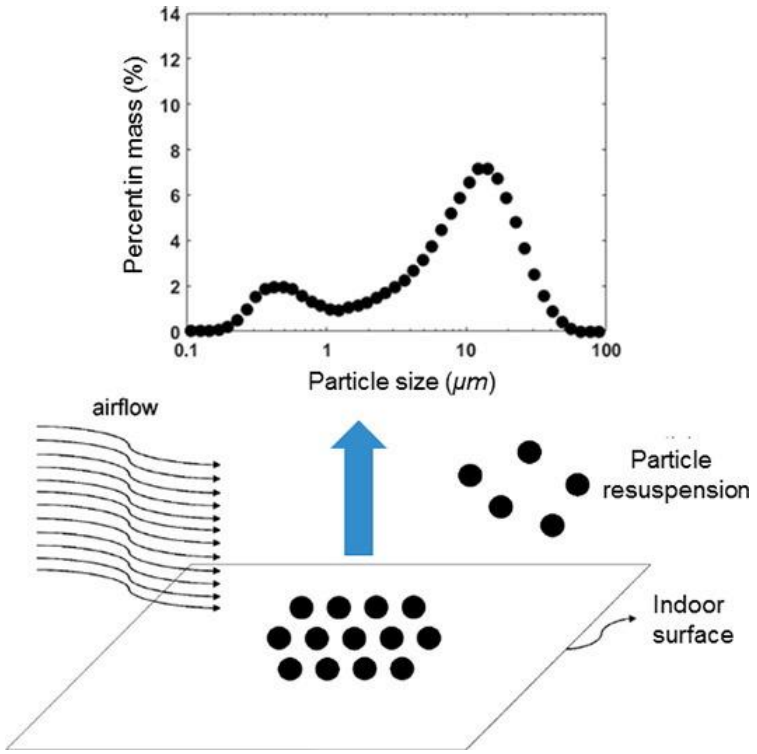

Highlights

- We examine resuspension of biological particles from floor and duct surfaces.
- Resuspension rates of dust mite particles notably vary with humidity level.

- Humidity effect on resuspension of dog fur and cat fur particles is moderate.
- Air swirl near the duct surface substantially affects particle resuspension.

Abstract

Human exposure to airborne particles can lead to adverse health outcomes such as respiratory and allergic symptoms. Understanding the transport mechanism of respirable particles in occupied spaces is a first step towards assessing inhalation exposure. Several studies have contributed to the current knowledge of particle resuspension from indoor surfaces; however, few published studies are available on resuspension of biological particles from indoor surfaces. The objective of this study is to investigate the impacts of humidity and air swirl on resuspension of biological particles from floor and duct surfaces. Controlled laboratory experiments were conducted under varying degrees of humidity and airflow conditions. Resuspension rates of five types of particles (quartz, dust mite, cat fur, dog fur, and bacterial spore-*Bacillus thuringiensis* as an anthrax simulant) were determined for two types of floor surface (carpet and linoleum) and a duct surface (galvanized sheet metal). The results show that the particle property of being hydrophilic or hydrophobic plays an important role in particle resuspension rate. Resuspension rates of hydrophilic dust mite particles increase up to two orders of magnitude as relative humidity (RH) decreased from 80% to 10% at 25 °C. However, resuspension rates of cat fur and dog fur particles that are hydrophobic are within the measurement error range (± 15%) over 10–80% RH. With regard to resuspension of bacterial spores (*Bacillus thuringiensis*) from a duct surface, the resuspension rates are substantially affected by air swirl velocity and particle size. However, no discernible increase in particle resuspension was observed with duct vibration.

Keywords

Particle resuspension; Indoor allergens; Dust mite; Cat fur; Dog fur; Anthrax.

A.1. Introduction

Human exposure to airborne particulate matter (PM) is closely linked to adverse health effects (Clancy et al., 2002; Dockery et al., 1993; Pope III and Dockery, 2006). As people spend most of their time indoors, prolonged exposure to indoor PM can lead to respiratory and allergic symptoms. Indoor particles that contain biologically-derived protein allergens can trigger initiation of allergy responses such as wheezing, red and itching eyes, and nasal dripping among susceptible individuals (Bardana Jr, 2001; Barnes et al., 2001; Ormstad, 2000; Raja et al., 2010; Roberts et al., 1999). Control of infectious biological particles is also one of the main concerns related to patient safety in healthcare facilities (Siegel et al., 2007). To accurately estimate breathing zone concentration and indoor exposure to biological particles, it is crucial to understand particle transport mechanisms indoors.

Transport of indoor particles involves deposition and resuspension processes. Particles are either directly generated from indoor sources or introduced from outdoors via ventilation and infiltration (Nazaroff, 2016). These particles can deposit on indoor surfaces such as floors, ventilation ducts, and filters due to gravitational settling, diffusion, thermophoretic, electrostatic, and turbulent transport. The particles deposited on the floor can resuspend by occupant activities such as walking and vacuuming (Ferro et al., 2004; Thatcher and Layton, 1995). Some portion of particles on duct surfaces can be transported into the air by turbulent airflow and duct vibration (Sippola and Nazaroff, 2002). Understanding particle resuspension mechanisms in occupied

spaces and heating, ventilation, and air conditioning (HVAC) system is prerequisite to control of indoor bioaerosols.

Previous studies have identified humidity to be an influential factor in particle resuspension (Sehmel, 1980). Experimental data have shown that particle to surface adhesion force becomes greater as relative humidity (RH) and particle size increase (Corn, 1961a, 1961b). However, the results of experimental studies on the effects of humidity on particle resuspension have not been very clear. Some of the previous investigations show conflicting results, indicating that resuspension may increase or decrease with indoor humidity. Early resuspension studies such as (Corn, 1961a, 1961b) and (Corn and Stein, 1965) showed that adhesion forces rapidly increase with RH under conditions of RH > 30%. Rosati et al. (2008) revealed particle resuspension rate both increasing and decreasing with humidity depending on the surface material composition. Qian and Ferro (2008) reported that walking-induced resuspension rate of Arizona Test Dust (ATD) in the size range of 0.1–10 μm was not significantly affected by variation of RH in the range of 30–50%. However, they suggested that the effect of RH should be investigated in a wider range, considering both organic and inorganic particles. A recent study by Tian et al. (2014) showed varied effects of RH (40% vs. 70%) on particle resuspension depending on the flooring type. Taken together, humidity effects on particle resuspension seem to vary with particle type and surface; however, only few quantitative data are available to describe particle resuspension rate as a function of particle type and indoor surface characteristics.

Field studies have shown that occupant activities significantly affect particle resuspension from indoor surfaces (Clayton et al., 1992; Ferro et al., 2004; Weekly et al., 2013). Even light occupant activities such as walking can increase the mass concentration of airborne supermicron particles by 100% (Thatcher and Layton, 1995). Several laboratory-based studies have characterized particle resuspension considering various indoor activities (Luoma and Batterman, 2001; Cheng et al., 2010; Qian et al., 2014). Gomes et al. (2007) investigated particle

resuspension from a floor surface by mimicking walking-induced swirl air velocities and floor vibration in a controlled chamber. Their results revealed that air swirl created by walking has discernable impact on the particle resuspension rate, while walking-induced floor vibration has negligible effect. Special emphasis has been placed on particle dynamics in building air distribution systems, especially for resuspension of chemical and biological agents such as Bacillus anthracis (anthrax) from duct surfaces (Settles, 2006). Mukai et al. (2009) measured the relative resuspension of 1–20 μm particles from three indoor surface materials including a galvanized sheet metal duct at five bulk air velocity magnitudes (5 to 25 m/s). The study results show that bulk air velocity, turbulence intensity, and particle size have measurable effects on particle resuspension. Ibrahim et al. (2003) conducted an experimental study on resuspension of Lycopodium spore particles under turbulent airflows. They found that among the controlled variables, adhesion force and particle size are most influential on the airflow threshold velocity for particle resuspension. However, the impacts of turbulent air swirl and duct vibration on the resuspension of bacterial spores from duct surfaces have not been closely investigated.

Based on the background described above, the first objective of the present study is to examine the effect of humidity on particle resuspension considering four types of organic/inorganic particles (quartz, dust mite, dog fur, and cat fur) and two common indoor surfaces (carpet and linoleum). A secondary objective is to investigate the effects of turbulent air swirl and duct vibration on the resuspension of bacterial spores (*Bacillus thuringiensis* as an anthrax simulant) from a duct surface. The size-resolved particle resuspension rates studied herein can provide a basis for intervention and filtration design for control of biological particles in building environmental systems.

A.2. Methods

Two sets of experiments were performed. First, particle resuspension from carpet and linoleum surfaces was examined under varied humidity conditions. Second, experiments simulated particle resuspension from a duct under a range of air swirl velocities. This section describes: 1) particle sample preparation; 2) experimental set-up; and 3) estimation of particle resuspension rates and uncertainty analysis.

A.2.1. Particle sample preparation

We tested five types of particles: 1) crushed quartz, 2) dust mite, 3) dog fur, 4) cat fur, and 5) bacterial spore-*Bacillus thuringiensis*. Crushed quartz particles (10 bt 4339, Particle Technology Limited, UK) were used as a reference against which to evaluate resuspension of biological particles. Dust mite particle specimens were prepared with spent mite culture powder (Indoor Biotechnologies Inc., Charlottesville, VA, USA). Dog fur and cat fur particles were prepared using respective pet animal fur collected from local pet grooming companies. Raw fur was ball milled and sieved through a 325 mesh to produce sub-micron sized powder. Dust mite particles are carriers of Der p 1 and Der f 1 allergens. Dog fur and cat fur particles are carriers of Can f 1 and Fel d1 allergens, respectively. In addition, *Bacillus thuringiensis* spores were provided by the U.S. Army Center for Health Promotion and Preventive Medicine and prepared as an anthrax simulant. The volumetric mass density of particles was determined based on the Archimedes' principle. The net resultant force from particle's weight and water drag force as the particle was sinking into water was calculated. The particle densities were estimated as 2650 kg/m3 for quartz, 1140 kg/m3 for dust mite, and 1000 kg/m3 for dog fur, cat fur, and *Bacillus thuringiensis* spore. For fibrous dust samples of cat fur and dog fur, a fiber was immersed into

water which resulted in no vertical movement; therefore, particle density was estimated to be 1000 kg/m3. Two floor substrates were purchased from a retail store and tested as the common flooring surface types found in buildings; carpet and linoleum. The carpet was a low loop-pile carpet for residential and commercial uses. The carpet consisted of nylon, styrene-butadiene-rubber latex adhesive with calcium carbonate filler, and PVC backing with a face weight of 830 (g/m^2) and an average thickness of 5.0 mm. The linoleum surface consisted of conductive carbon, oxidized drying oils, and coloring pigments. The conductive backing provided a static resistant flooring having a controlled electrical resistance. The linoleum sample had a thickness of 2.0 mm with unknown face weight. The substrate used for the duct material was a 23 gauge (0.78-mm-thick) galvanized sheet steel with a face weight of 6.10 kg/m^3. The size of all three substrate samples was 9 × 9 cm.

Surface-seeded particle samples were prepared by depositing aerosolized particles onto a substrate surface using the following steps: 1) substrate samples (floor or duct material plates) were placed in the particle dispersion chamber; 2) a uniform dust cloud was created in the chamber by injecting the particles at the center of the chamber via a bottom pulse injection delivery system. While injecting the particles, four mixing fans were running at four floor-corners of the dispersion chamber to ensure a well-mixed airflow inside the chamber; and 3) the particle seeding time period was adjusted to provide sufficient particle concentration on the substrate with a mass density target of 1.5 g/m^2 for each particle sample. In general, about 14 h of settling time was given to each sample after particle injection to have proper settling of particles on the substrate surface.

To confirm whether the surface-seeded particle samples mimicked the particle size distribution of typical indoor particles with a significant proportion in the size range of 1–20 μm (Montoya and Hildemann, 2005; Gomes et al., 2007; Raja et al., 2010), particle size distributions were characterized using Wet and Dry Laser Diffraction (Mastersizer S, Malvern, UK). For

quartz particles (reference particles), 99% of particles were distributed over the size range from 1 to 20 μm, while 30–70% of allergen-containing and *Bacillus thuringiensis* spore particles were distributed over the same size range. Detailed size distributions of the surface-seeded particles are shown in Figure A5 (Supplementary Information).

A.2.2. Experimental set-up

Resuspension of the settled particles was examined in a bench-scale chamber under a range of relative humidity (RH): 10%, 45%, and 80% RH at 25 °C. The particle samples on the carpet and linoleum floor surfaces were tested in the resuspension chamber (40 × 20 × 20 cm). Figure A1a shows the schematic diagram of the resuspension chamber system. Particle-free air was supplied into the resuspension chamber at a volume flow rate of 32.4 L/min that resulted in a laminar flow with a bulk air velocity of 0.0135 m/s. Six 45° inclined copper tubes delivered the burst air and created the air swirl near the substrate surface. Figure A1b shows the schematic diagram of these air swirl jet tubes. Figure A1c shows the positions of the air jet tubes over the substrate sample and nine locations of air velocity measurements. The air swirl velocity imposed on the substrate surface simulated vortices induced at the edges of the foot during human walking. To verify the achievement of desired air swirl velocity on the substrate sample, hot wire anemometer (510e/127MS, Solomat-GrayWolf, Shelton, CT) was used to measure the air swirl velocity above the 9 × 9 cm substrate sample and at the exit of the each jet tube. With an airflow rate of 20 L/min in the jet tubes, the average air velocity at the exit of jet tubes ranged between 3.90 and 4.10 m/s that yield Reynolds number in the range of 1060–1460. Airflow velocities measured at the nine locations 2.5 mm above the test surface (see Figure A1c) ranged from 0.22 to 2.50 m/s with an average of 1.12 m/s. This swirl velocity range agrees with the walking-induced air swirls near the floor observed by Gomes (2004) in which horizontal air swirl velocity

peaked at 1.5–2.0 m/s. Figure A6 and Tables A1–A2 (Supplementary Information) provide more detailed information of air velocity measurements.

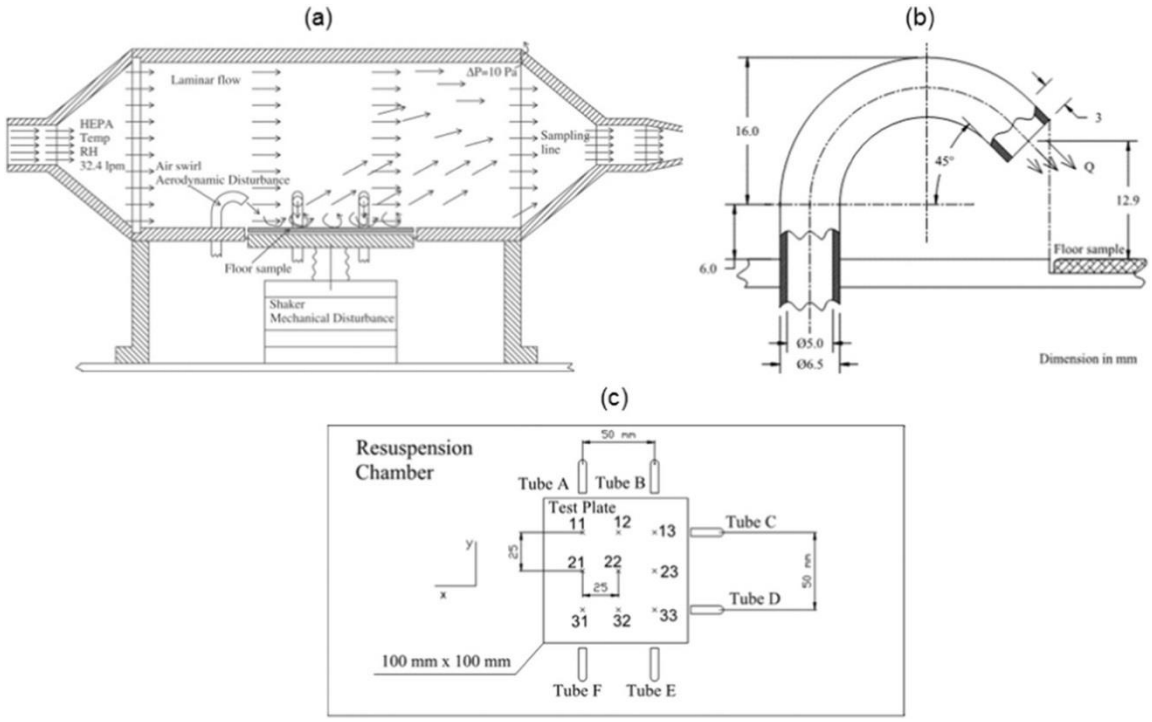

Figure A1. Schematic diagram of experiment set-up: (a) resuspension chamber system; (b) air swirl jet tubes (Gomes, 2007); (c) top view of the air velocity measurements at nine locations 2.5 mm above the test surface.

An environmental chamber (226 L, SM-8-3800, Thermotron, MI-USA) was used to condition air temperature and relative humidity (RH). The environmental chamber has the capability of conditioning the air temperature in the range from − 70 to 180 °C range with a RH in 35–97% range. For 10% RH test case where RH is below the range provided by environmental chamber, an extra step of drying the air was taken by adding a parallel desiccant line after the environmental chamber. First, the environmental chamber was set to provide airflow with 40% RH. Then 7.6 L/min of the total 32.4 L/min conditioned airflow was sent through the desiccant line that reduced the RH to < 2%. The final mixed air RH was at 10%. It should be noted that the portion of the supply airflow that required extra dehumidification for the final mixed air to be

exactly at 10% RH was empirically tested and verified, and therefore is slightly different than the theoretically calculated mixing ratio. The schematic diagram of the humidity control of the resuspension chamber is shown in Figure A7 (Supplementary information). The conditioned air was pumped into the resuspension chamber. The resuspension chamber's interior was thoroughly cleaned and particle-free air was supplied to flush out any remaining particles, as well as to pre-condition the surface sample over 12 h.

A Wilcoxon Research F4 electromagnetic mechanical chamber shaker was used to transmit the mechanical vibration to the substrate sample in the resuspension chamber. Figure A2a shows the vibration signal that simulates occupants walking (Gomes et al., 2007). At each experiment, 16-sec floor mechanical vibration signal were repeatedly applied to simulate walking-induced floor vibration. At each relative humidity level, the number of particles resuspended from the floor surface sample caused by the air swirl was measured by two optical particle counters (Climet, CA, USA and Semtech PM300, Sensors Inc., MI, USA) that covered the lower and higher end of the particle size spectrum of interest (0.3–25 μm) in this study.

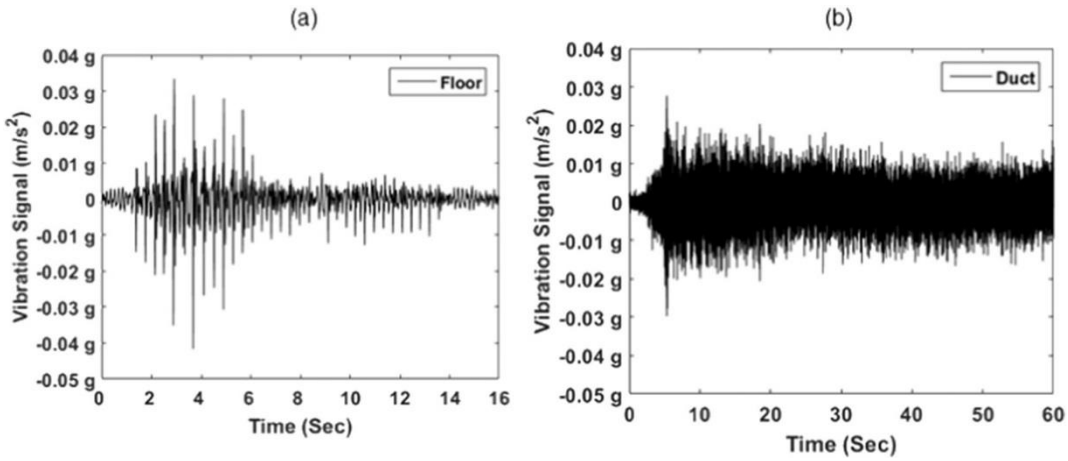

Figure A2. Vibration wave forms applied to the resuspension chamber via a mechanical shaker: (a) floor vibration; (b) duct vibration.

Along with the humidity effect on particle resuspension, the second set of measurements were performed to determine the impacts of air swirl and duct vibration on resuspension of bacterial spores from the duct surface. Multiple tests were conducted at imposed air swirl velocities of 0, 0.3, 0.9, 1.5, and 2.5 m/s that represent varying degrees of turbulence in a duct system (Salimifard et al., 2015). By adjusting the airflow rates provided through the jet tubes, specific air swirl velocities above the samples surface were simulated. Note that this simplified approach assumes turbulence phenomena lumped into a "net" swirl velocity and the results show general impacts of air swirl velocity on the particle resuspension in a duct system. Given the variability in duct airflow across buildings, the air swirl velocity simulated in this study does not represent time- and space-dependent turbulent flow field in a specific duct system.

Vibration waveforms representing duct vibrations in buildings were applied to the substrate sample using the chamber shaker. The vibration waveforms were acquired based on measurements of low-mass, broad band accelerometers attached to a surface of a full-scale test duct. Figure A2b shows 60-sec vibration waveforms created for the duct surface. While the amplitudes of the floor and duct vibration waveforms are about the same order, duct vibration spectrum covers a much wider range of frequencies than floor vibration spectrum.

A.2.3. Estimation of resuspension rate and uncertainty analysis

Using the time- and size-resolved particle concentrations collected from the two sets of experiments, particle resuspension rates were calculated using the following equation:

$$RR_d = \frac{G_d}{C_{surface,d}} \qquad \text{(Equation A1)}$$

where, RR_d is resuspension rate for particles of size d (min^{-1}), $C_{surface,d}$ is surface concentration for particles of size d ($\frac{\#}{m^2}$), and G_d is surface removal rate for particles of size d ($\frac{\#}{m^2.min}$), which is defined as follows.

$$G_d = \frac{\int_t Q_{sweep,flow} \cdot C_{air,d}\, dt}{A_{surface} \cdot \left(\frac{1\,min}{60\,s}\right) \cdot \int_t dt} \qquad \text{(Equation A2)}$$

Where, $Q_{sweep,flow}$, flow is the air cross-flow over the floor sample ($\frac{m^3}{s}$), $C_{air,d}$, d is air dust concentration for particles of size d ($\frac{\#}{m^3}$), Asurface is the sample surface area (m^2), and dt is time interval (s).

Uncertainty estimation of particle resuspension rate was obtained by propagating the uncertainties of all input parameters in Equations A1 and A2 (Taylor, 2009). Uncertainty in determining resuspension rate attributed to measurement and device uncertainties was evaluated to be about 15%, based on the airflow measurement error (± 3%), measurement uncertainty of airborne particle concentrations (± 5–10%) and surface concentration measurements (± 10–12%). Detailed uncertainty propagation analyses are presented in the "Uncertainty Analysis" section of Supplementary Information.

A.3. Results & Discussion

A.3.1. Humidity effect on particle resuspension from flooring surfaces

Figures A3a–h shows the size-resolved resuspension rates of quartz, dust mite, cat, and dog fur particles under 10% and 80% relative humidity (RH) at 25 °C observed with two different floor substrates: 1) carpet and 2) linoleum. The simulated air swirl velocity was typical of human

walking that has the peak horizontal velocity 2.5 mm above the surface sample in a range of 1.5–2.0 mm with the swirl diameter of 10–20 cm.

Figures A3a–h suggest that particle size plays a critical role in the resuspension rate across all tested conditions. Although differences exist in resuspension rates by orders of magnitude depending on humidity and the surface type, resuspension rate increases with particle size in the range of 0.5–10 μm. This trend has been observed by several other previous studies (Gomes et al., 2007; Qian and Ferro, 2008; Qian et al., 2014). In such particle size range, detachment of a particle from the surface occurs when the lifting forces are greater than adhesion force. According to adhesion theory, adhesion forces increase with particle size. However, the removal forces, such as vibration-induced and convective drag forces are proportional to the third and second power of the particle size, respectively (Corn, 1961a, 1961b). Therefore, larger particles are easier to resuspend than smaller particles, despite the larger adhesion force between larger particles and surface. For particles < 0.5 μm, Brownian diffusion is the driving force for the particle resuspension (Soltani and Ahmadi, 1995). For this region, as the particle size decreases, Brownian diffusion becomes the dominant force for the particle transport (Hinds, 2012). However, the dip in the resuspension curve around 0.5 μm represents the region where neither Stokes drag force nor Brownian diffusion are large enough to resuspend particles from the surface.

According to Figures A3a–d, resuspension rates of quartz and dust mite particles notably decrease as humidity increases from 10% to 80% RH. With regard to the surface effect, humidity impact is greater for linoleum surface than carpet surface. Unlike quartz and dust mite particles, resuspension rates of cat fur and dog fur particles are moderately affected by humidity change (Figures A3e–h). In these cases, the surface effect is negligible as the differences due to humidity change are mostly within the estimation uncertainty regardless of the surface type.

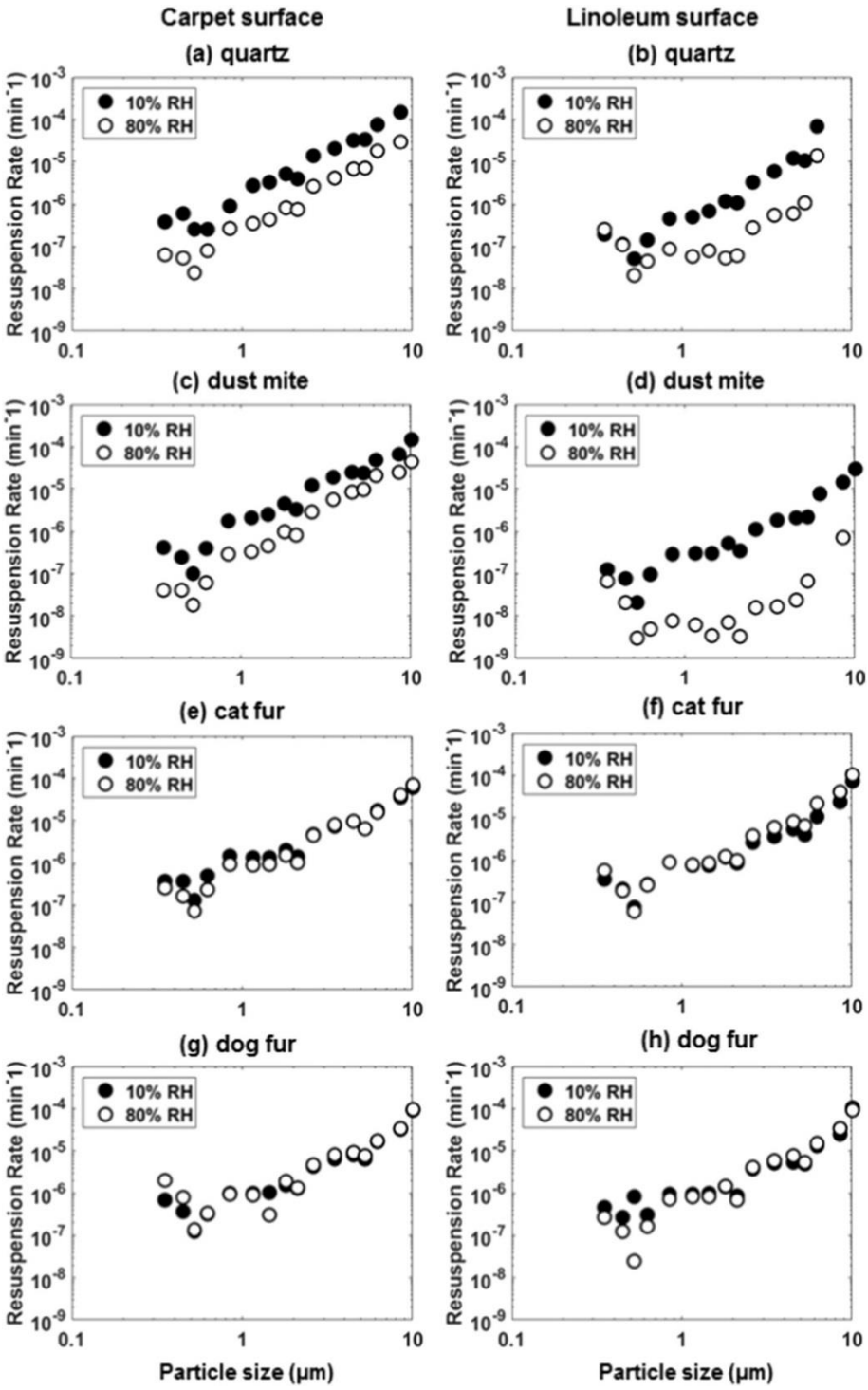

Figure A3. Size-resolved resuspension rates of four types of particles (quartz: a–b; dust mite: c–d; cat fur: e–f; dog fur: g–h) under 10% and 80% relative humidity levels for carpet (a, c, e, g) and linoleum (b, d, f, h) surfaces. The average swirl velocity was 1.5 m/s with a dust loading of the substrate sample of 3 g/m2.

It appears that particle resuspension strongly depends on the particle property of being hydrophilic or hydrophobic. Dust mite and quartz particles are hydrophilic and readily adsorb moisture from the air. Increase in humidity can decrease particle resuspension for hydrophilic particles via a capillary condensation film adhesion layer forming between the particle and reservoir surfaces (Qian et al., 2014). The water film can significantly reduce resuspension of hydrophilic particles by increasing the adhesion of the particle to the reservoir surface and also by decreasing the potential for electrostatic field strength to develop. However, cat fur and dog fur particles are hydrophobic and less sensitive to the indoor humidity variation. Hydrophobic particle surface inhibits the ability of a water film to form, thereby reducing the variability of the resuspension rates caused by humidity and surface type.

For both quartz and dust mite particles, substrate surface seems to have a discernable impact given the orders of magnitude change in the resuspension rate observed with different RH conditions. In general, carpet surface yields higher resuspension rate than linoleum surface at the same humidity level perhaps due to smaller adhesion force on the carpet. However, the impact of humidity appears to be greater for linoleum surface than carpet surface. For example, resuspension rates of dust mite particles increase up to two orders of magnitude for the linoleum surface as RH decreases from 80% to 10%.

The particle resuspension rate ranges between 10^{-9} and 1.5×10^{-4} min^{-1} for all tested particle sizes, surface type, and humidity level. This range is comparable to the results of previous studies in literature. Qian and Ferro (2008) reported based on their full-scale chamber experiment the walking-induced resuspension rates of $1.7\times10^{-7} – 1.7\times10^{-4}$ min^{-1} for carpet and vinyl floor under humidity conditions between 30 and 50% RH. Thatcher and Layton (1995) reported resuspension rates of $1.65\times10^{-8} – 5.6\times10^{-7}$ min^{-1} for a particle size range of 0.3 to 25 μm observed with normal activities of four occupants such as walking and vacuuming. Another study

by Qian et al. (2008) reported resuspension rate as high as 2.3×10^{-6} min^{-1} for house dust from carpet surface due to one occupant walking and sitting in a room.

A.3.2. Particle resuspension from duct surfaces depending on swirl flow velocity

Figure A4 displays size-resolved resuspension rates of *Bacillus thuringiensis* spore particles observed with air swirl velocity magnitude ranging from 0 to 2.5 m/s at a height of 2.5 mm above the duct surface. In the figure, the line graph for 0 m/s swirl velocity presents the baseline particle resuspension rates observed only with duct vibration under a laminar flow regime that has a bulk air speed of 0.011 m/s and Reynolds number of 140. Despite the higher vibration frequencies of the duct surface than floor surface, the resuspension rates due to duct vibration were between 10^{-8} and 5×10^{-6} min^{-1}. This range is similar to the range (10^{-8} to 10^{-6} min^{-1}) associated with the floor vibration typical of human walking (Gomes et al., 2007). This result suggests that particle acceleration due to duct vibration is not sufficiently high enough to overcome gravitational and adhesion forces in the boundary layer of the duct surface.

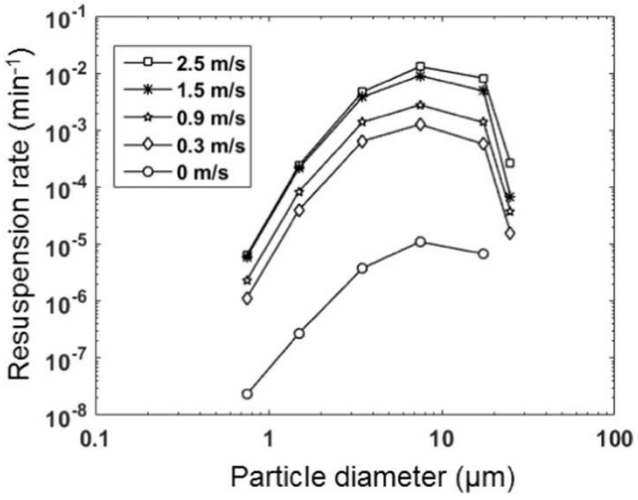

Figure A4. Resuspension rates of *Bacillus thuringiensis* spore particles from a galvanized sheet metal duct surface observed at varying air swirl velocities between 0 and 2.5 m/s.

According to Figure A4 particle resuspension rate increases with particle size and air swirl velocity, although the increase is not linear. With regard to size-specific resuspension rate, 7- to 10-μm particles have high resuspension rates in the duct system, which is generally consistent with varied air swirl velocities. The resuspension rate is dramatically elevated (up to larger than 2 orders of magnitude) with the swirl velocity increase from 0 m/s to 0.3 m/s. However, compared to the swirl velocity increase from 0 to 0.3 m/s, the increase from 1.5 to 2.5 m/s yields much smaller increases in resuspension rates. Mukai et al. (2009) have reported that turbulence intensity is not a major factor determining particle resuspension over galvanized metal surfaces under a bulk air velocity range from 5 to 25 m/s. However, our study results show that the presence of even a small air swirl (0.3 m/s swirl velocity) near the duct surface results in a substantial increase in particle resuspension, although the increase is marginal when the air swirl velocity is above 1.5 m/s. These findings also support that particle resuspension rate reaches the peak values under transient airflow regimes such as initial period of fan operating in the duct (Krauter and Biermann, 2007; Wang et al., 2012).

A.4. Conclusion

The present study examined resuspension rates of biological particles from floor and ventilation duct surfaces with a focus on the effects of the relative humidity and air swirl near the surface. Laboratory chamber experiments were conducted to measure particle resuspension rates of dust mite, cat fur, and dog fur particles from carpet and linoleum surfaces. Resuspension of bacterial spore particles (*Bacillus thuringiensis* as an anthrax simulant) was observed with a range of air swirl flow velocities in a galvanized steel duct system.

The results show that resuspension rates of dust mite particles strongly depend on humidity level, while resuspension of dog fur and cat fur particles are marginally affected by

humidity variation. The resuspension rates of dust mite particles from linoleum surface notably increased up to two orders of magnitude with RH decreases from 80% to 10%. This result suggests that indoor humidity is a key factor determining particle resuspension rates of hydrophilic dust mite particles. This finding also implies that increasing humidity levels indoors, particularly in winter season, could be a potential strategy for reducing the resuspension of dust mite particles from indoor surfaces.

The experiments with the duct system suggest a notable effect of air swirl velocity on the resuspension of bacterial spore particles. Resuspension rate increases over two orders of magnitude with a relatively small swirl velocity of 0.3 cm/s near the duct surface. The presence of air swirl near the duct surface seems to have a significant influence on the particle resuspension from the duct surface. This finding highlights the critical role of turbulent swirl flow in dispersion of the bacterial spores in duct systems. However, normal duct vibration does not yield discernible increase in particle resuspension compared to the floor vibration.

Acknowledgements

This research was funded by Penn State Institutes of Energy and the Environment Seed Grant (PSIEE 415-17) and ASHRAE (American Society of Heating, Refrigerating, and Air-conditioning Engineers) Graduate Student Grant-in-aid. The authors thank U.S. Army Center for Health Promotion and Preventive Medicine for providing the samples of *Bacillus thuringiensis* spores.

A.5. Supplementary Information

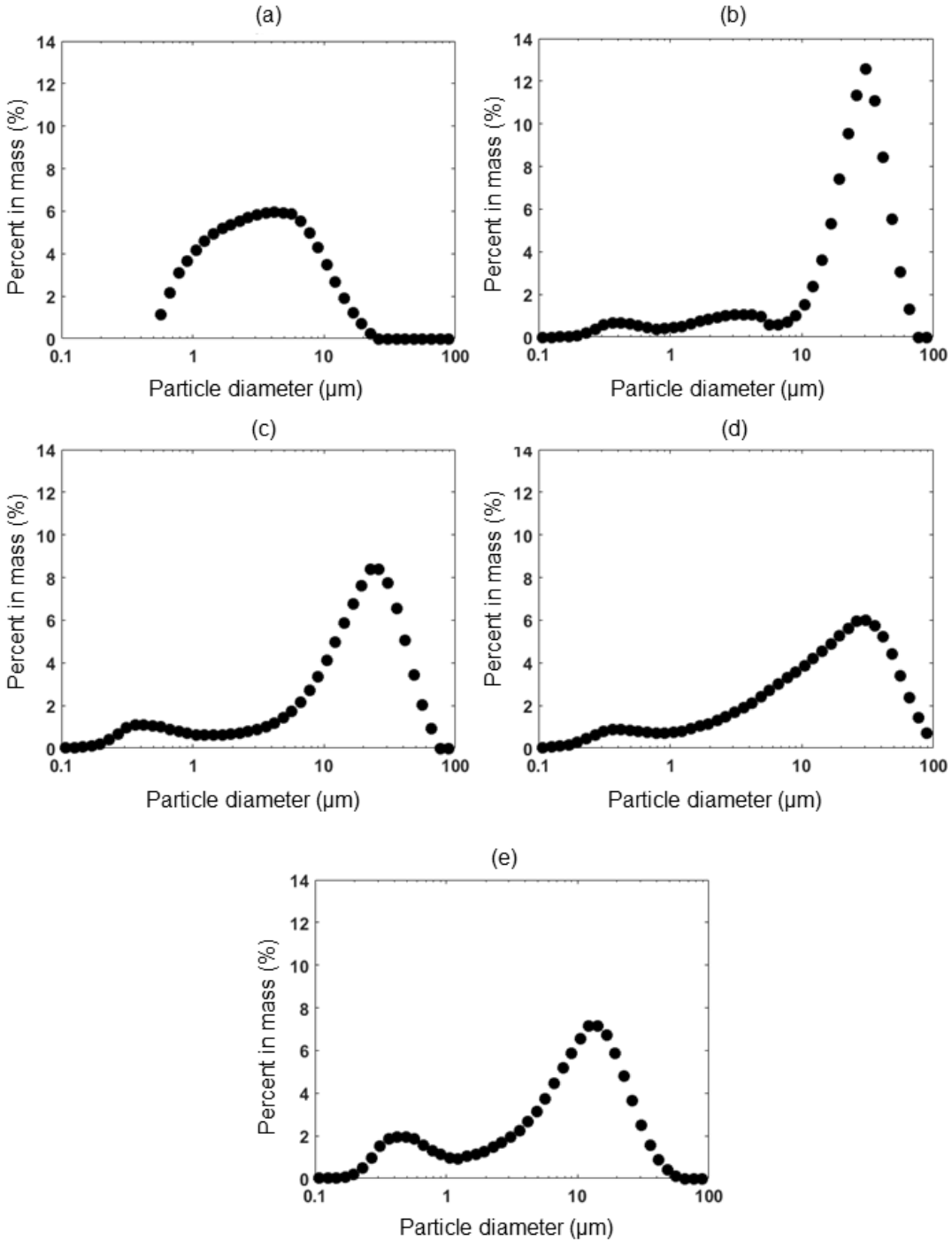

Figure A5. Size distribution of settled particles on sample surfaces: (a) quartz; (b) dust mite; (c) dog fur; (d) cat fur; (e) bacterial spore-*Bacillus thuringiensis*

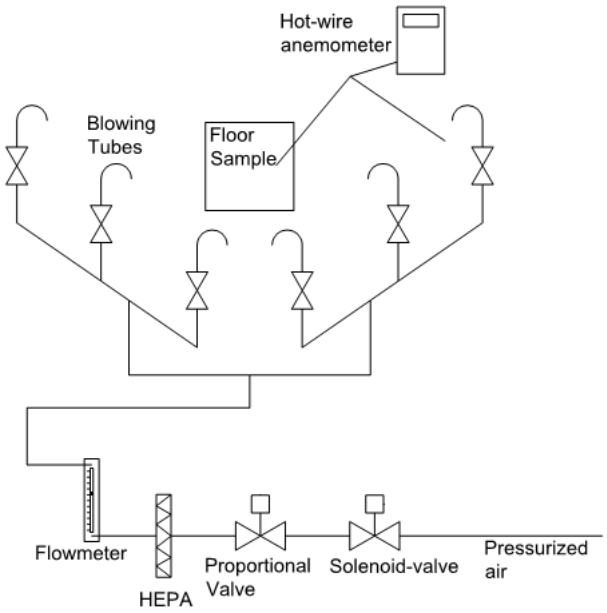

Figure A6. Schematic diagram of the floor disturbance air-swirl system. A proportional valve (SD8202G1V, ASCO, NJ-USA) and normally-closed valve (8262G90, ASCO, NJ-USA) control the airflow that passes through the HEPA filter (HEPA CAP36, Whatman, UK) and is supplied to the copper jet tubes.

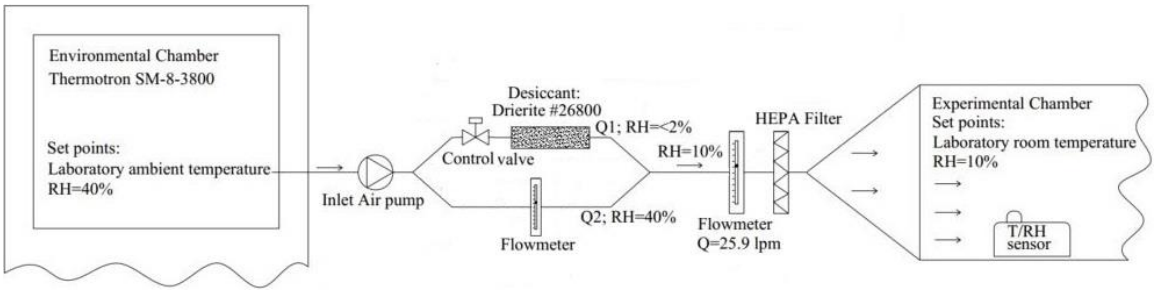

Figure A7. Schematic diagram of temperature and humidity control of the resuspension chamber: For 80% and 45% RH test cases, the environmental chamber can directly provide the supply airflow with desired temperature and RH level. For 10% RH test case, 6 L/min of the conditioned air by the environmental chamber (at 40% RH) is sent through a desiccant line which reduces the air RH to less than 2%. The final mixed air RH is 10%.

Table A1. Air velocity map over floor samples.

	x-direction (m/s)			y-direction (m/s)			x,y-equivalent (m/s)		
Location	**min**	**avg**	**max**	**min**	**avg**	**max**	**min**	**avg**	**max**
11	0.00	0.00	0.00	0.84	0.91	0.99	0.84	0.91	0.99
12	0.37	0.50	0.70	0.00	0.01	0.14	0.37	0.50	0.71
13	1.25	1.72	2.11	0.48	1.82	2.22	1.34	2.50	3.06
21	0.20	0.49	0.72	0.66	0.91	1.07	0.69	1.03	1.29
22	0.54	0.69	0.90	0.16	0.20	0.24	0.56	0.72	0.93
23	0.00	0.00	0.00	0.00	0.16	0.20	0.00	0.16	0.20
31	0.00	0.10	0.19	1.27	1.49	1.77	1.27	1.49	1.78
32	0.00	0.22	0.42	0.00	0.00	0.00	0.00	0.22	0.42
33	2.04	2.19	2.34	1.07	1.27	1.42	2.30	2.53	2.74
Average		**0.66**			**0.75**			**1.12**	

Table A2. Air velocity exiting the air-swirl system tubes.

Tube	avg (m/s)	Re number
A	4.10	1360
B	4.40	160
C	4.20	1390
D	3.90	1290
E	3.20	1060
F	4.00	1330

Uncertainty Analysis

Uncertainty of estimate of resuspension rate was analyzed based on error propagation of all input parameters in Equations A1 and A2. The uncertainty of the calculated resuspension rate values were obtained by propagating the uncertainty of each measured variable using Equation A3 (Taylor, 2009).

$$U_y = \sqrt{\sum_i \left(\frac{\partial Y}{\partial X_i}\right)^2 . {U_{X_i}}^2} \qquad \text{(Equation A3)}$$

U_y is the standard uncertainty of the calculated parameter Y that is a function of measured variables X_1, X_2,…, X_n; and U_{X_i} is the uncertainty associated with variable X_i. Here Y is the RR_d and U_y is the propagated uncertainty of the resuspension rate. Similarly, X_i and U_{X_i} represent the variables used in Equations A1 and A2, and their associated uncertainties, respectively. A summary of measured variables used to calculate the RR_d and their associated uncertainties are given in Table A3.

Table A3. Uncertainty of measured variables

Measured Variable (X_i)	**Uncertainty (U_{X_i})**	**Notes**
$\mathbf{Q_{sweepflow}}$	5%	Repeated measurement
$\mathbf{C_{surf,d}}$	5%	device (PM300)
$C_{air,d}$	5%	device (PM300)
$C_{air,d}$	10%	device (Climet)
$m_{surf,total}$	0.1 mg	Repeated measurement

Tables A4 and A5 present the result of uncertainty analysis for two different experiment sets with different conditions. Table A4 reports the size-resolved resuspension rate of quartz particles from carpet surface under 2.5 air swirl velocity at 45% RH and 25°C and its associated uncertainty rate. Dust loading of the substrate sample in this case is 5 g/m2. The uncertainty values are representing the propagated uncertainty level of the calculated resuspension rate for each particle size bin. The proportion of the uncertainty level to the resuspension rate value is reported as variation (%). Table A5 reports the propagation uncertainty analysis result for the test case of dust mite particles from linoleum substrate at 45% RH and 25°C under 0.9 m/s air swirl velocity. The substrate loading of this test was set at 3 g/m2. As it can be seen in the uncertainty results of both test cases, the combined equipment and measurement uncertainty has introduced a fairly uniform error percentage of 15% in calculated resuspension rate across all size bins.

Table A4. Estimation uncertainties of particle resuspension rates. Case I: quartz particles on the carpet, air swirl velocity: 1.5 m/s, surface dust load: 5 g/m^2, relative humidity: 45%.

d_p [µm]	RR_d [min^{-1}]	Uncertainty	% Variation
0.3-0.4	2.61×10^{-7}	3.96×10^{-8}	15.2%
0.4-0.5	4.62×10^{-7}	6.97×10^{-8}	15.1%
0.5-0.55	2.07×10^{-7}	3.11×10^{-8}	15.1%
0.55-0.7	7.21×10^{-7}	1.08×10^{-7}	15.0%
0.7-1.0	2.18×10^{-6}	3.21×10^{-7}	14.7%
1.0-1.3	2.43×10^{-6}	3.58×10^{-7}	14.7%
1.3-1.6	2.83×10^{-6}	4.14×10^{-7}	14.6%
1.6-2.0	4.63×10^{-6}	6.70×10^{-7}	14.5%
2.0-2.2	3.89×10^{-6}	5.70×10^{-7}	14.6%
2.2-3.0	1.29×10^{-5}	1.85×10^{-6}	14.4%
3.0-4.0	2.12×10^{-5}	3.10×10^{-6}	14.6%
4.0-5.0	3.20×10^{-5}	4.77×10^{-6}	14.9%
5.0-5.5	3.22×10^{-5}	4.86×10^{-6}	15.1%
5.5-7.0	6.39×10^{-5}	9.67×10^{-6}	15.1%

Table A5. Estimation uncertainties of particle resuspension rates. Case II: dog fur particles on the linoleum surface, air swirl velocity: 0.9 m/s, surface dust load: 3 g/m2, relative humidity: 45%.

d_p [µm]	RR_d [min^{-1}]	Uncertainty	% Variation
0.3-0.4	7.12×10^{-8}	1.10×10^{-8}	15.5%
0.4-0.5	6.09×10^{-8}	9.41×10^{-9}	15.5%
0.5-0.55	4.47×10^{-9}	6.90×10^{-10}	15.4%
0.55-0.7	6.29×10^{-8}	9.71×10^{-9}	15.4%
0.7-1.0	1.59×10^{-7}	2.46×10^{-8}	15.4%
1.0-1.3	1.13×10^{-7}	1.74×10^{-8}	15.4%
1.3-1.6	9.31×10^{-8}	1.43×10^{-8}	15.3%
1.6-2.0	1.11×10^{-7}	1.69×10^{-8}	15.3%
2.0-2.2	5.51×10^{-8}	8.38×10^{-9}	15.2%
2.2-3.0	3.74×10^{-7}	5.62×10^{-8}	15.0%
3.0-4.0	3.53×10^{-7}	5.23×10^{-8}	14.8%
4.0-5.0	3.66×10^{-7}	5.36×10^{-8}	14.7%
5.0-5.5	3.92×10^{-7}	5.78×10^{-8}	14.7%
5.5-7.0	1.58×10^{-6}	2.30×10^{-7}	14.6%

Appendix B

Paper 2. Performance Evaluation of Low-Cost Particle Sensors in Monitoring Common Indoor Bioaerosols: a Controlled Chamber Experimental Study

Graphical Abstract

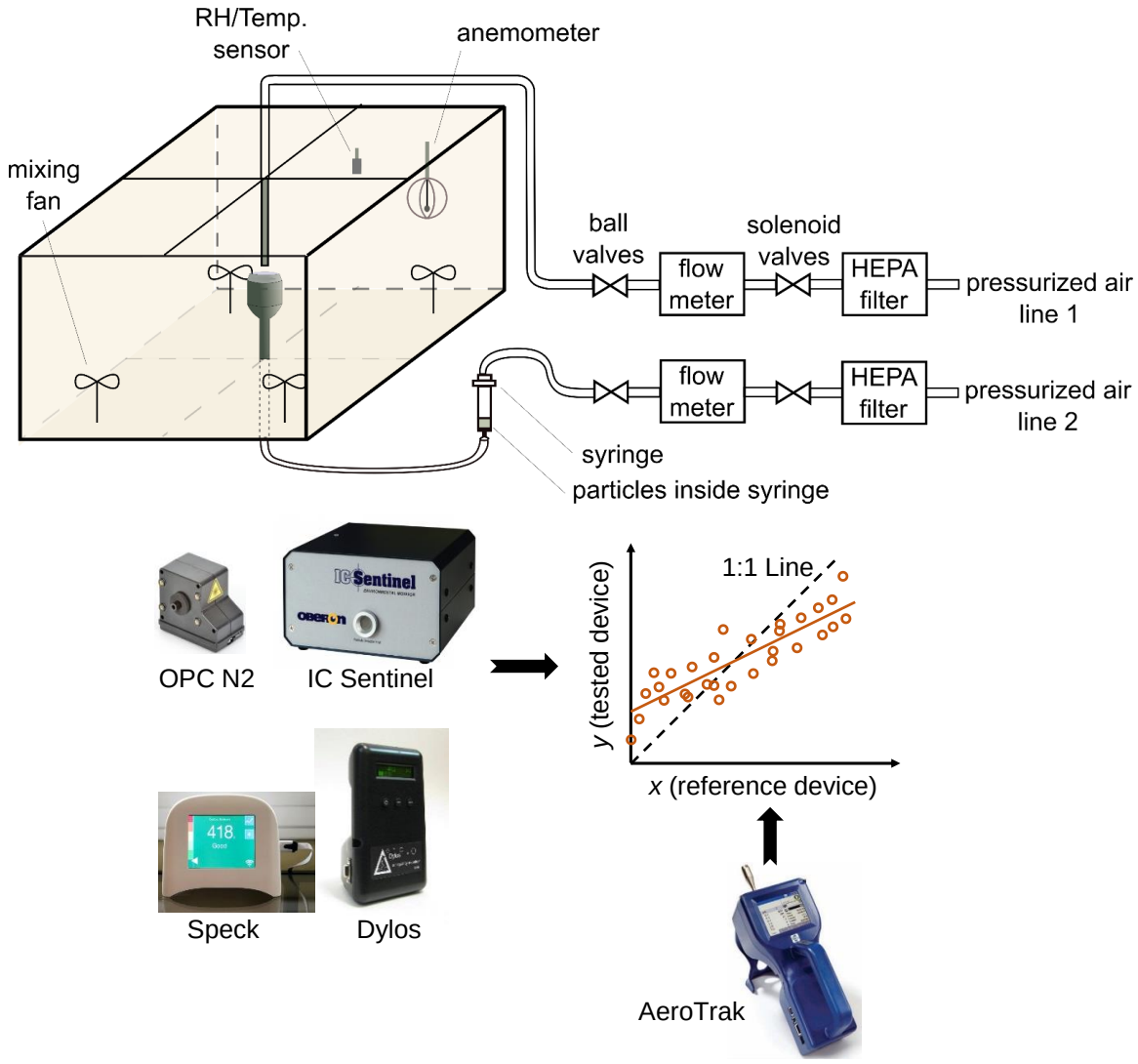

Highlights

- Particle concentration significantly influences the low-cost sensors' performance.
- The response pattern of tested low-cost sensors to bioaerosols are fairly similar.
- Tested sensors response to bioaerosols converge together in concentrations > 5/cm^3.
- Linear calibration equations for the aggregate of tested bioaerosols are developed.
- Particle-specific linear calibration equations are also provided.

Abstract

Low-cost particulate matter (PM) sensors have garnered significant interest in PM exposure field. Although, previous studies found that low-cost PM sensor performance could vary considerably when exposed to various particles, very little information about the performance of low-cost sensors in monitoring bioaerosols is available. Given the significance of bioaerosols in exposure studies and their associated adverse health effects, this study investigates the performance of low-cost optical particle counters (OPC) in detecting the common indoor bioaerosols.

To investigate the effects of particle characteristics and concentrations, PM sensor responses were examined under exposure to varying concentrations of biological (dust mite, pollen, cat fur, and dog fur) and non-biological (monodisperse silica and melamine resin particles in different sizes) aerosols. Each particle sample was dispersed into a chamber (76×76×42 cm) using a computer-controlled syringe injection system. Size-resolved particle number concentration was measured by four tested low-cost OPCs (OPC N2, Alphasense; IC Sentinel, Oberon Inc.; Speck, Airviz Inc.; and Dylos, Dylos) and the reference sensor (AeroTrak, TSI) simultaneously. Linear regression analysis was used to compare the sensor responses to that of the reference sensor.

Results showed different combined effects of aerosol size, optical characteristics, and concentration on the tested sensors' responses. Particle concentration has the most dominant effect on the

linearity of the low-cost sensors. In lower particle number concentration ranges, low-cost PM sensors showed a nonlinear response, whereas, in higher concentration ranges they exhibited high linearity. The dividing line between the nonlinear and linear concentration regions varied with the sensor and the tested non-biological aerosol type and size. The fairly homogenous response to the bioaerosols allowed for determining a dividing line ($5/cm^3$) between nonlinear and linear response regions that was common amongst all the tested low-cost OPCs. The findings of this study imply that low-cost OPCs can be used in monitoring specific concentration ranges of bioaerosols, once they are calibrated prior to deployment.

Keywords

Indoor air quality, particulate matter, bioaerosol, optical particle counter, sensor calibration.

B.1. Introduction

Human exposure to airborne particulate matter (PM) is detrimental to human's health and well-being (Goldsmith, 1999; Pope III et al., 2002). The high cost of PM sensors has been a barrier for long-term PM monitoring across sufficient spatial sampling density nodes (Castell et al., 2017). The recent emergence of low-cost PM sensors technology has enabled the real-time PM monitoring with high spatiotemporal resolution (Rai et al., 2017). The new capabilities that this low-cost sensing technology brings about have opened new horizons in exposure study field by deploying these sensors for various applications; from increasing public awareness about air pollution through projects such as Citizen Scientists (Aoki et al., 2008; Jovašević-Stojanović et al., 2015); to stablishing outdoor PM monitoring networks with high spatiotemporal resolutions (Jiao et al., 2016); and integrating PM sensors into building ventilation controls to mitigate the building occupants exposure to indoor PM (Kumar et al., 2016a, 2016b). In order to reliably use low-cost sensors for any of these applications, their performance under conditions specific to any of those applications should be examined first. Previous research (Snyder

et al., 2013) has warned against the possible detrimental consequences of rushing to apply low-cost sensors without proper performance evaluation.

To address the necessity of independent scientific investigation of low-cost sensors' performance, several researchers have conducted field and lab studies of observational and experimental nature. They have examined the performance of low-cost PM sensors –which are mostly light scattering based optical particle counters (OPC)- in indoor (Patel et al., 2017; Steinle et al., 2015; Weekly et al., 2013) and outdoor (Gao et al., 2015; Holstius et al., 2014; Kelly et al., 2017; Mukherjee et al., 2017; Piedrahita et al., 2014; Steinle et al., 2015; Zikova et al., 2017) environment applications. Sousan et al. (2016) tested Dylos1700 (Dylos, Riverside, CA) sensor in a chamber with salt, Arizona road dust (ARD), welding fume, and diesel exhaust particles. Their results showed that particle detection efficiency ranged from 0.04% to 108% for particle sizes of 0.1 to 5 µm. This sensor performance was found to be strongly influenced by particle type and concentration level. DC1700 showed a linear response with respect to reference sensor for low particle number concentrations; however, it displayed a nonlinear response for concentrations above 106 cm^{-3}. The linear calibration slope for linear response region (< 106 cm^{-3}) varied dramatically for different particle types; from 2.6 for salt to 54 for diesel fume particles. Similar influence of particle type on the PM sensor performance was found by Manikonda et al. (2016) while testing Dylos1700, Dylos1100 pro (Dylos, Riverside, CA), and Speck (Airviz Inc., Pittsburgh, PA) sensors in a chamber under exposure to cigarette smoke and Arizona Test Dust (ATD). In another laboratory chamber study by Wang et al. (2015), three light scattering sensors (PPD42NS (Shinyei), DSM501A (Samyoung), and GP2Y1010AU0F (Sharp)) were tested. Comparison of the sensor responses to atomized NaCl, sucrose, NH_4NO_3 particles, and atomized PSL spheres in 300, 600, 900 nm suggested that their response highly varied with particle composition, size, and concentration level. Taken together, controlled laboratory studies have shown that particle type, size, and concentrations being measured are major influencing factors for the performance of low-cost OPCs (See Table B1 for a summary of previous studies' findings on performance evaluation of four different low-cost OPCs). These results imply the

need for calibration of low-cost PM sensors for specific particle types, sizes, and concentration levels of interest before deploying them in the field. (Kelly et al., 2017).

Several particle properties influencing the light-scattering sensors' response are confounded in what is referred to as particle type. These properties include shape, optical properties, as well as composition. Research has shown that particles of biological and non-biological (Bohren and Huffman, 2004), or organic and inorganic (Wang et al., 2015) nature can draw different responses from optical sensors. Wang et al. (2015) found that response to the organic particle of sucrose was markedly distinct (output signal response to Sucrose was up to 10 times higher than those of NaCl and NH_4NO_3). Organic particles absorb higher fractions of light compared to inorganic particles and thus phototransistor in PM sensors receive less scattered light from organic aerosols. Subsequently, PM sensors may overestimate concentrations of organic aerosols compared to inorganic aerosols (Wang et al., 2015).

Despite mounting evidence for particle-dependence response of light-scattering based sensors and given the fact that exposure to indoor bioaerosols is linked to various adverse health effects in building occupants (Barnes et al., 2001; Nazaroff, 2016; Raja et al., 2010; Wallace, 1996), not much information is yet available about the low-cost sensors performance under exposure to bioaerosols. At the time of writing this paper, authors could not find previous experimental studies that examined the performance of low-cost PM sensors in measuring common indoor biological aerosols. Based on this background, the objective of this study is to assess the performance of low-cost PM sensors in monitoring common indoor biological aerosols of various type, size, and concentration and how that would differ from non-biological aerosols.

Table B1. Summary of the low-cost PM sensors performance evaluation results from previous studies

Test sensor	Study type	Reference sensor	Test particles	Sensor performance compared to the reference sensor				
				Linearity*	R^{2}**	Dependence*** on		
						Particle	Size	Concentration
OPC-N2	lab (Sousan, Koehler, Hallett, et al., 2016a)	SMPS (TSI), APS 3321 (TSI), PAS-1.108 (Grimm Technologies)	salt aerosols generated with 0.9% NaCl solution, welding fume, Arizona road dust	0.03-2.7	0.94-0.99	0.05-1.6	high	not analyzed
Speck (DSM501A)	lab (Manikonda et al., 2016)	Grimm1.109 (Grimm Technologies), APS 3321 (TSI), FMPS 3091 (TSI)	cigarette smoke, Arizona test dust	0.6-300	0.58-0.97	0.0023-210.2 [2]	not analyzed	not analyzed
	lab (Northcross et al., 2013)	SidePak (TSI), SMPS (TSI), AirAssure (TSI)	incense, NaCl, sucrose, NH_4NO_3, PSL (300,600,900 nm)	59.7-159	0.88-0.90	significant	significant	59.7-159 [5]
	lab (Sousan et al., 2017)	SMPS (TSI) + APS (TSI)	salt aerosols generated with 0.9% NaCl solution, welding fume, Arizona road dust	0.1-0.58	not analyzed	significant [3]	not analyzed	not analyzed
Dylos (DC1700)	lab (Sousan, Koehler, Thomas, et al., 2016b)	SMPS (TSI) + APS (TSI)	salt aerosols generated with 0.9% NaCl solution, welding fume, Arizona road dust, diesel exhaust	0.018-0.385[1]	0.91-0.99	high	high [4]	high [6]
	lab and field (Northcross et al., 2013)	DustTrak (TSI), Met-One (E-bam beta attenuation monitor)	PSL (0.49 µm), ammonium sulphate (0.01 M (NH4)2SO4), wood smoke, urban ambient particles	0.953-55.556	0.97-0.99	significant	not significant	not significant
	lab (Manikonda et al., 2016)	Grimm1.109 (Grimm Technologies), APS 3321 (TSI), FMPS 3091 (TSI)	cigarette smoke, Arizona test dust	0.1-15	0.65-0.95	0.052-0.44 [2]	not analyzed	not analyzed
Dylos (DC100 Pro)	lab (Manikonda et al., 2016)	Grimm1.109 (Grimm Technologies), APS 3321 (TSI), FMPS 3091 (TSI)	cigarette smoke, Arizona test dust	0.1-15	0.87-0.94	0.054-0.41 [2]	not analyzed	not analyzed

*: comparison between test sensor and reference measurements, regression fit slope.
**: comparison between test sensor and reference measurements, regression fit R^2 (coefficient of determination).
***: difference between low and high slope values under different test conditions.

1: regression equations refer to number concentrations (particles/cm^3) measured by DC1700 versus mass concentration (µg/m^3) measured by reference sensor for particle concentration levels below 106 (particles/cm^3).
2: regression fit slope of number counts of test sensor versus reference sensor (APS 3321).
3: non-linear response for salt, logarithmic curve for ARD, and fairly linear response for welding fume.
4: detection efficiency changed for different particle sizes; <5% for 0.3 µm, 60% for 1.3 µm, and ~100% for 3 µm particles.
5: slope of linear regression between the test sensor and the reference sensor (SidePak) under 100 and 1000 µg/m^3 concentration levels, respectively.
6: linear and nonlinear responses were observed for particle number concentrations below and above 106 (particles/cm^3), respectively.

B.2. Methods

Four low-cost PM sensors were investigated against a reference sensor in a controlled environmental chamber while varying particle type, size, and concentration level. The following sections describe details of data collection (section B.2.1.), sensors specifications (section B.2.2.), tested particles characteristics (section B.2.3.), and data analysis method (section B.2.4.).

B.2.1. Test chamber set-up and experimental protocol

The laboratory experimental set-up used for this experiment is shown in Figure B1. A 0.76 × 0.76 × 0.42 m particle dispersion chamber was used to test the low-cost sensors in a controlled environment. A computer-controlled injection system was designed to inject the particles into the chamber. Two separate lines (line 1 and line 2) of pressurized air flew through HEPA filters (TSI, Inc., Shoreview, MN) and the particle-free air was sent to ball valves and then solenoid valves (see Figure B1). Ball valves were used to modulate the airflow rate passing through each line. Solenoid valves were controlled by a computer program to open and close the airflow lines. There is a flow meter after each solenoid valve that measures the airflow rate in each line. Particle-free air (line 1) was supplied to chamber via an inlet at the top center of the chamber, while particle-free air in line 2 was sent to a syringe containing test particles and then the test particles were injected into the chamber through an inlet (TSI, Inc., Shoreview, MN) at the bottom center of the chamber. The particle-laden and particle-free air streams collided and dispersed the particles in the chamber, while four mixing fans were running at the four corners of the chamber to ensure a well-mixed condition in the chamber.

Relative humidity (RH) and temperature of the air inside the chamber were measured with a probe sensor (HMT100, Vaisala), while air velocity inside the chamber is measured with an anemometer. Location of the RH, temperature, and anemometer sensors are shown in Figure B1.

Nine 2.5-hour particle-decay test cases were conducted. Each test was performed using the following six steps:

1) Before each test, all surfaces inside the chamber as well as the particle injection line were thoroughly cleaned and washed to remove any residual particles from previous tests.
2) The specific amount of test particles needed to create the desired maximum particle number concentration in the chamber was calculated, measured, and added to the syringe.
3) Particle-free air at a volumetric flow rate of 9 L/min was supplied to the chamber for at least 30 minutes to flush the chamber until the reference PM sensors report PM counts of close to zero. Four mixing fans were running at the four corners of the chamber to achieve a well-mixed condition.
4) Background measurement was performed by all sensors (minutes 0 to 5 of the test).
5) A signal was sent to the solenoid valve in line 2 to supply 18 L/min of filtered airflow to the syringe and inject the particles into the chamber for 2 minutes (minutes 5 to 7 of the test).
6) The solenoid valve in line 2 was closed and the particles decay started. Particle concentration was monitored until it reached the background level again (minutes 7 to 150 of the test).

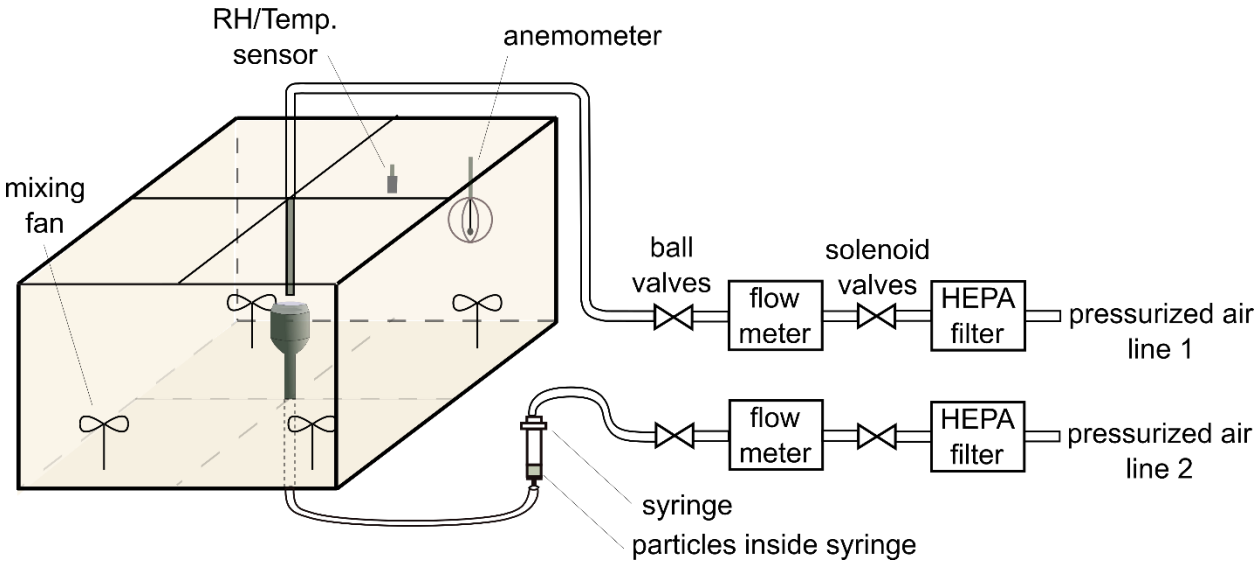

Figure B1. Schematic of the chamber experiment set-up.

B.2.2. Sensor specifications

The present study examined performance of four different low-cost PM sensors: 1) OPC N2 (Alphasense Ltd., Essex, United Kingdom), 2) IC Sentinel (Oberon Inc., State College, PA), 3) Speck (Airviz Inc., Pittsburgh, PA), and 4) Dylos (Dylos, Riverside, CA). Figure B2 shows four low-cost sensors, and the reference sensor examined in this study. All low-cost sensors are optical-based particle counters that report the particle number concentrations across different size bins. AeroTrak (TSI 9306, TSI, Inc., Shoreview, MN) was used as the reference monitor, given that it is a lab-grade optical particle counter and can measure particle number concentrations in the 0.3–10 μm diameter range with six particle size bins (0.3–0.5 μm, 0.5–1.0 μm, 1.0–2.5 μm, 2.5–5 μm, 5–10 μm, and >10 μm). Table B2 summarizes the characteristics and specifications of these sensors as provided by their respective manufacturers.

Table B2. Sensors' characteristics as reported by the manufacturer

Low-cost & reference sensors	Light source wavelength (nm)	Detection size range (µm)	# of bins	Bin size cuts (µm)	Flow rate (L/min)	Measurement time resolution (sec)	Detection concentration range
OPC N2 (Alphasense)	658 [2]	0.38-17	16	0.46, 0.66, 0.92, 1.20, 1.47, 1.83, 2.54, 3.50, 4.50, 5.75, 7.25, 9.00, 11.00, 13.00, 15.00, 16.75	sampling: 0.22, total:1.2	1	10,000 particles/sec
IC Sentinel	650 [3]		4	0.5, 1, 5, 10	1.5	120	3×10^6 particles/ft^3
Speck [1]	850 [4]	0.5–3	1	2	NA	30	NA
Dylos (DC1100)	650	>1	2	1,5	NA	60	NA
AeroTrak (TSI 9306)	785 [5]	0.3-25	6	0.3, 0.5, 1.0, 3.0, 5.0, 10.0	2.83	1	3×10^6 particles/ft^3 at 5% coincidence loss

1: uses DSM501A (Syhitech DSM501, Syhitech Co., Ltd) sensor,
2: Laser diode,
3: Laser diode, 10 mW,
4: LED,
5: enhanced active cavity HeNe laser.

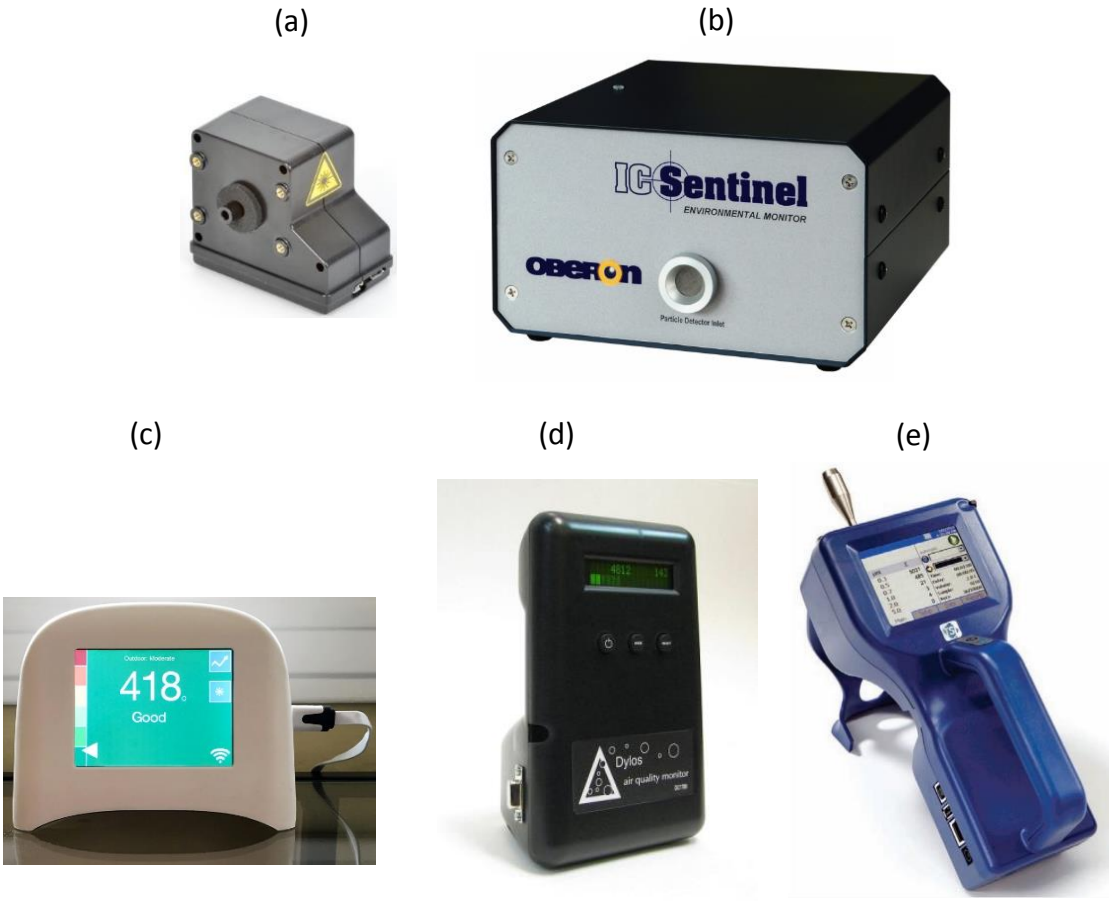

Figure B2. Sensors examined in this study.
a) OPC N2 (Alphasense Ltd., Essex, United Kingdom),
b) IC Sentinel (Oberon Inc., State College, PA),
c) Speck (Airviz Inc., Pittsburgh, PA),
d) Dylos (Dylos, Riverside, CA), and
e) Handheld AeroTrak (TSI, Inc., Shoreview, MN), reference sensor.

B.2.3. Tested particles characteristics

PM sensors were tested with 9 different particle batches. These 9 particle batches included various biological and non-biological, as well as monodisperse and polydisperse particles. Four types of common biological particles in indoor spaces (Bardana Jr, 2001) were used to test the PM sensors; 1) dust

mite (Indoor Biotechnologies Inc., Charlottesville, VA, USA), 2) pollen, 3) cat fur, 4) and dog fur. The preparation of cat fur and dog fur particles is described in a previous study (Salimifard et al., 2017b). Non-biological particles included two types of monodisperse particles (microparticles Gmbh, Berlin, Germany) with varied diameters and one polydisperse particle respectively: 1) melamine resin (MF-R), 2) silicon dioxide (SiO_2-R), and 3) quartz (crushed quartz #10 bt#4339, Particle Technology Limited, UK).

Table B3. Tested particles' characteristics

Particle type	Size distribution type	Size range (µm)	Biological / Non-Biological	Density (kg/m^3)	Shape	Roughness	Refractive Index	Hydrophobicity
dust mite	polydisperse	0.58-48	biological	1140	rounded **	smooth	-	hydrophilic
pollen	polydisperse	-	biological	1000	near spherical [a]	-	1.5 [b]	hydrophilic
cat fur	polydisperse	0.58-409	biological	1000	fibers	rough	1.35-1.43 [c]	hydrophobic
dog fur	polydisperse	0.58-351	biological	1000	fibers	rough	1.37-1.55 [c]	hydrophobic
melamine resin (MF-R)	monodisperse	1.041 ± 0.03 *, 2.81 ± 0.06 *	non-biological	1510	spherical	smooth	1.68 [d]	hydrophilic
silicon dioxide (SiO2-R)	monodisperse	0.977 ± 0.026 *, 2.81 ± 0.1 *	non-biological	1850	spherical	smooth	1.5 [e]	hydrophilic
crushed quartz (>95% of SiO_2)	polydisperse	0.58-22.5	non-biological	2650	varied ***	smooth	1.544 [a]	hydrophilic

* size ± standard deviation
** with prismatic edges resulted from the ball mill crushing effect)
*** varied from squares to rectangles (5/1 ratios maximum)
a: (Hinds, 2012)
b: (Gullvåg, 1964)
c: (Yan et al., 2015)
d: as provided by the manufacturer
e: (Radhakrishnan, 1947)

B.2.4. Data analysis method

In analyzing the performance of the low-cost sensors, particles smaller than 2.5 µm are particularly the focus of this study for two reasons; the gravity health concerns relevant to exposure to particles of this size range (Polichetti et al., 2009), as well as, consistently being the size range focus of measurement for all low-cost sensors tested in this study. As particle number concentration readings from different sensors may cover different size ranges, from each sensor, size bins representing the particle smaller than 2.5 µm which had the closest overlap with each other were selected. For instance, Speck sensor covers a particle size bin of 0.5-3 µm, while AeroTrak measures particles in a size range of 0.3-3 µm. In order to address this issue, from each sensor, only size bins which had the closest overlap with other sensors were selected. As in the case of the reference sensor, although AeroTrak provides measurements of particles as small as 0.3, the number counts in the smallest size bin were not included in the analysis. Information about the size range and geometric mean of the particle counts measured by each sensor are summarized in Table B4.

Table B4. Tested sensors' size bins representing particles smaller than 2.5 µm

Low-cost & reference sensors	Size range (µm)	Geometric mean (µm)
OPC N2 (Alphasense)	0.38-3	1.23
IC Sentinel	0.5-5	1.26
Speck	0.5-3	1.22
Dylos (DC1100)	1-5	2.24
AeroTrak (TSI 9306)	0.5-3	1.22

The OPC sensors tested in this study had different time resolutions ranging from 1 sec to 2 min. (see Table B2). In order to fairly compare sensor readings against each other, all the recorded data were time-averaged in 2-minute intervals. After synchronizing the monitoring time-interval for all sensors, the performance of low-cost sensors is examined using the linear regression analysis.

Linear regression coefficients provide straightforward indicators of sensor performance compared to the reference instrument. If sensor readings perfectly match the reference instrument readings, the regression model exhibits an intercept of 0 and a slope of 1. If the intercept and slope coefficients are significantly different from 0 and 1, respectively, it suggests fixed and proportional systematic biases from the reference sensor (schematics shown in Figure B3). The coefficient of determination (R^2) measures the correlation between the test and reference sensors, while the root mean square error (RMSE) gauges the test sensor's precision compared to reference sensor (Magari, 2002; Yanosky et al., 2002). Linear regression is commonly used in the literature for analyzing the performance of a sensor of interest (dependent variable) versus the reference sensor (independent variable). Amongst the regression models, Ordinary Least Squares (OLS) is the suitable and most commonly used model in sensor performance and calibration analysis (Holstius et al., 2014; Manikonda et al., 2016; Miller et al., 1991; Patel et al., 2017; Sousan et al., 2017, 2016b; Wang et al., 2015; Yanosky et al., 2002).

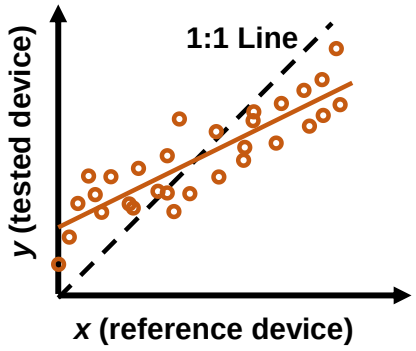

Figure B3. Linear regression analysis is used to evaluate the performance of the low-cost sensors. The tested sensors' measurements are considered as the dependent variable while the reference device measurements as the independent variable. The intercept and slope values different from 0 and 1 represent the fixed and proportional biases of the tested sensors with respect to the reference sensor.

Once the linear regression model (Equation B1) for a low-cost sensor is developed, a calibration equation (Equation B3) can be calculated to address the fixed and proportional biases.

$$y = FB + PB \times x \quad \text{(Equation B1)}$$

$$x = -\frac{FB}{PB} + \left(\frac{1}{PB}\right) y \quad \text{(Equation B2)}$$

$$NC_{LCS,corrected} = -\frac{FB}{PB} + \left(\frac{1}{PB}\right) NC_{LCS} \quad \text{(Equation B3)}$$

Where,

- x (independent variable) is the number concentration measured by the reference sensor ($\#/cm^3$),
- y (dependent variable) is the number concentration measurement of the low-cost sensor estimated by the linear regression model ($\#/cm^3$),
- FB is the fixed bias (intercept of the regression model) ($\#/cm^3$),
- PB is the proportional bias (slope of the regression model),
- NC_{LCS} is the number concentration measured by the low-cost sensor ($\#/cm^3$), and
- $NC_{LCS,corrected}$ is the corrected low-cost sensor number concentration ($\#/cm^3$).

B.3. Results and Discussion

B.3.1. Temporal particle concentration measurement

Figure B4 shows the time profiles of dust mite particle number concentration ($\#/cm^3$) recorded by the four low-cost sensors and the reference sensor over background, emission, and decay periods. Note that tests with other types of particles exhibited similar trends of concentration profiles. OPC N2 and IC Sentinel readings are fairly close to those of reference sensor when measuring higher concentration ranges (emission and early decay period); however, they underestimate concentrations in lower concentration ranges (background and late decay sampling periods). Speck and Dylos sensors consistently underestimate particle concentrations regardless of the concentration ranges being measured. The discrepancies in the concentration profile and decay rate between the reference sensor and low-cost sensors reflect fixed and proportional biases inherent to the low cost sensors. The following section provides details of such biases with using regression analysis results.

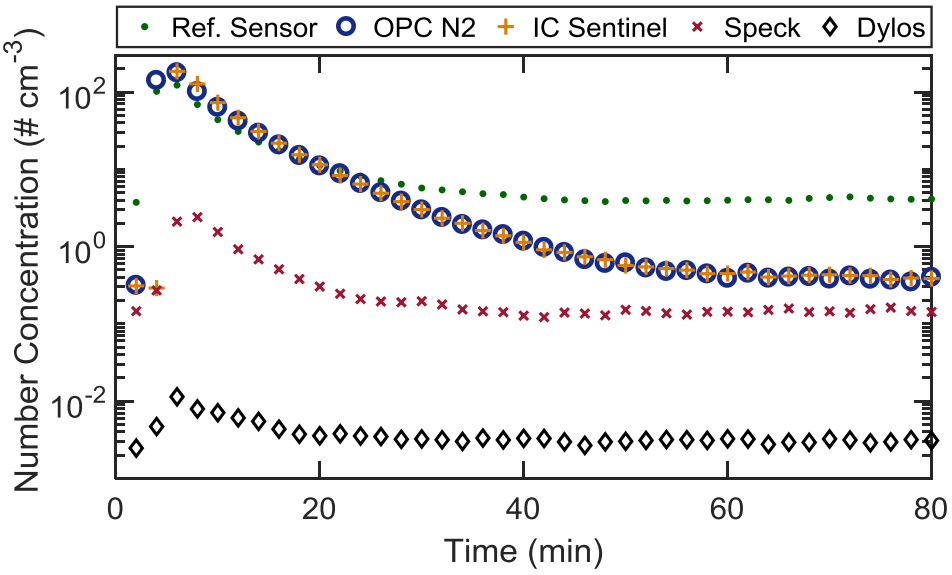

Figure B4. Time-series of dust mite particle number concentrations for a size range < 2.5 µm measured by four low-cost sensors and the reference sensor. The test consists of three phases; 1) background level (minutes 0-5), 2) particle injection (minutes 5-7), and 3) particle concentration decay (minutes 7-150). Note that other test cases with different particle types and sizes had similar temporal concentration profile trends.

B3.2. Performance evaluation using regression analysis

Analyzing the regression analysis results for four biological aerosols based on the comparison between the reference sensor and each low-cost sensor revealed that the performance of low-cost sensors is a strong function of particle concentration. It turns out that a number concentration of 5/cm^3 is the concentration threshold that divides the non-linear response region (0-5/cm^3) and the linear response region (>5/cm^3) (shown in Figure B10 in the Supplementary Information). For the non-linear response region, the median R^2 values are smaller than 0.308 for all four sensors regardless of the biological particles tested. However, for the linear response region (>5/cm^3), the median R^2 values are in the range of 0.957-0.998 for all sensors (more details

are in Table B6 in the Supplementary Information). The clear contrast in the R^2 values between the low and high concentration region emphasizes the effect of concentration on the linearity of low-cost sensor response.

Figure B5 shows the response of the low-cost sensors to tested bioaerosols in the linear response region (>5/cm^3). In the linear response region, the regression slope (proportional bias) varies with the particle type, although the variations are distinctly smaller for OPC N2 and IC Sentinel (Figures B5a and B5b) compared to Speck and Dylos (Figures B5c and B5d). Also, note that the regression slopes for OPC N2 and IC Sentinel are closer to 1 than are Speck and Dylos. These results suggest that when monitoring biological particles, OPC N2 and IC sentinel sensors exhibit smaller proportional biases than Speck and Dylos sensors regardless of particle type. However, Speck and Dylos sensors exhibit relatively large changes in the regression slope depending on the particle type.

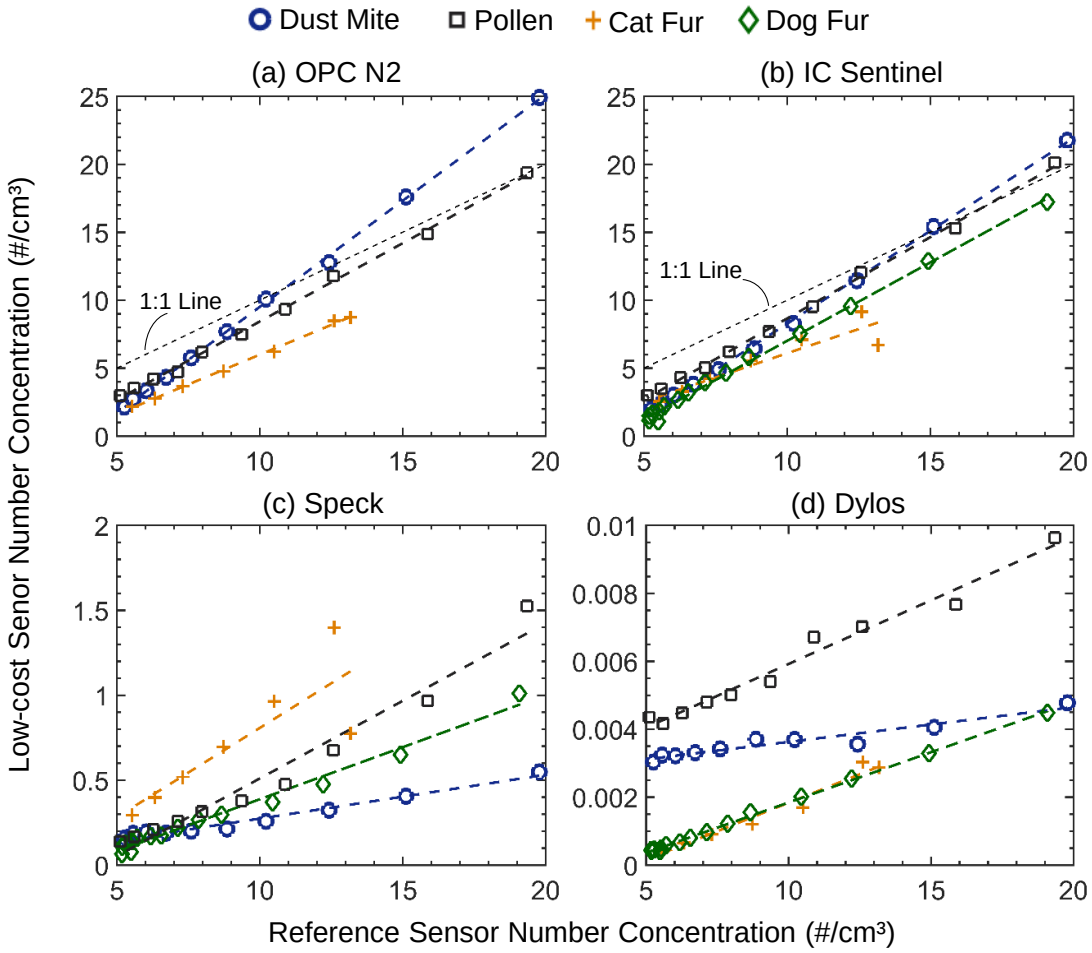

Figure B5. Particle number concentrations measured by low-cost sensors (y-axis) versus the reference sensor (x-axis). Subplots a, b, c, and d represent the OPC N2, IC sentinel, Speck, and Dylos responses to bioaerosols with number concentrations of 5-20/cm^3 where the tested sensors exhibited a linear response. OPC N2 did not record data during dog fur test.

Figures B6a-c illustrates varied regression slopes (PB), intercepts (FB), and values of R^2 for the linear response region among the tested low-cost sensors. Combination of PB and FB reveals whether the sensor underestimates or overestimates the PM concentration. For OPC N2 and IC sentinel sensors, the slope is above 1 and intercept is below 0, therefore it can be concluded that at low concentrations they underestimate, whereas, at higher concentrations, they overestimate the PM concentration. For Speck and Dylos sensors, the intercept is negative and the slope is below 1, suggesting that they underestimate the PM concentration. Despite the presence

of the fixed and proportional biases, high coefficient of determination (R^2) values for the linear response region (Figure B6c) reveal the potential for developing calibration curves before sensor deployment, considering the proportional and fixed biases of a low-cost sensor. The RMSE (Figure B6d) represent the precision of corresponding calibration equations derived from the regression results. Concentration range- and bioaerosol-specific calibration equations can be developed using Equation B3 and linear regression results provided in Table B6 in the Supporting Information section.

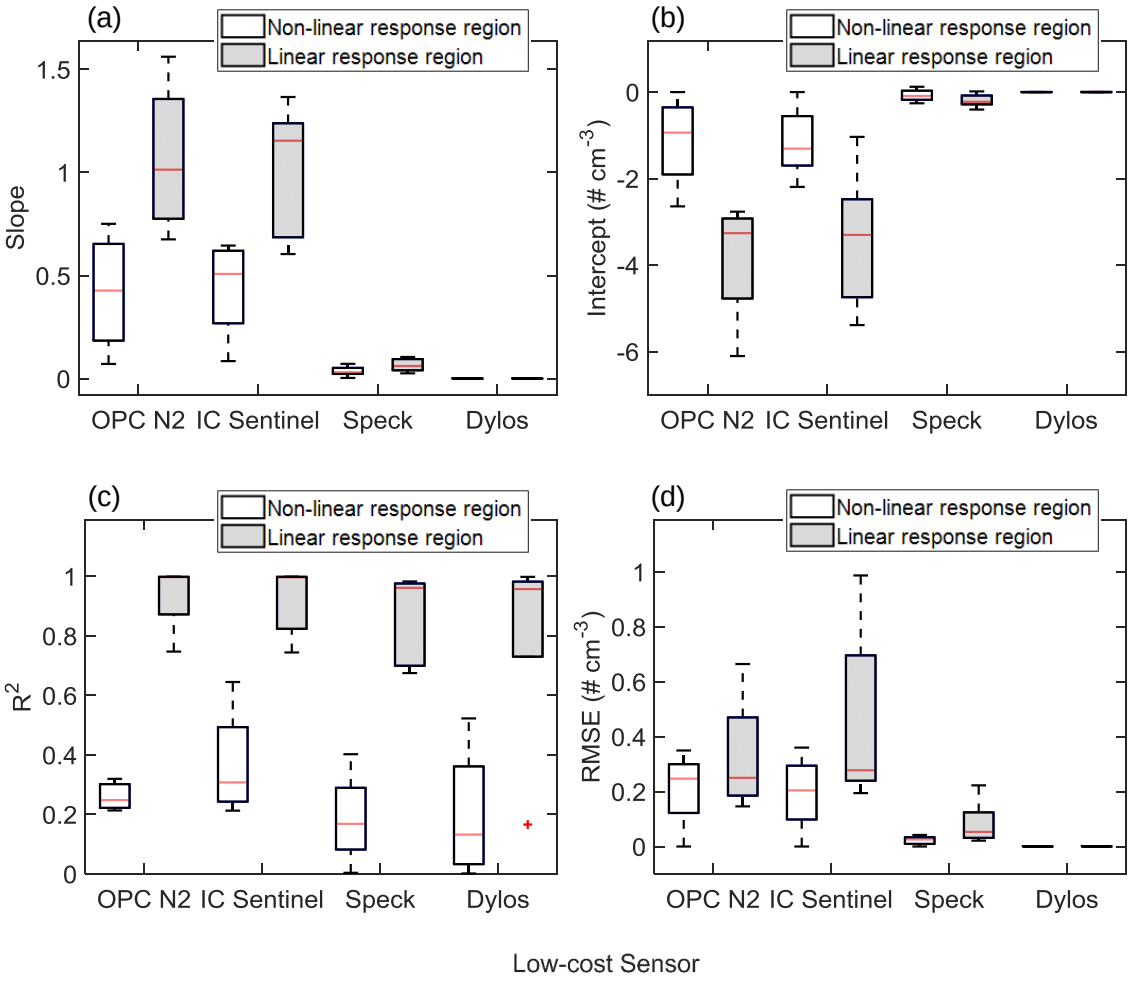

Figure B6. Distribution of linear regression analysis results of low-cost sensors with respect to the reference sensor under exposure to low and high concentration levels of various common indoor bioaerosols. (a): slope (proportional bias), (b): intercept (proportional bias), (c) R^2 (linearity), and (d): RMSE (calibration precision).

All the tested low-cost sensors are all particle counters and measure particle number concentration. Some of the low-cost sensors provide estimates of mass concentrations using propriety equation, which is a function of particle density, and particle shape factor. However, these mass calculations are merely approximate values, since the particle density and shape also vary across particle size distribution. Alternatively, some other low-cost sensors use calibration curves to estimate mass concentrations based on measured number concentrations calibrated against a mass concentration measurement device. Even the low-cost sensors manufacturers themselves do not claim these mass concentration estimates to be accurate. For example, Speck manufacturer calls the provided mass concentration value "a bit of a guess" (Airviz Inc.). Therefore, in this study, the performance evaluation of the low-cost sensors was based on the particle number concentration. However, many low-cost PM sensor calibration studies provide mass-based calibration curves, whether the low-cost was evaluated against a mass-based reference sensor readings or a mass concentration estimates from a particle counter reference device. Hence, to put the particle number concentration based results of this study into the context of mass concentration applications and compare with previous studies findings, the key borderline number concentrations are converted into mass concentration, as being measured by the reference sensor. To estimate the PM2.5 mass concentration, the following equation was used:

$$m = n\,\rho\,\frac{\pi}{6\times10^{6}}\,D^{3} \qquad \text{(Equation B4)}$$

where, m is mass concentration (µg/m^3), ρ is the number concentration, ρ is density (g/cm^3), and D is geometric mean of the bin sizes representing PM2.5. Shape factor was not introduced in the mass concentration calculation, and density was assumed constant. The lower (5/cm^3) and upper (20/cm^3) number concentration limits used in the low-cost sensors linear response region calibration analysis were estimated to be approximately 5 and 22 µg/m^3 for dust mite ($\rho \simeq 1.14$ g/cm^3), 5 and 19 µg/m^3 for pollen, cat fur, and dog fur ($\rho \simeq 1$ g/cm^3), using Equation B4. This

mass concentration range covers the PM2.5 long-term exposure threshold (annual mean averaged over 3 years) set by EPA in National Air Quality Standards (NAAQS) table for primary (12 $\mu g/m^3$) and secondary PM2.5 (15 $\mu g/m^3$) (EPA, 2017).

Various studies have conducted field co-location tests in the indoor and outdoor environment and reported the mean PM2.5 concentration range and the low-cost sensor performance within those environments. Zikova et al. (2017) tested 66 units of Speck in co-location with Grimm 1.19 (Grimm Technologies) in both indoor and outdoor microenvironments in Potsdam, NY. They identified 10 $\mu g/m^3$ as the limit of detection for Speck, while RMSE was often around 10 $\mu g/m^3$. In the co-location field tests they conducted, the indoor air had higher PM2.5 concentration than the outdoor air. The median indoor PM2.5 mass concentration measured by 62 speck units was 12.8 $\mu g/m^3$, while it was 4.6 $\mu g/m^3$ according to Grimm. The median of outdoor PM2.5 mass concentration measurements by Speck units and Grimm sensor were 7.3 $\mu g/m^3$ and 1.6 $\mu g/m^3$ for the first outdoor campaign, and 7.6 $\mu g/m^3$ and 1.3 $\mu g/m^3$ for the second outdoor campaign, respectively. PM2.5 concentrations in both indoor and outdoor environment were below the EPA NAAQS 24-hr average threshold of 35 $\mu g/m^3$. As authors of that study pointed out, the ambient air PM2.5 at their test location was relatively low due to lack of major local PM sources and high vegetation. Another outdoor co-location test conducted in Richmond, California reported a higher outdoor PM2.5 concentration range of 0.8-39 $\mu g/m^3$ (Northcross et al., 2013). Outdoor PM2.5 concentration varies in different locations. Subsequently, indoor PM2.5 concentration in locations with higher outdoor PM concentration is expected. A PM monitoring field study in nurseries in Seoul, Korea reported the significant influence of outdoor sources on the indoor PM2.5 with its mean ranging from 6.6 to 30.6 $\mu g/m^3$. Therefore, depending on the building location, indoor PM2.5 concentration range, and subsequently, the low-cost PM sensor calibration curve varies.

B.3.3. Biological versus non-biological particles

Figure B7 shows differences in low-cost sensor responses between biological and non-biological particles. Biological particles include dust mite, pollen, cat fur, and dog fur while non-biological particles are quartz and melamine resin (MF-R) particles. The figure illustrates the particle number concentrations measured by a low-cost sensor (IC sentinel) versus the reference sensor. Figure 6a shows that the sensor responses to four biological particles follow a similar pattern and converge to a linear line as number concentration increases above 5 cm^{-3}. As for non-biological particles, the sensor responses are widely varied depending on the particle type and particle size, especially in the concentration range < 30 cm^{-3}. Furthermore, the convergence of low-cost sensors responses to a linear line at much higher concentrations compared to those of biological particles.

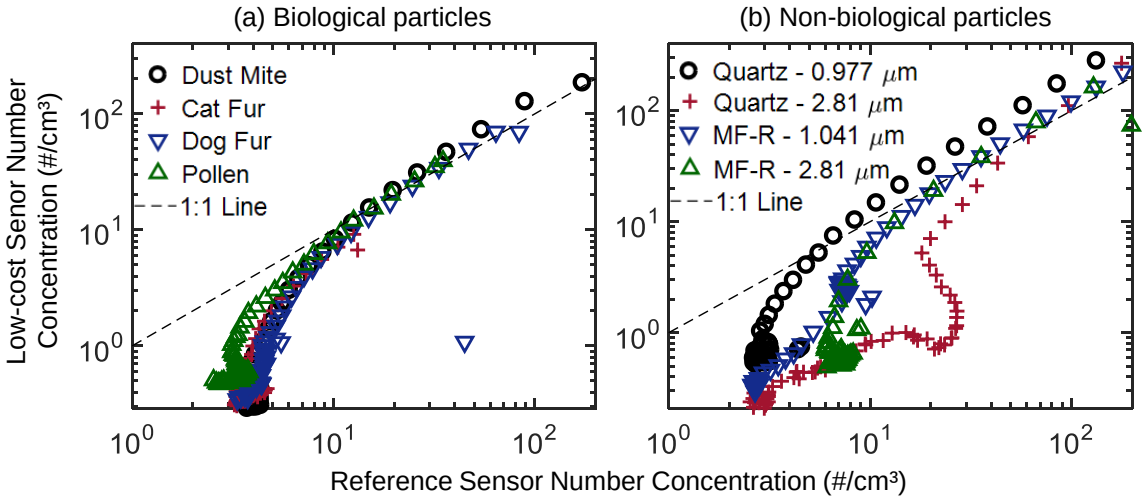

Figure B7. The response of IC sentinel sensor under exposure to biological (a) and non-biological (b) aerosols with respect to the reference sensor. Note that the x- and y- axis scales are log scales.

The similarity of bioaerosols response and its convergence to linear line denoted the possibility of developing a linear calibration equation that can be applied to all four bioaerosols. Therefore, for each tested low-cost sensor, linear regression analysis was conducted on the

aggregate of all bioaerosols. Table B5 presents the linear regression results for concentrations in 5-20/cm^3 range and the corresponding calibration equations. IC Sentinel and OPC N2 with R^2 values of 0.95 and 0.92 showed good performance, while Speck and Dylos have low R^2 values of 0.59 and 35, respectively.

All the tested bioaerosols are important in asthma, however, the relative importance of these bioaerosols varies in different regions of the world (Ormstad, 2000). In the UK, dust mite a significant source of asthma sensitization (Mygind et al., 1996), while in Scandinavia, mite allergens are not of significant concern. In Sweden, allergens in cat and dog fur and pollen are more prevalent than dust mite and also found to be common cause asthma sensitization in children (Croner and Kjellman, 1994; Munir, 1994). Therefore, depending on the building location, specific allergen carrier particles could be of monitoring interest. In regions where a specific bioaerosol is the target of PM monitoring, bioaerosol-specific calibrated sensors in those microenvironments could be applied. However, regardless of having an identified particle for monitoring target or not, PM sensors are exposed to various particles of different type and size. Hence, calibrating sensors with a combination of particles existing at the monitoring site microenvironment yields more realistic results for practical application.

Table B5. Linear calibration equations developed from tested bioaerosols (dust mite, pollen, cat fur, and dog fur) in 5-20/cm^3.

Low-cost sensor	**Linear Regression analysis results**				**Linear calibration equation**
	FB (#/cm^3)	PB	R^2	RMSE (#/cm^3)	
OPC N2	-4.918	1.319	0.920	1.663	$NC_{LCS,corrected} = 3.730 + 0.760\ NC_{LCS}$
IC Sentinel	-4.546	1.219	0.953	1.151	$NC_{LCS,corrected} = 3.728 + 0.820\ NC_{LCS}$
Speck	-0.176	0.063	0.593	0.222	$NC_{LCS,corrected} = 2.776 + 15.801\ NC_{LCS}$
Dylos	1.69E-5	3.25E-4	0.373	0.002	$NC_{LCS,corrected} = -0.052 + 3079.724\ NC_{LCS}$

B.4. Conclusion

This study tested 4 different low-cost OPC sensors with 9 particle batches of different types and sizes in a fully-controlled chamber environment. Ordinary least squares linear regression model was used to investigate the performance of the low-cost sensors (OPC N2, IC Sentinel, Speck, and Dylos) against the reference sensor (AeroTrak TSI). The linear regression analysis results indicated varying performance levels intra-sensors as well as intra-test conditions.

The effect of particle optical properties and size and the degree to which these parameters influence the sensors' response varies amongst the tested sensors. Therefore, none of these parameters can be dismissed and both size and optical properties of aerosols of interest merit due attention while calibrating the low-cost sensors. Showing more robust and higher R^2 values, OPC N2 and IC Sentinel presented superior performance than Speck and Dylos. In general, OPC N2 and IC Sentinel showed very similar performance across all test cases. These two sensors had slope values of closer to 1, indicating that when used uncalibrated, they provide more accurate measurements compared to Speck and Dylos.

Particle concentration level was the most influential factor on the sensor response linearity in relation to the reference sensor measurements. In low concentration ranges, low-cost sensors showed a non-linear response. For concentration ranges of above a specific threshold, low-cost sensors exhibited a linear response. The dividing line between low and high concentration regions ($5/cm^3$) where non-linear and linear responses occurred matched closely for the tested bioaerosols.

Examining low-cost PM sensors' performance showed that these sensors can provide promising measurement data with close agreement to the lab-grade sensor if they are calibrated for specific application conditions. The calibration curves for each low-cost sensor varies depending on the particle type, size, and concentration. Therefore, it is suggested to calibrate the

low-cost PM sensors for the specific particle of interest and the specific site conditions before deployment.

Despite the higher accuracy of particle-specific calibrated sensors, in most field PM exposure monitoring applications, sensors are exposed to a combination of PM, and not to isolated batches of specific particle type and size. Subsequently, although the highest precision would be provided by using particle-specific and size-specific calibration curves, using such calibration curves is not actually practical when it comes to field applications. The findings of this study showed promising results in terms of using linear calibration curves that work well for monitoring common indoor bioaerosols in particle number concentration range of $5/cm^3$ - $20/cm^3$.

This study tested the sensors under temperature and relative humidity levels representative of the conditioned indoor environment. Further investigation of these low-cost sensors' performances under varying temperature and relative humidity levels is suggested for future studies.

Acknowledgements

This research was funded by ASHRAE (American Society of Heating, Refrigerating, and Air-conditioning Engineers) Graduate Student Grant-in-aid. Authors would like to acknowledge the assistance of former lab manager of Penn State Architectural Engineering Department at the time this experiment was conducted, Mr. Paul Kremer, as well as the undergraduate research assistants who helped with conducting the experiments during their research experience training, Mr. Sean Michael Eagan, and Ms. Camilla Victoria McCrary.

B.5. Supplementary Information (SI)

B.5.1. Combined effects of particle size, type (optical properties), and concentration

To examine the combined effects of particle size and concentration, the low-cost sensors' response to varying concentrations of two different sizes of the same monodisperse particle type were inspected. Figure B8 shows the variation of sensors' response to quartz and MF-R particles in 1 and 2.8 sizes. To investigate the combined effect of particle type and concentration on the sensors' performance, the response of low-cost sensors under exposure to varying concentrations of two different monodisperse particles of the same size is examined. Both monodisperse particles are round in shape; therefore, their difference in refractive index could be referred to as the cause of possible particle type effect on the tested light-scattering based sensors responses.

B.5.1.1. Speck

Speck readings in all test cases demonstrate a curvilinear relationship with the reference sensor until it reaches a saturation point followed by an inverse curvilinear relationship with the increase in particle concentration. The concentration level at which Speck becomes saturated seems to be a function of particle size (Figure B8). The larger the particle size is, the lower the concentration saturation point is. It is usually expected of PM sensors to reach a plateau in their measurement after saturation. However, in case of Speck, not only it fails to show the increasing rates of PM levels after saturation, but also it starts following a downward trend of reporting lower concentration values with further increase in particle concentration. Manikonda et al. (2016) observed a similar trend when comparing the PM2.5 mass concentration ($\mu g/m^3$) levels calculated

from measurements by Speck versus Aerodynamic Particle Sizer (APS3321, TSI). Likewise, Wang et al. (2015) observed a curvature in the DSM sensor (the PM sensor used in Speck) response in higher concentration levels. A saturation concentration of 4 mg/m^3 was detected when testing Speck with incense particles against reference sensor (SidePak). Least squares linear regression of DSM response against the SidePak at 100, 300, and 1000 $\mu g/m^3$ concentration levels had R^2 values 0.9506, 0.9755, and 0.8914, and slope values of 159, 119, and 59.7, respectively.

Besides affecting the saturation point, particle size seems to have an effect on the Speck's linearity of response too. Both quartz and MF-R particles in 1 µm test cases present a more linear response pattern than 2.8 µm test cases for Speck sensor (Figure B8).

Figure B9 shows MF-R particles have higher number concentration representation by Speck sensor than quartz particles –for both sizes- due to the higher refractive index of MF-R. This effect of particle optical property on the Speck response is more pronounced for the larger particle size of 2.8 compared to 1 µm. Wang et al. (2015) found a similar effect of particle size on DSM501A sensor response; DSM501A sensor measured a higher concentration with increase in PSL particles size (300, 600, and 900 nm). Another study by Sousan et al. (2017) observed that depending on the tested particle type, Speck response varied significantly; nonlinear for NaCl and logarithmic for ARD, while fairly linear for welding fume particles.

Comparing the linearity range and patterns of Speck's responses to different tested particles (Figures B8 and B9) implies an overall stronger influence of particle size than type.

B.5.1.2. Dylos

Dylos measurements seem to have a curvilinear pattern with various changing points. However, the curvature in its pattern seems to be less than that in the Speck sensor. Dylos failed to record

data during the 2.8 µm quartz test. Therefore, the effect of particle size on Dylos's response could be explored by comparing only MF-R particles in 1 and 2.8 µm test cases (Figure B8). At the same concentration level measured by the reference sensor, Dylos reports a higher number concertation for 2.8 µm than 1 µm MF-R. Besides particle size, Dylos response is affected by the aerosol optical properties as well. As shown in Figure B9, for the same aerosol size of 1 µm, MF-R number concentration is reported higher than quartz. This effect of particle type can be inferred to the higher refractive index of MF-R (1.68) compared to quartz (1.5) particles. The Dylos response to MF-R and quartz particles of 1 µm are closer compared to 1 and 2.8 µm MF-R particles, indicating a stronger influence of particle size rather than optical properties. The results of this study confirm previous chamber assessment of this sensor, which showed its particle type dependence. Manikonda et al. (2016) compared the number concentration (#/cm^3) of particles smaller than 2.5 µm measured by Dylos (DC100 Pro) versus the APS3321 for cigarette smoke and Arizona test dust (ATD) particles. The linear regression model slope for cigarette and ATD particles were 0.054, and 0.44 respectively. It should be noted that they used an aerodynamic particle sizer as reference sensor which is inherently different from the reference sensor of this study.

B.5.1.3. IC Sentinel

The comparison of IC Sentinel response to 1 and 2.8 µm quartz particles depicts a significant effect of particle size, whereas such size effect is not observed for MF-R particles of the same sizes. Refractive indices of MF-R and quartz particles are 1.68 and 1.5, respectively. IC Sentinel's response to quartz particle with the lower refractive index is size dependent, while for MF-R with higher refractive index, its response does not vary significantly with size. These patterns imply the interrelatedness of particle type and size effects on IC Sentinel response. At the

time of writing this paper, no previous studies on IC Sentinel are available to which we can compare our results.

B.5.1.4. OPC N2

OPC N2 failed to record data during the MF-R (1 and 2.8 µm) and quartz (1 µm) tests. The reason for this data collection is unknown to the authors. Since this incident happened in repetition testes of different particles, regardless of particle type, size, shape, or optical properties, it could not be concluded that OPC N2 was failing to respond to a specific particle type or size. Authors speculate that an error in the sensor data logging software could be the culprit. To be able to examine the effect of particle size on OPC N2, its response to monodisperse 2.8 µm quartz is compared to another test case with polydisperse quartz particles (Figure B8). OPC N2 shows a fairly linear response to polydisperse quartz particles, while under exposure to 2.8 µm quartz particles shows a nonlinear response for concentration levels of up to ~30/cm3, and then a linear response for higher concentration levels. The results of this study are in agreement with the previous test of OPC N2 by Sousan et al. (2016). They observed significant variation in the slope of OPC N2 response to fine and welding fume and Arizona road dust particles which vary considerably in size.

OPC N2's response to 2.8 µm quartz is very similar to IC Sentinel. Both OPC N2 and IC Sentinel seem to have a linear response as the particle concentration goes higher than specific thresholds – depending on the particle type and size- and the response to different tested particles converge as the concentration level increases. This convergence pattern indicates the possibility of developing linear calibration curves which could be more robust with respect to particle type and size variation.

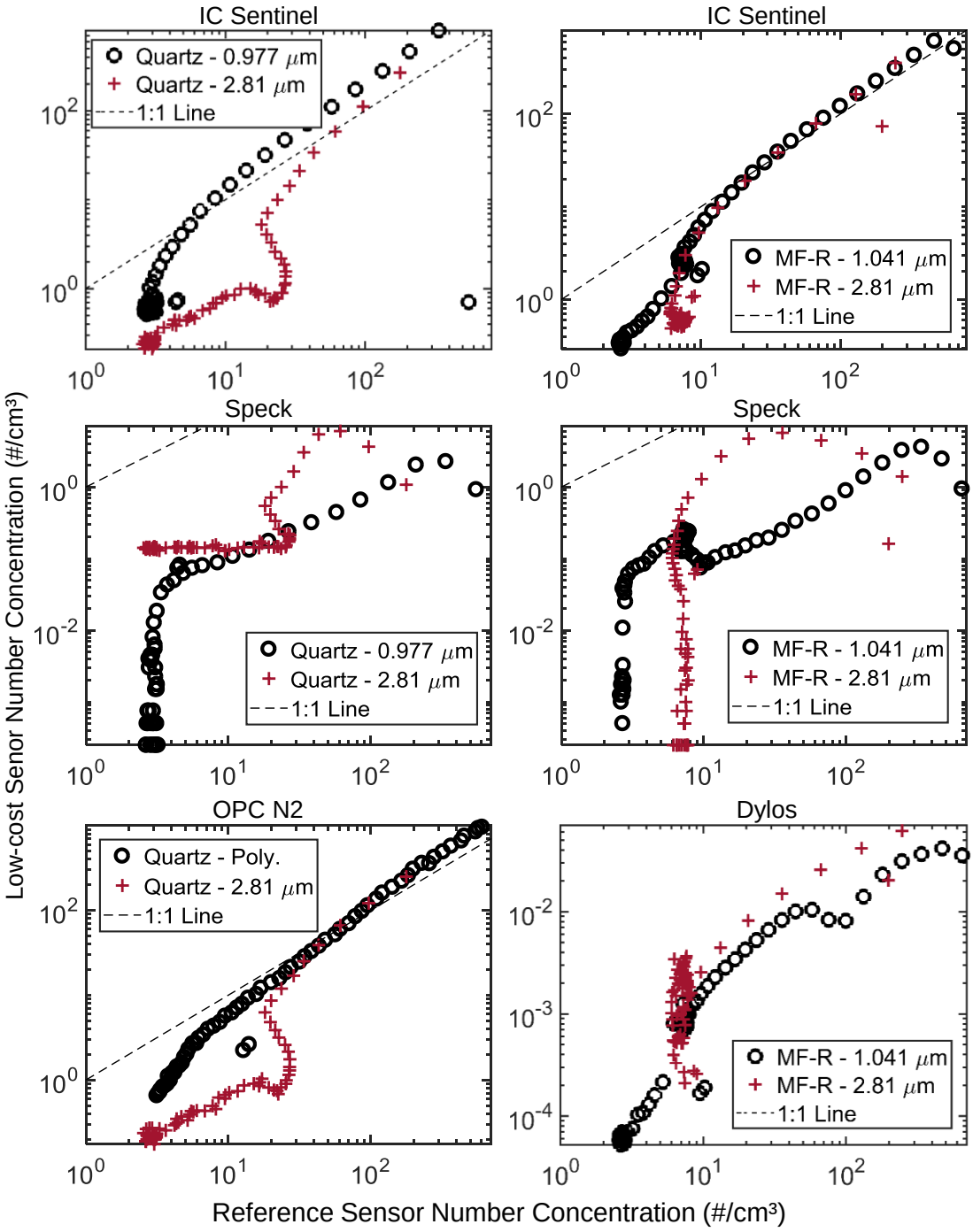

Figure B8. The combined effect of particle size and concentration on the response of the tested sensors in relation to the reference sensor.

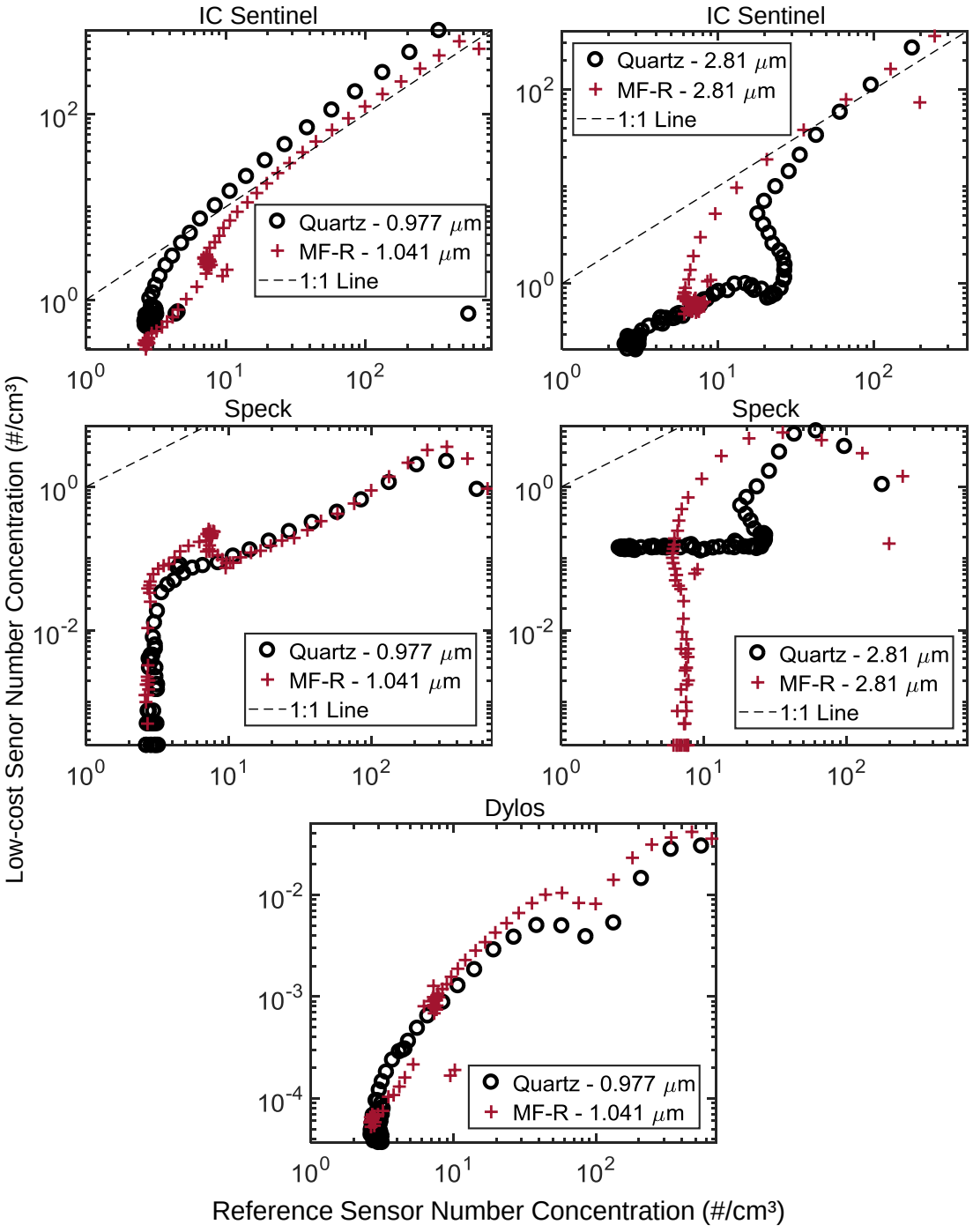

Figure B9. The combined effects of particle type and concentration on the response of the tested sensors in relation to the reference sensor.

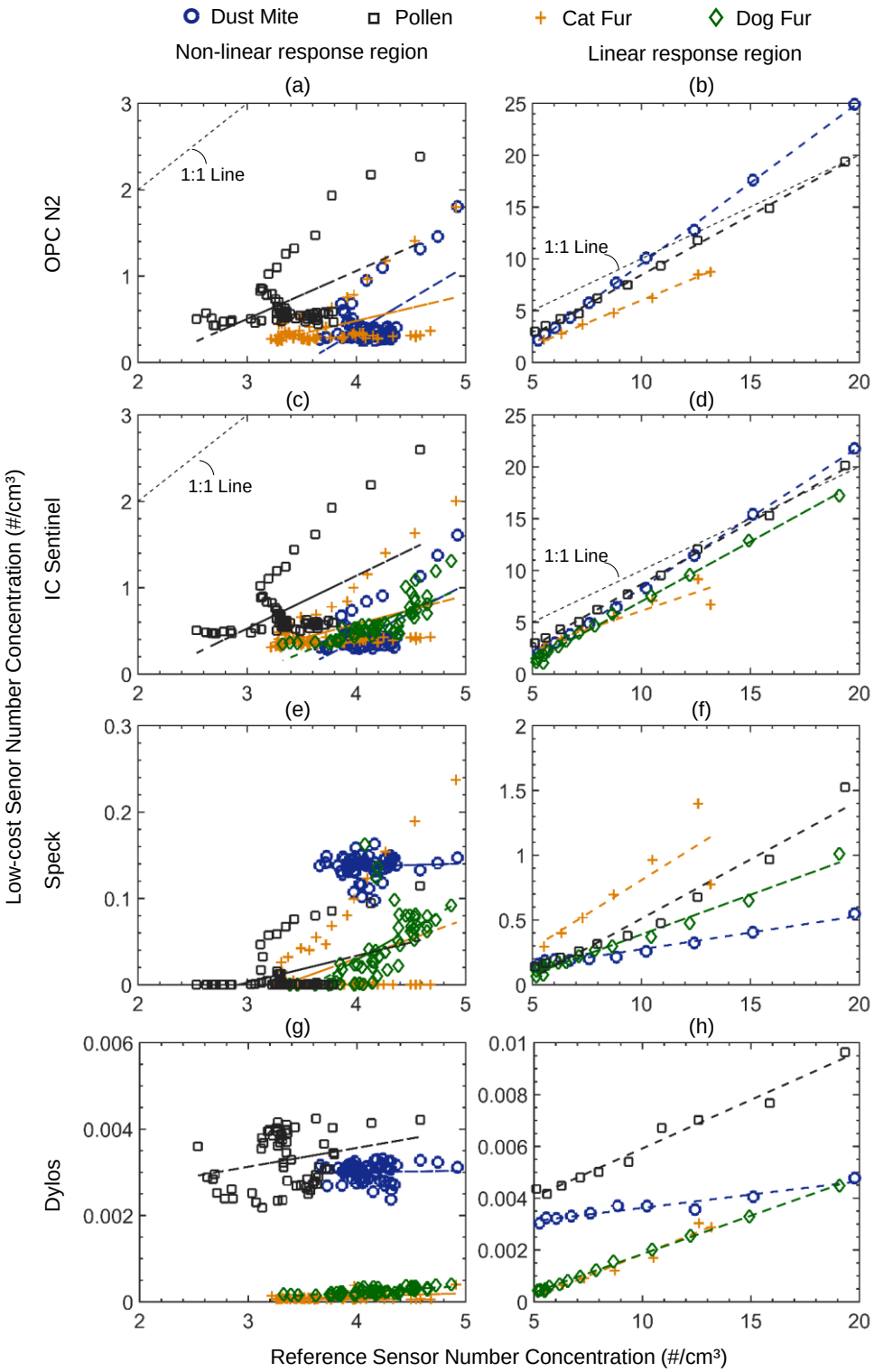

Figure B10. Particle number concentrations measured by low-cost sensors (y-axis) versus the reference sensor (x-axis). Subplots in the left column (a, c, e, and g) represent the non-linear response region (0-5/cm^3). Subplots in the right column (b, d, f, and h) represent the linear response region.

Table B6. Summary of regression model results for the different tested bioaerosols comparing each low-cost sensor to the lab-grade sensor.

Particle type	Concentration range* (#/cm^3)	OPC N2				IC Sentinel			
		FB** (#/cm^3)	PB***	R^2	RMSE (#/cm^3)	FB (#/cm^3)	PB	R^2	RMSE (#/cm^3)
Dust mite	0-5	-2.643	0.751	0.320	0.250	-2.193	0.645	0.342	0.204
	5-20	-6.105	1.561	0.999	0.225	-5.388	1.366	0.999	0.194
Pollen	0-5	-1.165	0.556	0.248	0.350	-1.308	0.611	0.274	0.360
	5-20	-3.083	1.151	0.998	0.276	-3.303	1.196	0.998	0.255
Cat fur	0-5	-0.710	0.298	0.213	0.244	-0.740	0.330	0.213	0.272
	5-20	-2.766	0.875	0.997	0.146	-1.036	0.713	0.850	0.987
Dog fur	0-5	N/A				-1.533	0.508	0.645	0.131
	5-20					-4.528	1.154	0.997	0.278
Particle type	**Concentration range* (#/cm^3)**	**Speck**				**Dylos**			
		FB** (#/cm^3)	PB***	R^2	RMSE (#/cm^3)	FB (#/cm^3)	PB	R^2	RMSE (#/cm^3)
Dust mite	0-5	0.123	0.003	0.004	0.013	-2.193	0.645	0.342	0.204
	5-20	0.016	0.026	0.974	0.021	-5.388	1.366	0.999	0.194
Pollen	0-5	-0.091	0.031	0.161	0.026	-1.308	0.611	0.274	0.360
	5-20	-0.404	0.091	0.961	0.091	-3.303	1.196	0.998	0.255
Cat fur	0-5	-0.151	0.045	0.176	0.042	-0.740	0.330	0.213	0.272
	5-20	-0.244	0.105	0.708	0.223	-1.036	0.713	0.850	0.987
Dog fur	0-5	-0.259	0.072	0.402	0.031	-3.55E-4	1.44E-4	0.523	4.80E-5
	5-20	-0.225	0.061	0.983	0.035	-1.12E-3	2.96E-4	0.998	5.09E-5

*: as measured by the reference sensor
**: fixed bias, intercept of the regression model
***: proportional bias, slope of the regression model

Appendix C

Paper 3. An Experimental Comparison of Aerodynamic and Optical Particle Sensing for Indoor Aerosols

Graphical Abstract

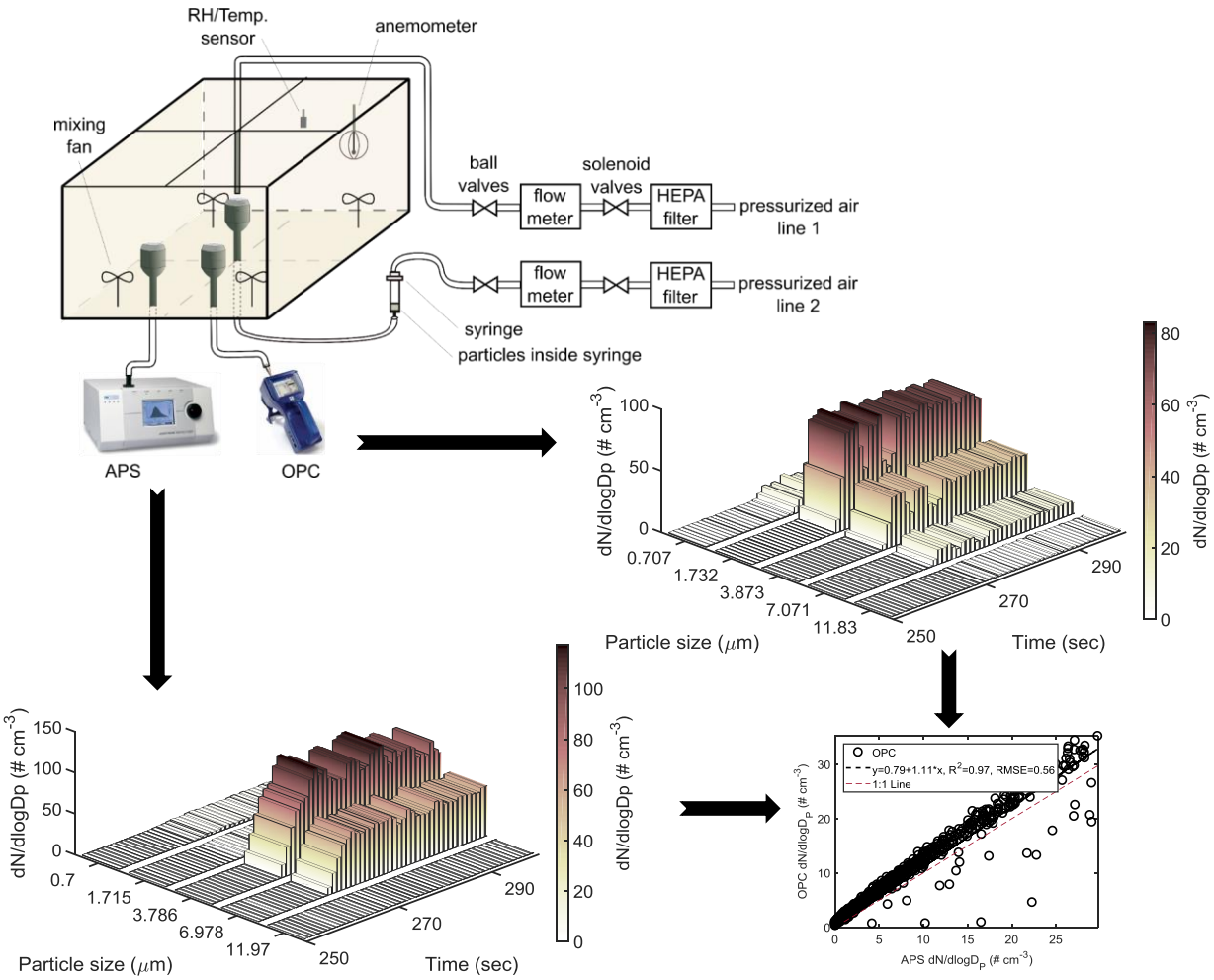

Abstract

Particle size is one of the most influential factors in particle transport and human exposure. A number of studies have investigated the relationship between optical and aerodynamic particle size. However existing literature is inconclusive due to limited available data on particles with varying size distribution, shape, density, and optical characteristics. The objective of this study is to experimentally investigate the relationship between optical and aerodynamic sizing techniques for a wide range of biological and monodisperse particles.

Biological particles included cat fur, dog fur, *Bacillus thuringiensis* spore, pollen, dust mite and monodisperse particles involved silica, melamine resin, and methyl methacrylate in the range of 1- 10 µm. In addition, NIST indoor reference dust, quartz, and aluminum oxide particles were used as reference particles. Each particle was dispersed into a dispersion chamber (76×76×42 cm) with a computer-controlled syringe injection system. Particle sizes and concentrations were simultaneously measured by aerodynamic particle sizer (APS3321, TSI) and optical particle counter (Handheld AeroTrak OPC, TSI).

Comparison between APS and OPC results showed that the relationship between optical and aerodynamic diameters strongly depends on the particle size itself for all tested particles with varying shape factors, density, and refractive indices. Generally, OPC measures a higher number count compared to APS in smaller size bins whereas as size bin increases this relationship is reversed. The cut point at which the inverse proportion of OPC and APS is happening increases from about 1 to 3 µm with respect to the size of the tested particle. This study further investigates the relationship between the APS and OPC measurements across various particle size fractions using linear regression analysis. Linear regression analysis results showed that the relationship between the APS and OPC measurements is both particle-dependent and size-dependent. This finding implies that researchers should avoid the interchangeable use of aerodynamic and optical particle sizing technique results without prior calibration of the optical sensor with the aerodynamic sensing device. Linear calibration equations to convert the optical size measured with OPC to aerodynamic size is provided for all sixteen tested particles for three

size brackets; total particles counted across all size bins of the sensors, particles smaller than 10 µm, and particles smaller than 2.5 µm.

Keywords

Aerodynamic equivalent diameter, optical particle counter, monodisperse particles, bioaerosols, particulate matter exposure.

C.1. Introduction

Exposure to respirable aerosols is linked to adverse health effects (Goldsmith, 1999; Pope III et al., 2002). In order to effectively control the exposure to particulate matter (PM), particulate matter size-resolved concentration should be accurately monitored, for particle size is one of the most influential factors in PM exposure field. One of the main challenges in particle size characterization is that particles are rarely of spherical shape. Therefore, to be able to characterize their size, equivalent sphere diameter sizes are defined for various practical purpose and application, such as volume equivalent diameter and aerodynamic equivalent diameter. It should be noted that, in PM exposure study applications, when PM size is discussed, it is referred to the aerodynamic equivalent size. PM resuspension, deposition, and transport is a function of particle aerodynamic size (Salimifard et al. 2017). PM filtration and removal mechanism are particle aerodynamic size dependent (Kasper et al., 2009; Stafford and Ettinger, 1972). Similarly, penetration of PM into the human body is a function of particle aerodynamic size; the smaller the particles are the deeper they can penetrate into the human body through respiratory system (Heyder, 2004).

Aerodynamic equivalent diameter size is the size of a spherical particle with unit density (density of water, 1 g/cm^3) that would have the same settling velocity as the actual particle. To measure the aerodynamic equivalent diameter size, two types of devices are used; cascade impactors, and time-of-

flight devices. Cascade impactors provide the aerodynamic size distribution of the measured particles; however, it does not provide temporal measurement. On the other hand, time of flight devices provide real-time size-resolved number concentration of the measured particles.

It is common practice in research (Salimifard et al., 2015) as well as field applications (Castell et al., 2017; Kumar et al., 2016a) to use optical-based sensors (mostly optical particle counters, OPC) to measure the PM size, in cases where the aerodynamic size is the measurement goal. The issue with such practice is that not only the optical and aerodynamic sensors have fundamentally different measurement principles, but also the relationship between their measurement results is not yet fully understood. Several researchers have investigated the relationship between the optical and aerodynamic based sensors measurements. Reponen et al. (2001) Compared different methods of size measurement for four fungal species (Penicillium brevicompactum, Penicillium melinii, Cladosporium cladosporioides, and Aspergillus versicolor) and two actinomycete species (Streptomyces albus and Thermoactinomyces vulgaris). They used three microscopic methods to measure the spore sizes: using optical microscope from stained (wet) slides, optical microscope from unstained (dry) slides, and environmental scanning electron microscope (SEM) directly from microbial culture. An aerodynamic particle sizer (APS) was used to measure spore's aerodynamic diameter. Their results showed that there was no clear trend in the relationship between aerodynamic and physical diameter measured with any of the three microscopic methods. Another experimental study by Peters et al. (2006) compared size measurement response of two OPCs (Grimm 1.108 and 1.109) and a and an APS (TSI 3321). They tested three sizes of monodisperse (polystyrene latex spheres in 0.83, 1.0, and 3.0 μm) particles and polydisperse Arizona test dust. They found that that the number counts measured by OPC were higher than that of measured by APS for monodisperse PSL spheres, while the number and mass concentrations of polydisperse Arizona test dust were different depending on the particle size. A recent study by (Chien et al., 2016) examined the conversion equation that could correlate the volume equivalent diameter measured by OPC to the aerodynamic diameter size measured by APS. They tested monodisperse particles of oleic acid, and

sodium chloride with refractive indices of 1.46 and 1.54 respectively. They found that despite the common assumption that optical diameter represents the volume equivalent diameter, this assumption does not hold true for particles with a different refractive index than PSL particle that is used to calibrate the optical sensors. In addition to the effect of refractive index, they found the irregularity of particle shape to also influence the optical sensor measurement. All these studies suggested for further experimental study with additional particles to shed more light on the relationship between aerodynamic and optical size measurement.

Due to limited and inconclusive results in the literature, the objective of this study is to investigate the relationship between optical and aerodynamic size measurement for a wide spectrum of monodisperse and polydisperse aerosols.

C.2. Methods

Size-resolved particle number concentrations simultaneously measured by APS and OPC sensors were compared against each other. Tested aerosols were sampled from a controlled environmental chamber with various aerosol types, sizes and concentration levels. The following sections describe details of data collection (section C.2.1.), sensors specifications (section C.2.2.), tested particles characteristics (section C.2.3.), and data analysis method (section C.2.4.).

C.2.1. Test chamber set-up and experimental protocol

The laboratory experimental set-up used for this experiment is shown in Figure C1. A 0.76 × 0.76 × 0.42 m particle dispersion chamber was used to disperse and sample the tested particles from a controlled environment. A computer-controlled injection system was designed to inject the particles into the chamber. Two separate lines (line 1 and line 2) of pressurized air flew through HEPA filters (TSI,

Inc., Shoreview, MN) and the particle-free air was sent to ball valves and then solenoid valves (see Figure C1). Ball valves were used to modulate the airflow rate passing through each line. Solenoid valves were controlled by a computer program to open and close the airflow lines. There is a flow meter after each solenoid valve that measures the airflow rate in each line. Particle-free air (line 1) was supplied to chamber via an inlet at the top center of the chamber, while particle-free air in line 2 was sent to a syringe containing test particles and then the test particles were injected into the chamber through an inlet (TSI, Inc., Shoreview, MN) at the bottom center of the chamber. The particle-laden and particle-free air streams collided and dispersed the particles in the chamber, while four mixing fans were running at the four corners of the chamber to ensure a well-mixed condition in the chamber.

Relative humidity (RH) and temperature of the air inside the chamber were measured with a probe sensor (HMT100, Vaisala), while air velocity inside the chamber is measured with an anemometer (Model, manufacturer). Location of the RH, temperature, and anemometer sensors are shown in Figure C1.

Sixteen 2.5-hour particle-decay test cases were conducted. Each test was performed using the following six steps:

1) Before each test, all surfaces inside the chamber as well as the particle injection line were thoroughly cleaned and washed to remove any residual particles from previous tests.
2) The specific amount of test particles needed to create the desired maximum particle number concentration in the chamber was calculated, measured, and added to the syringe.
3) Particle-free air at a volumetric flow rate of 9 L/min was supplied to the chamber for at least 30 minutes to flush the chamber until the reference PM sensors report PM counts of close to zero. Four mixing fans were running at the four corners of the chamber to achieve a well-mixed condition.
4) Background measurement was performed by all sensors (minutes 0 to 5 of the test).

5) A signal was sent to the solenoid valve in line 2 to supply 18 L/min of filtered airflow to the syringe and inject the particles into the chamber for 2 minutes (minutes 5 to 7 of the test).

6) The solenoid valve in line 2 was closed and the particles decay started. Particle concentration was monitored until it reached the background level again (minutes 7 to 150 of the test).

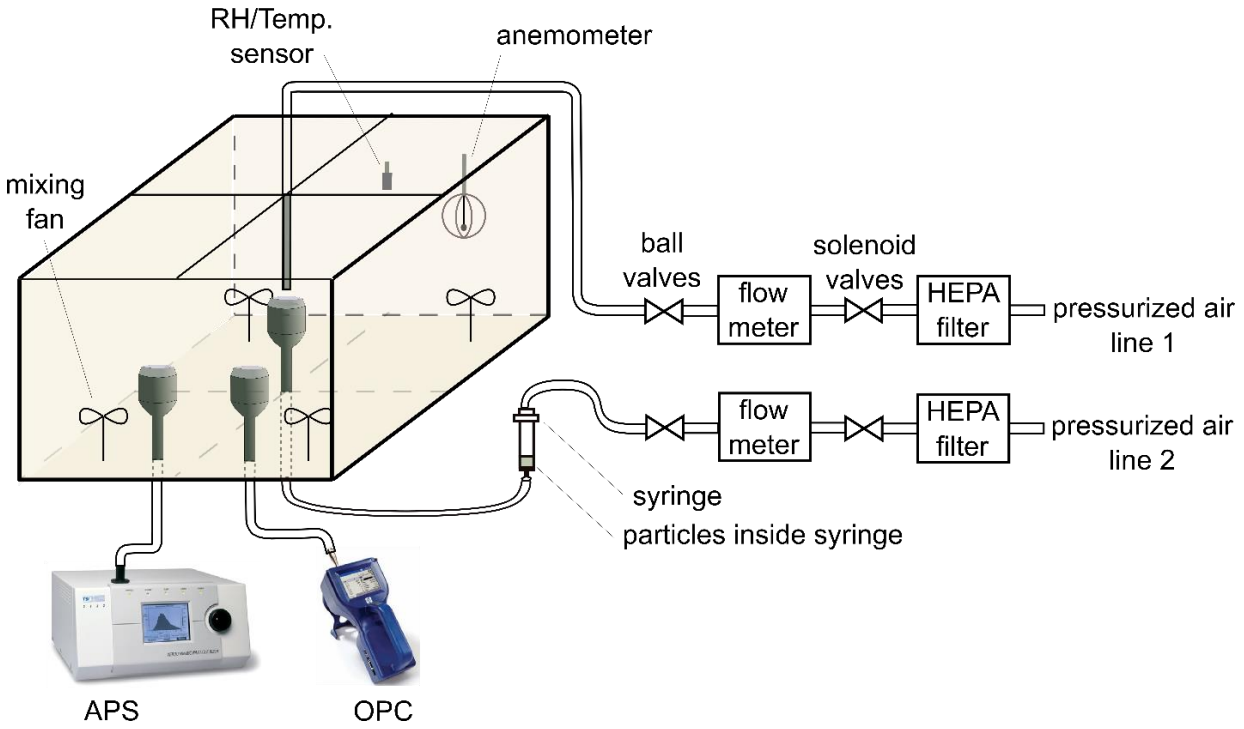

Figure C1. Schematic of the chamber set-up, particle injection and sampling, and the sensors' location.

C.2.2. Sensor specifications

To investigate the relationship between the aerodynamic and optical sensing, an aerodynamic particles counter (APS, TSI 3321, TSI, Inc., Shoreview, MN) and an optical particle counter (Handheld AeroTrak, TSI 9306, TSI, Inc., Shoreview, MN) are used. Figure 2 shows the picture of these two sensors and Table C1 summarizes the characteristics and specifications of these sensors as provided by their manufacturer.

Table C1. Sensors' specifications as reported by the manufacturer

Sensor	Measurement type	Light source wavelength (nm)	Detection size range (µm)	# of bins	Bin size cuts (µm)	Flow rate (L/min)	Time resolution (sec)	Detection concentration range
AeroTrak (TSI 9306)	optical – particle count	785 [1]	0.3-14		0.3, 0.5, 1.0, 3.0, 5.0, 10.0	2.83	1	3×10^6 particles/ft^3 at 5% coincidence loss
APS (TSI 3321)	aerodynamic – particle count	658	0.5-20	2	0.523, 0.542, 0.583, 0.626, 0.673, 0.723, 0.777, 0.835, 0.898, 0.965, 1.037, 1.114, 1.197, 1.286, 1.382, 1.486, 1.596, 1.715, 1.843, 1.981, 2.129, 2.288, 2.458, 2.642, 2.839, 3.051, 3.278, 3.523, 3.786, 4.068, 4.371, 4.698, 5.048, 5.425, 5.829, 6.264, 6.732, 7.234, 7.774, 8.354, 8.977, 9.647, 10.37, 11.14, 11.97, 12.86, 13.82, 14.86, 15.96, 17.15, 18.43, 19.81	sample flow rate: 1, total flow rate: 5	1	0.001 - 1000 particles/cm^3

1: enhanced active cavity HeNe laser.

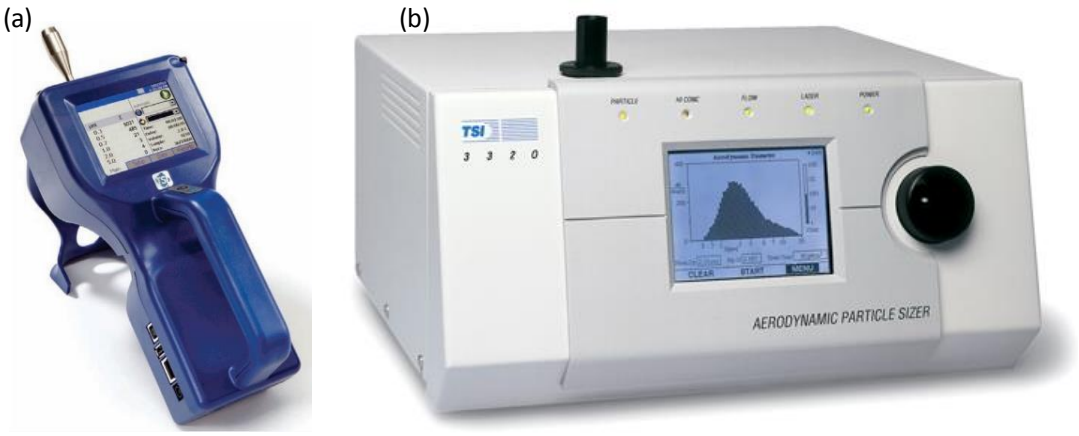

Figure C2. Sensors used in this study: (a) Handheld AeroTrak (TSI), (b) APS3321 (TSI).

C.2.3. Tested particles characteristics

Sixteen different particle batches of various size and composition are tested in this experimental study. These particles include eight monodisperse particle batches and eight polydisperse ones. Monodisperse particles (microParticles GmbH, Berlin, Germany) are poly methyl methacrylate (PMMA-R) in 5.1 and 9.9 µm, melamine resin (MF-R) in 1.041, 2.81, and 10.55 µm, and silicon dioxide –also known as silica or quartz- (SiO_2-R) in 0.977, 2.81, and 5.04 µm. There are eight polydisperse particle batches including both non-biological and biological particles. The non-biological particles are quartz (crushed quartz #10 bt#4339, Particle Technology Limited, UK), and aluminum oxide (Al_2O_3). The biological particles include pollen, dust mite (Indoor Biotechnologies Inc., Charlottesville, VA, USA), dog fur, cat fur, *Bacillus thuringiensis* (BT) spore, and NIST indoor dust. The preparation of cat fur and dog fur dust particles is described in a previous study (Salimifard et al., 2017b). The physical properties of each tested particle are summarized in Table C2.

Table C2. Tested particles' characteristics

Particle type	Size distribution type	Size range (µm)	Biological / Non-biological	Density (kg/m^3)	Shape	Roughness	Refractive Index	Hydrophobicity
poly (methyl methacrylate) (PMMA-R)	monodisperse	5.1 ± 0.13[1], 9.9 ± 0.22[1]	non-biological	1190	spherical	smooth	1.48 [h,i]	hydrophobic
melamine resin (MF-R)	monodisperse	1.041 ± 0.03[1], 2.81 ± 0.06[1], 10.55 ± 0.14[1]	non-biological	1510	spherical	smooth	1.68 [i]	hydrophilic
silicon dioxide (SiO2-R)	monodisperse	0.977 ± 0.026[1], 2.81 ± 0.1[1], 5.04 ± 0.2[1]	non-biological	1850	spherical	smooth	1.42 [i]	hydrophilic
crushed quartz (>95% of SiO_2)	polydisperse	0.58-22.5	non-biological	2650	varied [3]	smooth	1.544 [g]	hydrophilic
aluminum oxide (Al_2O_3)	polydisperse	-	non-biological	3950	-		1.768 [a]	-
pollen	polydisperse	-	biological	1000	near spherical [l]		1.5 [b]	-
dust mite	polydisperse	0.58-48	biological	1140	rounded [2]	smooth	-	hydrophilic
dog fur	polydisperse	0.58-351	biological	1000	fibers	rough	1.37-1.55 [d]	hydrophobic
cat fur	polydisperse	0.58-409	biological	1000	fibers	rough	1.35-1.43 [d]	hydrophobic
Bacillus thuringiensis (BT) spore	polydisperse	0.58-56.2	biological	1000	round	smooth	1.84 [e]	hydrophobic [k]
NIST indoor dust	polydisperse	-	-	-	-	-	-	-

1: size ± standard deviation, 2: with prismatic edges resulted from the ball mill crushing effect, 3: varied from squares to rectangles (5/1 ratios maximum).
a: (Weber, 1986), b: (Gullvåg, 1964), d: (Yan et al., 2015), e: (Fromentin et al., 2008), g: (Hinds, 2012), h: (Sultanova et al., 2009), i: as provided by the manufacturer, j: (Radhakrishnan, 1947), k: (Koshikawa et al., 1989; Tufts et al., 2014), l: (Hinds, 2012).

C.2.4. Data analyses

Size-resolved normalized number concentration distribution of the tested particles is developed from both APS and OPC measurement at each sampling time. To compare the size distribution profiles captured by the two sensors, first, the time at which the sampled aerosols have the peak number concentration during that test is identified. This peak number concentration moment usually happens around the injection period. After injection period, particle concentration inside chamber decays and therefore the size distribution of the sampled aerosols would deviate from the parent particle batch and shift toward smaller sizes as time goes on during the concentration decay period. Although, the objective of this study is solely comparing the APS and OPC measurement if the same aerosol samples at any point in time and not the particle size distribution characterization, the peak concentration moment was preferably chosen for this comparison as it would be closer to the parent particle batch size distribution. It should also be noted that the size distribution profiles are developed based on the geometric mean (channel midpoints) of each size bin for both sensors.

APS measures the aerodynamic equivalent size of particles, while OPC measurements can be referred to as volume equivalent diameter size. Considering a constant density, it is assumed that aerodynamic equivalent size can be calculated from the volume equivalent size using the following equation.

$$D_{ae} = D_{ve}\sqrt{\frac{\rho}{\rho_0}} \qquad \text{(Equation C1)}$$

Where, D_{ae} is aerodynamic equivalent diameter, D_{ve} is volume equivalent diameter, ρ_0 is the unit density (1 g/cm^3), and ρ is the particle density. If this conversion equation holds true, the OPC size measurement should be equal to APS measurement divided by $\sqrt{\rho}$. After comparing the APS and OPC size distribution of tested aerosols o various size, density, and refractive indices at the peak number concentration moment, the relationship between the two sensors measurements across various particle

size fractions throughout each test is investigated using ordinary linear regression analysis. As aerodynamic size is the desired particle size variable, normalized number concentration measurements by APS and OPC are considered as independent and dependent variables, respectively (Equation C2). If there is a consistent relationship between the APS and OPC size measurements, it is expected that the linear regression analysis yields the same fixed (FB; intercept) and proportional (PB; slope) biases regardless of the tested particle properties. Finally, empirical linear conversion equations between the APS and OPC measurements for various particle size fractions is developed using Equation C3.

$$y = FB + PB \times x \qquad \text{(Equation C2)}$$

$$x = -\frac{FB}{PB} + \left(\frac{1}{PB}\right) y \qquad \text{(Equation C3)}$$

$$NNC_{OPC,ae} = -\frac{FB}{PB} + \left(\frac{1}{PB}\right) NNC_{OPC,ve} \qquad \text{(Equation C4)}$$

Where,

- *x* (independent variable) is the number concentration measured by APS ($\frac{dN}{dlogD_p}$, $\#/cm^3$),
- *y* (dependent variable) is the number concentration measurement of the low-cost sensor estimated by the linear regression model ($\frac{dN}{dlogD_p}$, $\#/cm^3$),
- *FB* is the fixed bias (intercept of the regression model) ($\frac{dN}{dlogD_p}$, $\#/cm^3$),
- *PB* is the proportional bias (slope of the regression model),
- $NNC_{OPC,ve}$ is the size (which is volume equivalent) resolved normalized number concentration measured by the OPC ($\frac{dN}{dlogD_p}$, $\#/cm^3$), and
- $NNC_{OPC,ae}$ is the aerodynamic equivalent size resolved normalized number concentration for OPC measurements calibrated by APS ($\frac{dN}{dlogD_p}$, $\#/cm^3$),

Three particle size fractions are selected as the focus of this study analysis; total particle size range being captured by the sensors, particles smaller than 10 µm, and particles smaller than 2.5 µm.

C.3. Results and Discussion

C.3.1. Size-resolved normalized number concentrations: effects of particle size, refractive index, and density

Size-resolved normalized number concentration profiles developed from APS and OPC measurement for each tested particle are presented in Figure C3 (monodisperse aerosols) and Figure C4 (polydisperse aerosols).

Comparing the size distribution plots of different sizes of the monodisperse particle type allows for probing the effect of particle size on sensors measurements. For 1.04 µm MF-R particles (Figure C3a), the particle size distribution reported by both sensors share a similar pattern. Both sensors report the same size mode, which is slightly higher than the aerosol size reported by the manufacturer. This larger size characterization could be due to the fact that these sensors are calibrated with PSL particles with a refractive index (1.59) smaller than that of the MF-R particles (1.68). For 2.81 µm MF-R particles (Figure C3c), APS reports a size mode of ~5 µm, while OPC reports the same size mode (~2 µm) it did for 1.04 µm MF-R particles. The difference in the number of size bins and the size bins width variation between the two sensors could be one of the contributing factors to the discrepancy between the size distribution profiles measured by APS and OPC sensors. OPC has a lower number of bins compared to APS. Both 1.04 and 2.81 µm particles would fall into the same size bin for OPC. Whereas, APS with a significantly higher number of bins is capable of capturing the size distribution with higher size resolution. Similarly, Figure 3-b and Figure C3d show the effect of size variation from 0.977 to 2.81 µm for silica (SiO_2) particles. The relationship between APS and OPC size distribution and its variation matches that of the MF-R particles.

The size distributions reported for 5 µm (Figure C3e and Figure C3f) and 10 µm (Figure C3g and Figure C3h) particles do not match the expected size modes. OPC size distribution for 5 µm particles does no report a monodisperse size and has more of a polydisperse pattern. For the same 5 µm particles, APS reports a polydisperse pattern for PMMA -with size mode of ~8 µm- and a bimodal pattern -with size modes of ~1 and ~8 µm- for silica. For 10 µm MF-R (Figure C3h), APS and OPC share similar size distribution pattern, considering their bin number and size width differences. Both sensors report a much smaller size mode of 2 µm which is significantly smaller than the 10 µm. Authors speculate that these larger tested particles of 5 and 10 µm might have broken into smaller particles during the particle injection and thus caused a polydisperse size distribution being captured by the sensors.

Although the size distribution measured by APS and OPC for 1 and 2.81 µm size are relatively close, for 5 and 10 µm sizes, their difference is higher and more substantial. This discrepancy could be related to the effect of particle density on the aerodynamic size measurement. Since APS measures the time of flight of particles at a high airflow velocity, the Reynolds number falls outside of Stokes regime and aerodynamic size measurement becomes density dependent. APS undersizes the particles with densities smaller than unit density (1 g/cm^3) and oversizes the particles with densities above unit density. This effect of density on the aerodynamic size measurement becomes more severe with a further deviation of measured particle density from 1 g/cm^3 and is more signified for larger particles (Wang and John, 1987). Although the proprietary stokes correction provided by the APS interface software was used to alleviate the effect of density, comparing the size distributions measured for increasing sizes of the monodisperse particle points out possible yet existing effect of density on size measurements, especially in larger particle sizes.

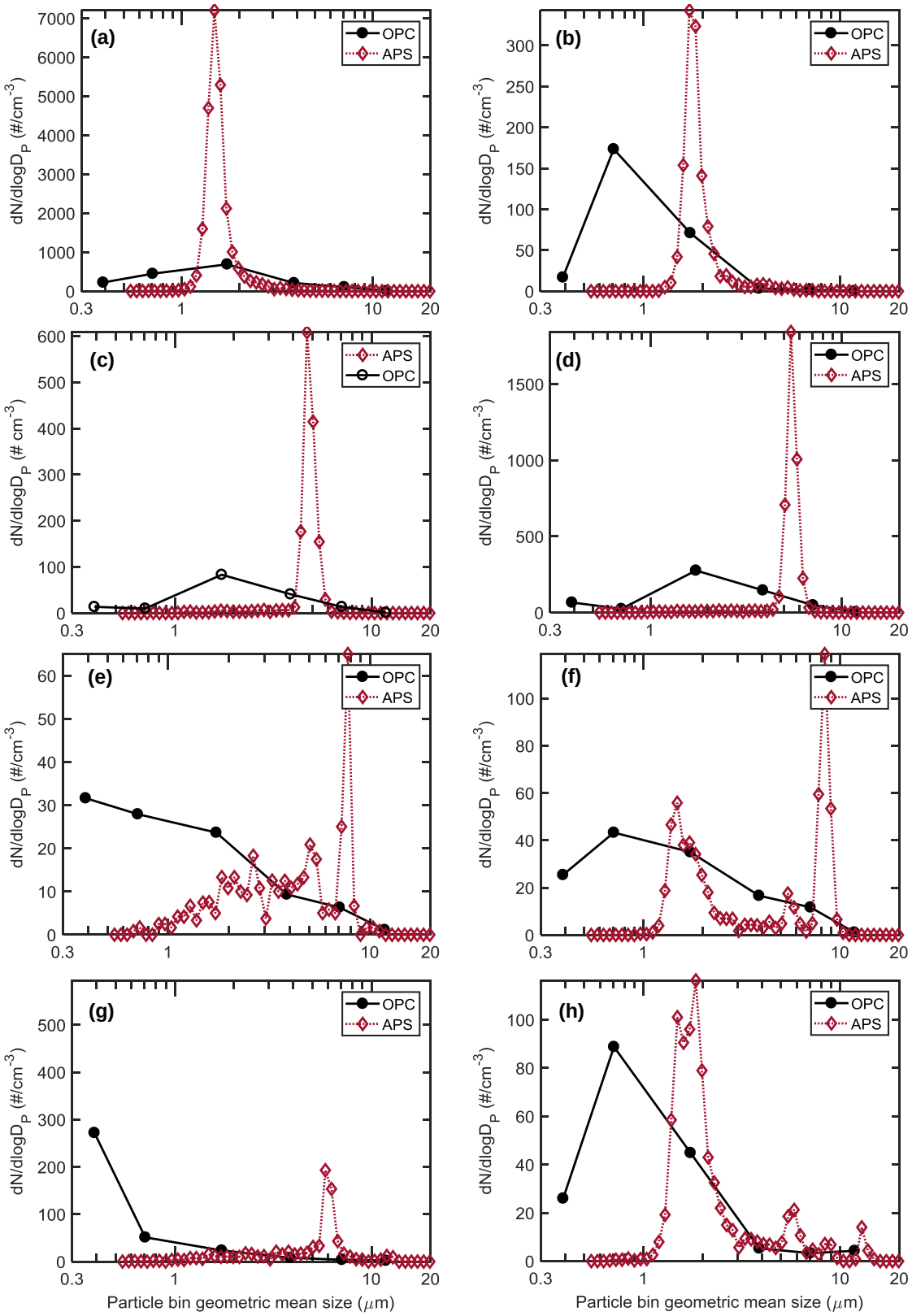

Figure C3. Size-resolved normalized number concentration distribution measured by APS and OPC sensors for monodisperse particles; a) MF-R in 1.041µm, b) SiO_2 in 0.977µm, c) MF-R in 2.81µm, d) SiO_2 in 2.81µm, e) PMMA-R in 5.1µm, f)SiO_2 in 5.04µm, g) PMMA-R in 9.9µm, h) MF-R in 10.55µm.

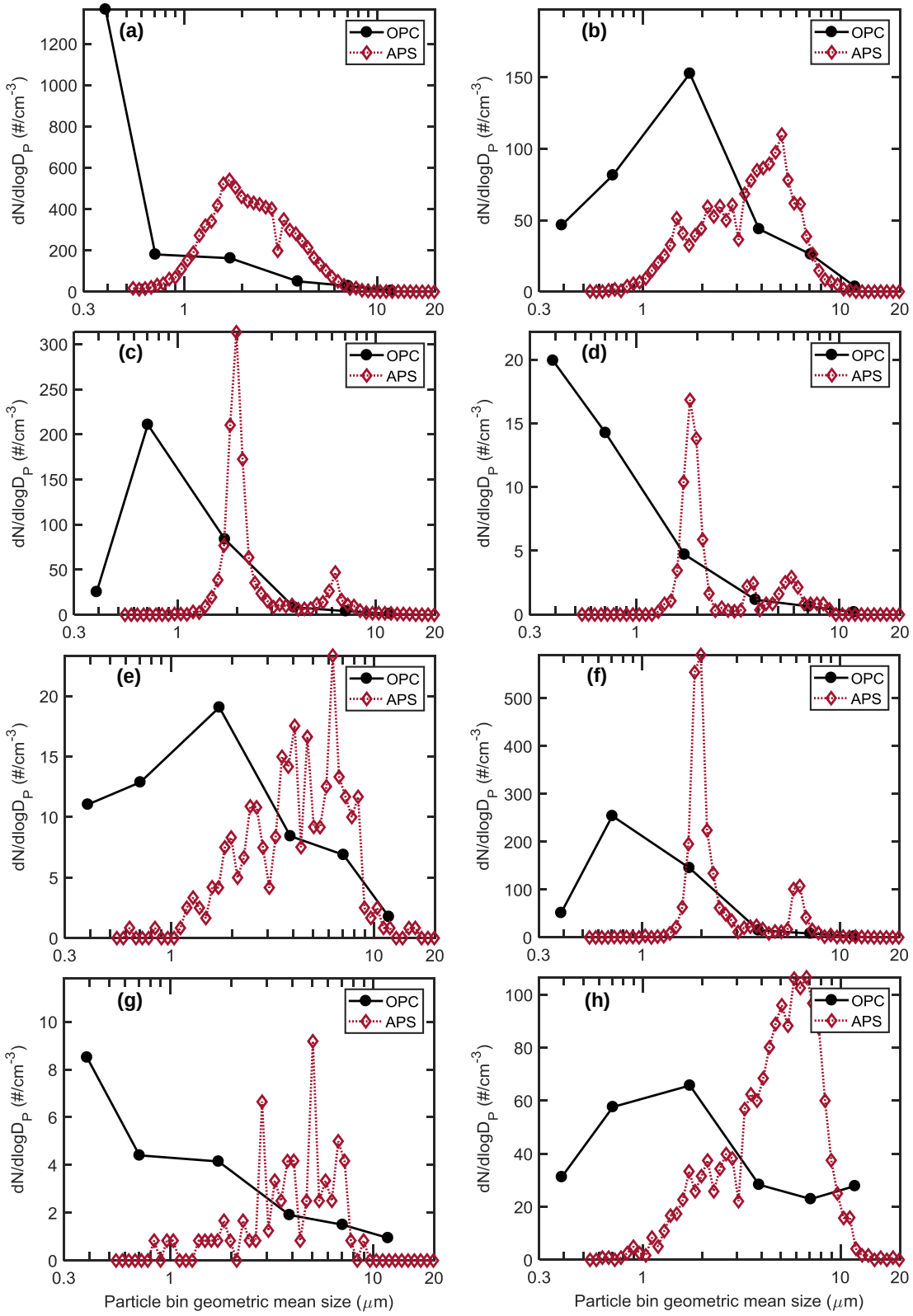

Figure C4. Size-resolved normalized number concentration distribution measured by APS and OPC sensors for polydisperse particles; a) quartz, b) aluminum oxide, c) dust mite, d) BT spore, e) pollen, f) NIST dust, g) cat fur, and h) dog fur.

C.3.2. Temporal particle concentration measurement

Figure C5 shows the normalized number concentration time-series profile of 2.81 µm MF-R simultaneously measured by APS and OPC during the background, emission, and decay periods. It can be seen that OPC reports a higher number concentration throughout the test. However, it should be noted the particle number concentration in this figure represents all of the counted particles across all size bins; this higher number concentration of OPC compared to APS does not hold true consistently across different size bins. When the particle number concentration measurement profile across different size brackets (Figure C6) are examined, a shift in OPC to APS number concentration proportion with respect to particle size fraction is observed (Figure C7). OPC to APS number concentration proportion is higher than 1 for particles larger than 0.5 µm, and also for particles larger than 1 µm, but to a less degree. APS surpasses OPC in number concentration for particles larger than 3 µm, and particles larger than 5 µm. This pattern was observed for all tested particles; OPC reports a higher number concentration than APS for smaller sizes, while the opposite happens for larger sizes. Peters et al.'s (2006) comparison of two OPCs with APS measurement of 0.83, 1.0, and 3.0 µm PSL particles resulted in higher number concentration reported by OPC than APS. This part of their finding is in agreement with this study results. However, they also found that the percent difference of OPCs and APS number concentration increased with particles size, which is in contradiction to this study results. Peters et al.'s test of the polydisperse particle of Arizona road dust showed APS has a lower number concentration in size ranges of smaller than 0.7 and larger than 2.5 µm while having a higher number concentration in size range of 0.7-2 µm. Current study results taken together with previous researchers findings conclude the size dependence of APS and OPC measurement relationship. To further investigate the relationship between APS and OPC relationship and its variation, linear regression analysis of the two sensors measurements across various size brackets is presented in the following section.

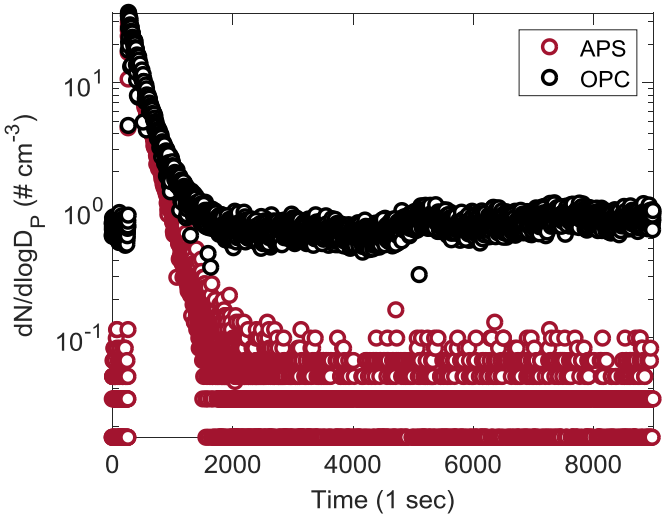

Figure C5. Time-series profile of the total normalized particle number concentration of tested particles measured by APS and OPC sensors across all of their size bins throughout one test duration. Each test runs for 2.5 hours which consists of three phases; 1) background level (minutes 0-5), 2) particle injection (minutes 5-7), and 3) particle concentration decay (minutes 7-150). All test cases with different particle types and sizes had similar temporal concentration profile trends. This figure presents the test case results with the monodisperse particle of MF-R in 2.81 µm.

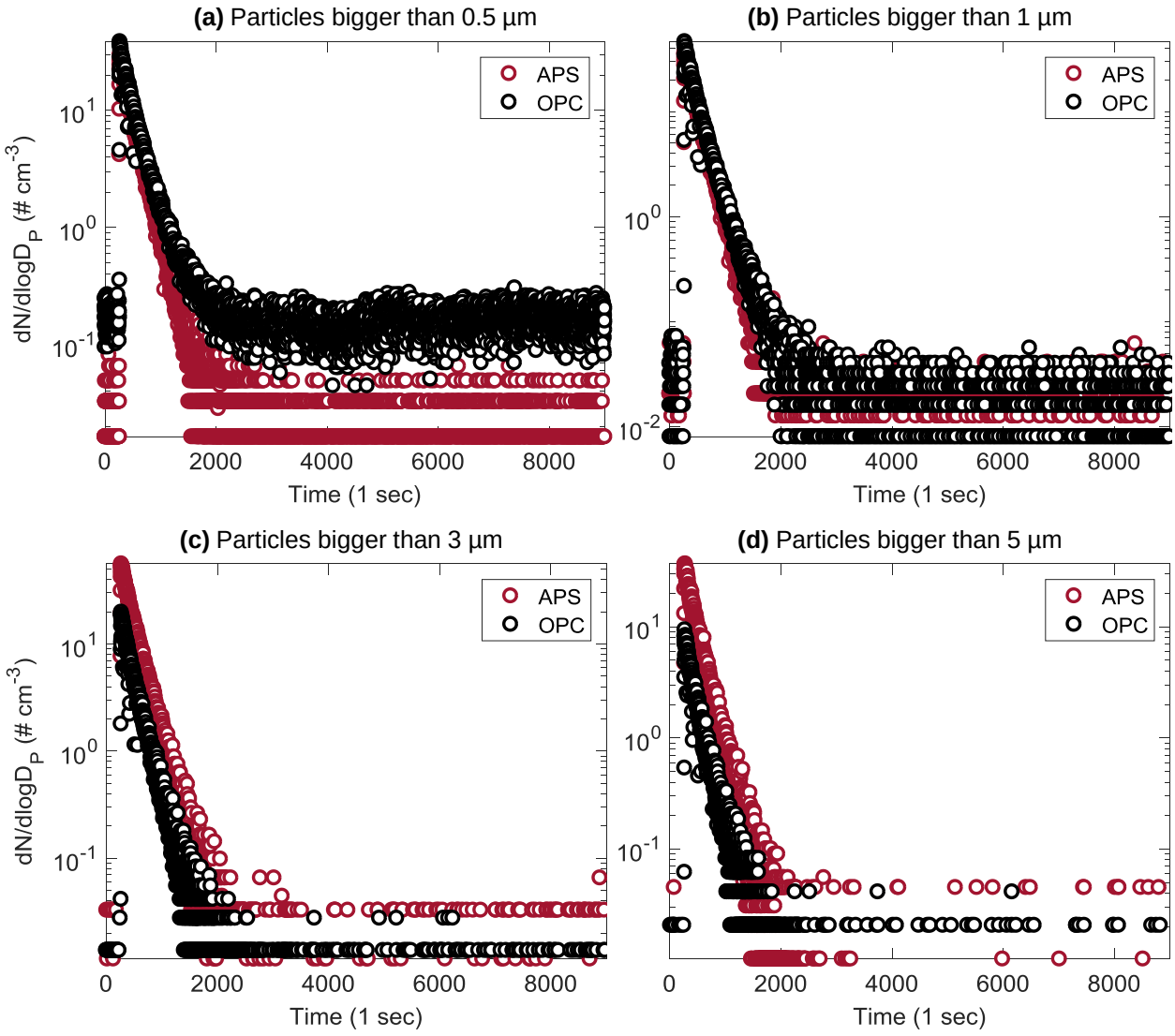

Figure C6. The normalized particle number concentration time-series profile measured by APS and OPC across various particle size fractions.

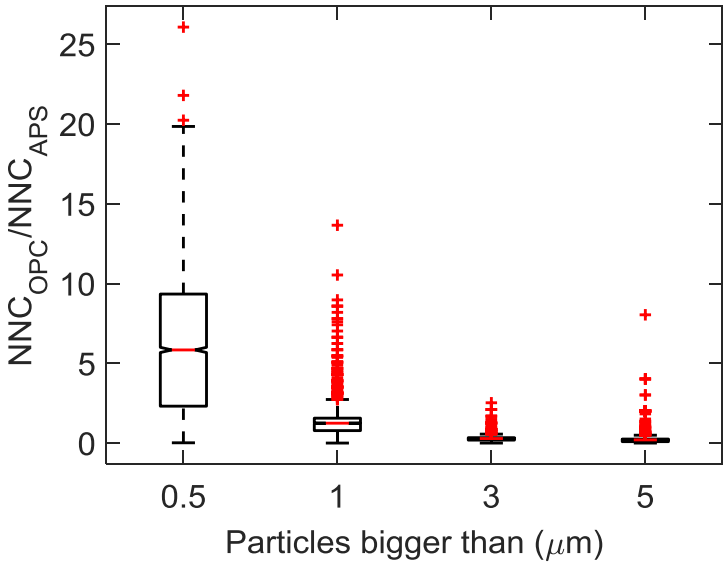

Figure C7. OPC to APS measurement proportion of normalized number concentration distribution across different size bins.

C.3.3. Linear relationship between APS and OPC between APS and OPC measurements

Figure C8a shows the normalized number concentration measurement by OPC versus that of APS for the total counted particles (2.81 µm MF-R) across all size bins of each sensor. It can be seen that there is a clear linear relationship between the two sensors closely following the 1:1 line, as the slope of the linear regression analysis is 1.11. Nonetheless, in exposure studies, it is rarely of interest to assess the total particle number concentration, but rather the particle number concentration within specific size ranges such as PM2.5 or PM10. Conducting the linear regression analysis for particles smaller than 2.5 of the same test case resulted in a significantly different linear relationship with a slope of 11.66 (Figure C8b).

Table C3 summarizes the linear regression analysis results of the APS and OPC measurements for each test case across three size brackets; total counted particles in all size bins, particles smaller than 10 µm (representing PM10), and particles smaller than 2.5 µm (representing PM2.5). It can be seen that not only the linear relationship between the APS and OPC measurements is size dependent, but also the

degree to which it is affected by the size varies amongst the tested particles. Thus, it can be concluded that particle-specific, size-specific linear calibration curves should be used to calculate the aerodynamic equivalent diameter size from optically measured size distributions.

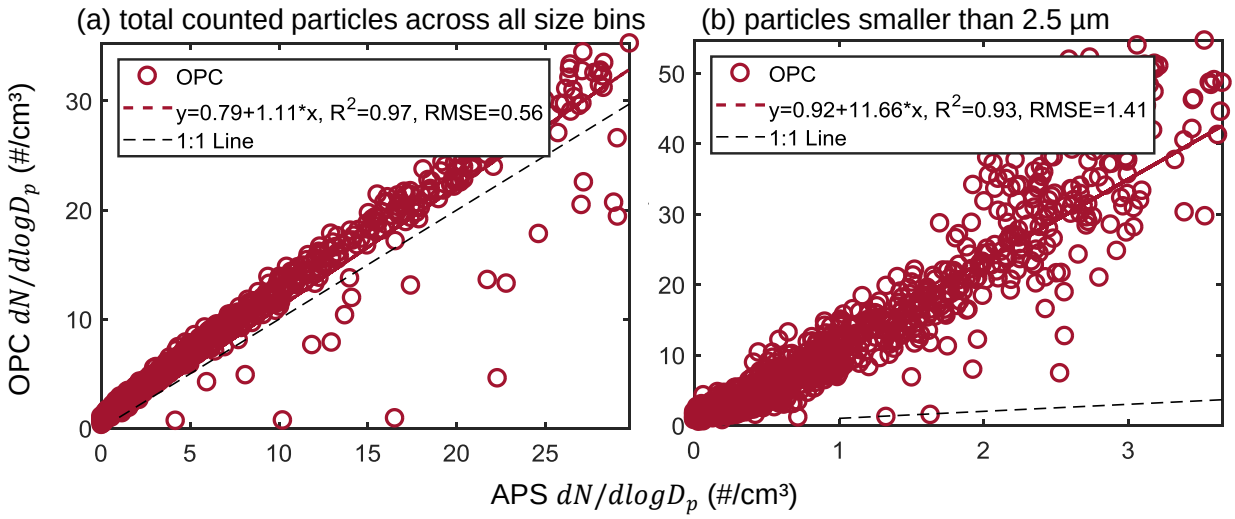

Figure C8. The linear relationship between APS and OPC measurements of 2.81 µm MF-R particles.

Table C3. Ordinary linear regression results of OPC versus APS normalized number concentration measurements for different size fractions

Tested particle	Size fraction (µm)	Intercept (#/cm^3)	Slope	R^2	RMSE (#/cm^3)
poly (methyl methacrylate) (PMMA-R) 5.1 µm	total counted	1.918	2.246	0.881	1.851
	PM10	0.939	1.857	0.896	1.733
	PM2.5	0.442	3.177	0.922	2.371
poly (methyl methacrylate) (PMMA-R) 9.9 µm	total counted	43.884	1.468	0.024	20.814
	PM10	8.712	1.590	0.460	4.614
	PM2.5	12.054	4.218	0.543	6.955
melamine resin (MF-R) 1.041 µm	total counted	8.686	0.949	0.856	32.447
	PM10	10.692	0.896	0.821	41.895
	PM2.5	18.021	0.889	0.814	70.077
melamine resin (MF-R) 2.81 µm	total counted	0.788	1.107	0.972	0.557
	PM10	0.205	1.131	0.973	0.674
	PM2.5	0.145	14.307	0.925	1.751
melamine resin (MF-R) 10.55 µm	total counted	1.455	1.587	0.971	0.580
	PM10	0.314	1.887	0.983	0.538
	PM2.5	0.475	2.120	0.984	0.861
silicon dioxide (SiO2-R) 0.977 µm	total counted	0.782	1.903	0.981	1.064
	PM10	0.278	1.977	0.982	1.280
	PM2.5	0.432	2.042	0.983	2.112
silicon dioxide (SiO2-R) 2.81 µm	total counted	1.779	1.079	0.913	3.811
	PM10	0.700	1.077	0.916	4.472
	PM2.5	-1.574	12.434	0.915	7.114
silicon dioxide (SiO2-R) 5.04 µm	total counted	1.670	1.826	0.902	0.639
	PM10	0.361	1.773	0.907	0.722
	PM2.5	0.492	2.587	0.908	1.120

Tested particle	Size fraction (μm)	Intercept (#/cm^3)	Slope	R^2	RMSE (#/cm^3)
crushed quartz	total counted	19.889	1.303	0.762	24.326
	PM10	8.550	1.262	0.813	23.799
	PM2.5	12.833	1.468	0.835	36.400
aluminum oxide	total counted	1.410	1.780	0.934	2.990
	PM10	0.897	1.755	0.935	3.366
	PM2.5	0.555	3.012	0.944	4.969
pollen	total counted	1.285	1.546	0.863	1.130
	PM10	0.809	1.474	0.878	1.224
	PM2.5	0.570	2.723	0.895	1.749
dust mite	total counted	1.073	2.175	0.972	1.028
	PM10	0.267	2.217	0.971	1.288
	PM2.5	0.349	2.476	0.972	2.112
dog fur	total counted	2.910	1.275	0.852	2.894
	PM10	1.954	1.122	0.858	3.004
	PM2.5	1.345	2.634	0.923	3.432
cat fur	total counted	0.972	1.959	0.904	0.269
	PM10	0.274	1.643	0.917	0.253
	PM2.5	0.321	2.964	0.910	0.407
Bacillus thuringiensis (BT) spore	total counted	1.514	3.020	0.769	0.303
	PM10	0.261	2.292	0.956	0.109
	PM2.5	0.425	2.692	0.952	0.188
NIST indoor dust	total counted	1.079	1.845	0.959	2.253
	PM10	0.557	1.863	0.952	3.050
	PM2.5	0.700	2.090	0.957	4.749

C.4. Conclusion

This study investigated the relationship between aerodynamic and optical aerosol size measurement by testing sixteen different particles of various sizes, compositions, densities, and refractive properties in a controlled chamber environment. Comparison of APS and OPC simultaneous sampling and measurement of tested aerosols resulted in the following findings:

- Aerosol size distribution measured by APS and OPC are significantly different, and their relationship varies depending on particle size, type, concentration levels.
- The linear relationship between the aerosol number concentration measured by APS and OPC is significantly different across different size ranges.
- The findings of this study warrant caution in using optical based size measurement where aerodynamic size measurement is intended. In applications where aerodynamic sensing is not possible or cannot be afforded, it is recommended to use particle-specific, size-specific calibration curves to convert the optically measured size distribution to aerodynamic equivalent one.
- This study provides size-specific, particle-specific calibration curves for the tested OPC with reference to APS measurements for various biological and non-biological aerosols of monodisperse and polydisperse type. Further empirically developed optical-to-aerodynamic size distribution conversion equations for other common indoor and outdoor commons aerosols is recommended for future studies.

Acknowledgements

This research was funded by ASHRAE (American Society of Heating, Refrigerating, and Air-conditioning Engineers) Graduate Student Grant-in-aid. Authors would like to acknowledge the assistance of former lab manager of Penn State Architectural Engineering Department at the time this experiment was conducted, Mr. Paul Kremer, as well as the undergraduate research assistants who helped with conducting the experiments during their research experience training, Mr. Sean Michael Eagan, and Ms. Camilla Victoria McCrary.

References

Airviz Inc. Speck: Support: FAQs. https://www.specksensor.com/support/faq (accessed 3.16.18).

Aoki, P., Honicky, R.J., Mainwaring, A., Myers, C., Paulos, E., Subramanian, S., Woodruff, A., 2008. Common sense: Mobile environmental sensing platforms to support community action and citizen science. Adjun. Proc. Ubicomp 2008 Paper 201 OR-Human Computer Interaction Institu. https://doi.org/10.1080/08839510701252676

ASHRAE, 2004. ANSI/ASHRAE Standard 62-2001: Ventilation for acceptable indoor air quality, American Society of Heating, Refrigerating and Air-conditioning Engineers, American Society of Heating, Refrigerating and Air-Conditioning Engineers. https://doi.org/ISSN 1041-2336

Bardana Jr, E.J., 2001. Indoor pollution and its impact on respiratory health. Ann. Allergy, Asthma Immunol. 87, 33–40. https://doi.org/10.1016/S1081-1206(10)62338-1

Barnes, C., Tuck, J., Simon, S., Pacheco, F., Hu, F., Portnoy, J., 2001. Allergenic materials in the house dust of allergy clinic patients. Ann. Allergy, Asthma Immunol. 86, 517–523. https://doi.org/10.1016/S1081-1206(10)62899-2

Bernstein, J.A., Alexis, N., Bacchus, H., Bernstein, I.L., Fritz, P., Horner, E., Li, N., Mason, S., Nel, A., Oullette, J., Reijula, K., Reponen, T., Seltzer, J., Smith, A., Tarlo, S.M., 2008. The health effects of non-industrial indoor air pollution. J. Allergy Clin. Immunol. 121, 585–91. https://doi.org/10.1016/j.jaci.2007.10.045

Bohren, C.F., Huffman, D.R., 2004. Absorption and scattering of light by small particles. Wiley.

Castell, N., Dauge, F.R., Schneider, P., Vogt, M., Lerner, U., Fishbain, B., Broday, D., Bartonova, A., 2017. Can commercial low-cost sensor platforms contribute to air quality monitoring and exposure estimates? Environ. Int. 99, 293–302.

https://doi.org/10.1016/j.envint.2016.12.007

Cheng, K.-C., Goebes, M.D., Hildemann, L.M., 2010. Association of size-resolved airborne particles with foot traffic inside a carpeted hallway. Atmos. Environ. 44, 2062–2066. https://doi.org/10.1016/j.atmosenv.2010.02.027

Chien, C.-H., Theodore, A., Wu, C.-Y., Hsu, Y.-M., Birky, B., 2016. Upon correlating diameters measured by optical particle counters and aerodynamic particle sizers. J. Aerosol Sci. 101, 77–85. https://doi.org/10.1016/J.JAEROSCI.2016.05.011

Clancy, L., Goodman, P., Sinclair, H., Dockery, D.W., 2002. Effect of air-pollution control on death rates in Dublin, Ireland: an intervention study. Lancet 360, 1210–1214. https://doi.org/10.1016/S0140-6736(02)11281-5

Clayton, C.A., Perritt, R.L., Pellizzari, E.D., Thomas, K.W., Whitmore, R.W., Wallace, L.A., Ozkaynak, H., Spengler, J.D., 1992. Particle Total Exposure Assessment Methodology (PTEAM) study: distributions of aerosol and elemental concentrations in personal, indoor, and outdoor air samples in a southern California community. J. Expo. Anal. Environ. Epidemiol. 3, 227–250.

Corn, M., 1961a. The adhesion of solid particles to solid surfaces II. J. Air Pollut. Control Assoc. 11, 566–584.

Corn, M., 1961b. The adhesion of solid particles to solid surfaces, I. A review. J. Air Pollut. Control Assoc. 11, 523–528.

Corn, M., Stein, F., 1965. Re-entrainment of particles from a plane surface. Am. Ind. Hyg. Assoc. J. 26, 325–336.

Croner, S., Kjellman, N.-I.M., 1994. Natural history of bronchial asthma in childhood. A prospective study from birth to 14 years of age. Allergy 47, 150–157.

Davidson, C.I., Phalen, R.F., Solomon, P.A., 2005. Airborne Particulate Matter and Human Health: A Review. Aerosol Sci. Technol. 39, 737–749.

https://doi.org/10.1080/02786820500191348

Dockery, D.W., Pope, C.A., Xu, X., Spengler, J.D., Ware, J.H., Fay, M.E., Ferris, B.G., Speizer, F.E., 1993. An Association between Air Pollution and Mortality in Six U.S. Cities. N. Engl. J. Med. 329, 1753–1759. https://doi.org/10.1056/NEJM199312093292401

EPA, U., 2017. National Ambient Air Quality Standards (NAAQS).

Ferro, A.R., Kopperud, R.J., Hildemann, L.M., 2004. Elevated personal exposure to particulate matter from human activities in a residence. J. Expo. Anal. Environ. Epidemiol. 14, S34–S40. https://doi.org/10.1038/sj.jea.7500356

Fromentin, P., Garet, F., Le Bouffant, E., Maleck-Rassoul, R., 2008. Study of two sporulated bacillus species by THz time domain spectroscopy, in: 2008 33rd International Conference on Infrared, Millimeter and Terahertz Waves. IEEE, pp. 1–2. https://doi.org/10.1109/ICIMW.2008.4665772

Gao, M., Cao, J., Seto, E., 2015. A distributed network of low-cost continuous reading sensors to measure spatiotemporal variations of PM2.5 in Xi'an, China. Environ. Pollut. 199, 56–65. https://doi.org/10.1016/j.envpol.2015.01.013

Goldsmith, C.-A.W., 1999. Particulate Air Pollution and Asthma: A Review of Epidemiological and Biological Studies. Rev. Environ. Health 14, 121–134. https://doi.org/10.1515/REVEH.1999.14.3.121

Gomes, C., 2007. Factors impacting allergen-containing particle resuspension.

Gomes, C., 2004. Resuspension of Allergen-Containing Particles Subject to Mechanical and Aerodynamic Disturbance - Introduction to an Experimental Controlled Methodology.

Gomes, C., Freihaut, J., Bahnfleth, W., 2007. Resuspension of allergen-containing particles under mechanical and aerodynamic disturbances from human walking. Atmos. Environ. 41, 5257–5270. https://doi.org/10.1016/j.atmosenv.2006.07.061

Gullvåg, B.M., 1964. Morphological and Quantitative Investigations of Pollen Grains and Spores

by Means of the Françon-Johansson Interference Microscope. Grana Palynol. 5, 3–23. https://doi.org/10.1080/00173136409429127

Heidarinejad, M., 2011. Using computational fluid dynamics (CFD) to study upper-room UVGI lamp disinfection effectiveness in the patients' rooms. The Pennsylvania State University. https://doi.org/10.13140/2.1.1541.8567

Heyder, J., 2004. Deposition of Inhaled Particles in the Human Respiratory Tract and Consequences for Regional Targeting in Respiratory Drug Delivery. Proc. Am. Thorac. Soc. 1, 315–320. https://doi.org/10.1513/pats.200409-046TA

Hinds, W., 2012. Aerosol technology: properties, behavior, and measurement of airborne particles.

Holstius, D.M., Pillarisetti, A., Smith, K.R., Seto, E., 2014. Field calibrations of a low-cost aerosol sensor at a regulatory monitoring site in California. Atmos. Meas. Tech. 7, 1121–1131. https://doi.org/10.5194/amt-7-1121-2014

Ibrahim, A.H., Dunn, P.F., Brach, R.M., 2003. Microparticle detachment from surfaces exposed to turbulent air flow: controlled experiments and modeling. J. Aerosol Sci. 34, 765–782. https://doi.org/10.1016/S0021-8502(03)00031-4

Jiao, W., Hagler, G., Williams, R., Sharpe, R., Brown, R., Garver, D., Judge, R., Caudill, M., Rickard, J., Davis, M., Weinstock, L., Zimmer-Dauphinee, S., Buckley, K., 2016. Community Air Sensor Network (CAIRSENSE) project: Evaluation of low-cost sensor performance in a suburban environment in the southeastern United States. Atmos. Meas. Tech. 9, 5281–5292. https://doi.org/10.5194/amt-9-5281-2016

Jovašević-Stojanović, M., Bartonova, A., Topalović, D., Lazović, I., Pokrić, B., Ristovski, Z., 2015. On the use of small and cheaper sensors and devices for indicative citizen-based monitoring of respirable particulate matter. Environ. Pollut. 206, 696–704. https://doi.org/10.1016/J.ENVPOL.2015.08.035

Kasper, G., Schollmeier, S., Meyer, J., Hoferer, J., 2009. The collection efficiency of a particle-loaded single filter fiber. J. Aerosol Sci. 40, 993–1009. https://doi.org/10.1016/J.JAEROSCI.2009.09.005

Kelly, K.E., Whitaker, J., Petty, A., Widmer, C., Dybwad, A., Sleeth, D., Martin, R., Butterfield, A., 2017. Ambient and laboratory evaluation of a low-cost particulate matter sensor. Environ. Pollut. 221, 491–500. https://doi.org/10.1016/j.envpol.2016.12.039

Klepeis, N.E., Nelson, W.C., Ott, W.R., Robinson, J.P., Tsang, A.M., Switzer, P., Behar, J. V, Hern, S.C., Engelmann, W.H., 2001. The National Human Activity Pattern Survey (NHAPS): a resource for assessing exposure to environmental pollutants. J. Expo. Anal. Environ. Epidemiol. 11, 231–52. https://doi.org/10.1038/sj.jea.7500165

Koshikawa, T., Yamazaki, M., Yoshimi, M., Ogawa, S., Yamada, A., Watabe, K., Torii, M., 1989. Surface Hydiophobicity of Spores of Bacillus spp. Microbiology 135, 2717–2722. https://doi.org/10.1099/00221287-135-10-2717

Krauter, P., Biermann, A., 2007. Reaerosolization of Fluidized Spores in Ventilation Systems. Appl. Environ. Microbiol. 73, 2165–2172. https://doi.org/10.1128/AEM.02289-06

Kumar, P., Martani, C., Morawska, L., Norford, L., Choudhary, R., Bell, M., Leach, M., 2016a. Indoor air quality and energy management through real-time sensing in commercial buildings. Energy Build. 111, 145–153. https://doi.org/10.1016/J.ENBUILD.2015.11.037

Kumar, P., Skouloudis, A.N., Bell, M., Viana, M., Carotta, M.C., Biskos, G., Morawska, L., 2016b. Real-time sensors for indoor air monitoring and challenges ahead in deploying them to urban buildings. Sci. Total Environ. 560–561, 150–159. https://doi.org/10.1016/j.scitotenv.2016.04.032

Luoma, M., Batterman, S.A., 2001. Characterization of Particulate Emissions from Occupant Activities in Offices. Indoor Air 11, 35–48. https://doi.org/10.1034/j.1600-0668.2001.011001035.x

Magari, R., 2002. Statistics for laboratory method comparison studies. BIOPHARM-EUGENE-.

Manikonda, A., Zíková, N., Hopke, P.K., Ferro, A.R., 2016. Laboratory assessment of low-cost PM monitors. J. Aerosol Sci. 102, 29–40. https://doi.org/10.1016/j.jaerosci.2016.08.010

Miller, J.N., Eyring, E.M., Mills, W.N., 1991. Basic statistical methods for Analytical Chemistry. Part 2. Calibration and regression methods. A review. Analyst 116, 3. https://doi.org/10.1039/an9911600003

Mohammadpour, A., 2014. Retrofitting Healthcare Facilities to Enhance Patient Safety and Energy Efficiency.

Montoya, L.D., Hildemann, L.M., 2005. Size distributions and height variations of airborne particulate matter and cat allergen indoors immediately following dust-disturbing activities. J. Aerosol Sci. 36, 735–749.

Mukai, C., Siegel, J.A., Novoselac, A., 2009. Impact of Airflow Characteristics on Particle Resuspension from Indoor Surfaces. Aerosol Sci. Technol. 43, 1022–1032. https://doi.org/10.1080/02786820903131073

Mukherjee, A., Stanton, L., Graham, A., Roberts, P., 2017. Assessing the Utility of Low-Cost Particulate Matter Sensors over a 12-Week Period in the Cuyama Valley of California. Sensors 17, 1805. https://doi.org/10.3390/s17081805

Munir, A.K.M., 1994. Exposure to allergens and relation to sensitization and asthma in children. Lindko¨ping University.

Mygind, N., Dahl, R., Pedersen, S. and Thestrup-Pedersen, K., 1996. Diagnosis of allergy, Essential Allergy. Oxford: Blackwell Science Ltd.

Nazaroff, W.W., 2016. Indoor bioaerosol dynamics. Indoor Air 26, 61–78. https://doi.org/10.1111/ina.12174

Northcross, A.L., Edwards, R.J., Johnson, M.A., Wang, Z.-M., Zhu, K., Allen, T., Smith, K.R., Shi, Y., Finkelstein, N., Calle, E.E., Thun, M.J., 2013. A low-cost particle counter as a

realtime fine-particle mass monitor. Environ. Sci. Process. Impacts 15, 433–439. https://doi.org/10.1039/C2EM30568B

Ormstad, H., 2000. Suspended particulate matter in indoor air: adjuvants and allergen carriers. Toxicology 152, 53–68. https://doi.org/10.1016/S0300-483X(00)00292-4

Patel, S., Li, J., Pandey, A., Pervez, S., Chakrabarty, R.K., Biswas, P., 2017. Spatio-temporal measurement of indoor particulate matter concentrations using a wireless network of low-cost sensors in households using solid fuels. Environ. Res. 152, 59–65. https://doi.org/10.1016/j.envres.2016.10.001

Perez-Padilla, R., Schilmann, A., Riojas-Rodriguez, H., 2010. Respiratory health effects of indoor air pollution. Int. J. Tuberc. Lung Dis. https://doi.org/20819250

Persily, A., 2015. Challenges in developing ventilation and indoor air quality standards: The story of ASHRAE Standard 62. Build. Environ. 91, 61–69. https://doi.org/10.1016/J.BUILDENV.2015.02.026

Peters, T.M., Ott, D., O'Shaughnessy, P.T., 2006. Comparison of the Grimm 1.108 and 1.109 portable aerosol spectrometer to the TSI 3321 aerodynamic particle sizer for dry particles. Ann. Occup. Hyg. 50, 843–850. https://doi.org/10.1093/annhyg/mel067

Piedrahita, R., Xiang, Y., Masson, N., Ortega, J., Collier, A., Jiang, Y., Li, K., Dick, R.P., Lv, Q., Hannigan, M., Shang, L., 2014. The next generation of low-cost personal air quality sensors for quantitative exposure monitoring. Atmos. Meas. Tech. 7, 3325–3336. https://doi.org/10.5194/amt-7-3325-2014

Polichetti, G., Cocco, S., Spinali, A., Trimarco, V., Nunziata, A., 2009. Effects of particulate matter (PM10, PM2.5 and PM1) on the cardiovascular system. Toxicology 261, 1–8. https://doi.org/10.1016/j.tox.2009.04.035

Pope III, C.A., Burnett, R.T., Thun, M.J., Calle, E.E., Krewski, D., Ito, K., Thurston, G.D., 2002. Lung Cancer, Cardiopulmonary Mortality, and Long-term Exposure to Fine Particulate Air

Pollution. JAMA 287, 1132. https://doi.org/10.1001/jama.287.9.1132

Pope III, C.A., Dockery, D.W., 2006. Health Effects of Fine Particulate Air Pollution: Lines that Connect. J. Air Waste Manage. Assoc. 56, 709–742. https://doi.org/10.1080/10473289.2006.10464485

Qian, J., Ferro, A.R., 2008. Resuspension of Dust Particles in a Chamber and Associated Environmental Factors. Aerosol Sci. Technol. 42, 566–578. https://doi.org/10.1080/02786820802220274

Qian, J., Ferro, A.R., Fowler, K.R., 2008. Estimating the Resuspension Rate and Residence Time of Indoor Particles. J. Air Waste Manage. Assoc. 58, 502–516. https://doi.org/10.3155/1047-3289.58.4.502

Qian, J., Peccia, J., Ferro, A.R., 2014. Walking-induced particle resuspension in indoor environments. Atmos. Environ. https://doi.org/10.1016/j.atmosenv.2014.02.035

Radhakrishnan, T., 1947. The dispersion, birefringence, and optical activity of quartz, in: Mathematical Sciences. pp. 260–265.

Rai, A.C., Kumar, P., Pilla, F., Skouloudis, A.N., Di Sabatino, S., Ratti, C., Yasar, A., Rickerby, D., 2017. End-user perspective of low-cost sensors for outdoor air pollution monitoring. Sci. Total Environ. https://doi.org/10.1016/j.scitotenv.2017.06.266

Raja, S., Xu, Y., Ferro, A.R., Jaques, P.A., Hopke, P.K., 2010. Resuspension of indoor aeroallergens and relationship to lung inflammation in asthmatic children. Environ. Int. 36, 8–14. https://doi.org/10.1016/j.envint.2009.09.001

Reponen, T., Grinshpun, S.A., Conwell, K.L., Wiest, J., Anderson, M., 2001. Aerodynamic versus physical size of spores: Measurement and implication for respiratory deposition. Grana 40, 119–125. https://doi.org/10.1080/00173130152625851

Rim, D., Persily, A., Emmerich, S., Dols, W.S., Wallace, L., 2013. Multi-zone modeling of size-resolved outdoor ultrafine particle entry into a test house. Atmos. Environ. 69, 219–230.

https://doi.org/10.1016/J.ATMOSENV.2012.12.008

Rim, D., Schiavon, S., Nazaroff, W., 2014. Impact of increasing outdoor ventilation rates on energy consumption for office buildings in tropical climates.

Roberts, J.W., Clifford, W.S., Glass, G., Hummer, P.G., 1999. Reducing Dust, Lead, Dust Mites, Bacteria, and Fungi in Carpets by Vacuuming. Arch. Environ. Contam. Toxicol. 36, 477–484. https://doi.org/10.1007/PL00022756

Rosati, J.A., Thornburg, J., Rodes, C., 2008. Resuspension of Particulate Matter from Carpet Due to Human Activity. Aerosol Sci. Technol. 42, 472–482. https://doi.org/10.1080/02786820802187069

Salimifard, P., 2014. Comparison of Part Load Model Prediction of Commercial Office Subsystem Energy Consumption with Sub-metered Data. The Pennsylvania State University. https://doi.org/10.13140/2.1.1033.2963

Salimifard, P., Delgoshaei, P., Xu, K., Freihaut, J.D., 2014. Comparison of actual supply air fan performance data to ASHRAE 90.1 Standard-2010 and DOE commercial reference buildings part load fan energy use formula, in: 2014 ASHRAE/IBPSA-USA Building Simulation Conference.

Salimifard, P., Kremer, P., Rim, D., Freihaut, J.D., 2015. Resuspension of Bacterial Spore Particles from Duct Surfaces. Boulder, CO. https://doi.org/10.13140/RG.2.1.5005.6407

Salimifard, P., Rim, D., Freihaut, J.D., 2017a. An Experimental Comparison of Aerodynamic and Optical Particle Sensing for Indoor Aerosols, in: American Association for Aerosol Research. Raleigh, NC.

Salimifard, P., Rim, D., Freihaut, J.D., 2016. Effect of Relative Humidity on Resuspension of Indoor Allergen Particles, in: American Association for Aerosol Research. Portland, OR.

Salimifard, P., Rim, D., Gomes, C., Kremer, P., Freihaut, J.D., 2017b. Resuspension of biological particles from indoor surfaces: Effects of humidity and air swirl. Sci. Total Environ. 583,

241–247. https://doi.org/10.1016/j.scitotenv.2017.01.058

Sehmel, G., 1980. Particle resuspension: a review. Environ. Int. 4.2.

Settles, G.S., 2006. Fluid Mechanics and Homeland Security. Annu. Rev. Fluid Mech. 38, 87–110. https://doi.org/10.1146/annurev.fluid.38.050304.092111

Siegel, J.D., Rhinehart, E., Jackson, M., Chiarello, L., 2007. 2007 Guideline for Isolation Precautions: Preventing Transmission of Infectious Agents in Health Care Settings. Am. J. Infect. Control 35, S65–S164. https://doi.org/10.1016/j.ajic.2007.10.007

Sippola, M.R., Nazaroff, W.W., 2002. Particle deposition from turbulent flow: Review of published research and its applicability to ventilation ducts in commercial buildings. Lawrence Berkeley Natl. Lab.

Snyder, E.G., Watkins, T.H., Solomon, P.A., Thoma, E.D., Williams, R.W., Hagler, G.S.W., Shelow, D., Hindin, D.A., Kilaru, V.J., Preuss, P.W., 2013. The Changing Paradigm of Air Pollution Monitoring. Environ. Sci. Technol. 47, 11369–11377. https://doi.org/10.1021/es4022602

Soltani, M., Ahmadi, G., 1995. Direct numerical simulation of particle entrainment in turbulent channel flow. Phys. Fluids 7, 647–657.

Sousan, S., Koehler, K., Hallett, L., Peters, T.M., 2017. Evaluation of consumer monitors to measure particulate matter. J. Aerosol Sci. 107, 123–133. https://doi.org/10.1016/j.jaerosci.2017.02.013

Sousan, S., Koehler, K., Hallett, L., Peters, T.M., 2016a. Evaluation of the Alphasense optical particle counter (OPC-N2) and the Grimm portable aerosol spectrometer (PAS-1.108). Aerosol Sci. Technol. 50, 1352–1365. https://doi.org/10.1080/02786826.2016.1232859

Sousan, S., Koehler, K., Thomas, G., Park, J.H., Hillman, M., Halterman, A., Peters, T.M., 2016b. Inter-comparison of low-cost sensors for measuring the mass concentration of occupational aerosols. Aerosol Sci. Technol. 50, 462–473.

https://doi.org/10.1080/02786826.2016.1162901

Stafford, R.G., Ettinger, H.J., 1972. Filter efficiency as a function of particle size and velocity. Atmos. Environ. 6, 353–362. https://doi.org/10.1016/0004-6981(72)90201-6

Steinle, S., Reis, S., Sabel, C.E., Semple, S., Twigg, M.M., Braban, C.F., Leeson, S.R., Heal, M.R., Harrison, D., Lin, C., Wu, H., 2015. Personal exposure monitoring of PM 2.5 in indoor and outdoor microenvironments. Sci. Total Environ. 508, 383–394. https://doi.org/10.1016/j.scitotenv.2014.12.003

Sultanova, N., Kasarova, S., Nikolov, I., 2009. Dispersion Properties of Optical Polymers. Acta Phys. Pol. A 116, 585–587. https://doi.org/10.12693/APhysPolA.116.585

Taylor, B.N., 2009. Guidelines for Evaluating and Expressing the Uncertainty of NIST Measurement Results (rev. DIANE Publishing.

Thatcher, T.L., Layton, D.W., 1995. Deposition, resuspension, and penetration of particles within a residence. Atmos. Environ. 29, 1487–1497. https://doi.org/10.1016/1352-2310(95)00016-R

Tian, Y., Sul, K., Qian, J., Mondal, S., Ferro, A.R., 2014. A comparative study of walking-induced dust resuspension using a consistent test mechanism. Indoor Air 24, 592–603.

Tufts, J.A.M., Calfee, M.W., Lee, S.D., Ryan, S.P., 2014. Bacillus thuringiensis as a surrogate for Bacillus anthracis in aerosol research. World J. Microbiol. Biotechnol. https://doi.org/10.1007/s11274-013-1576-x

Wallace, L., 1996. Indoor Particles: A Review. J. Air Waste Manage. Assoc. 46, 98–126. https://doi.org/10.1080/10473289.1996.10467451

Wang, H.-C., John, W., 1987. Particle Density Correction for the Aerodynamic Particle Sizer. Aerosol Sci. Technol. 6, 191–198. https://doi.org/10.1080/02786828708959132

Wang, S., Zhao, B., Zhou, B., Tan, Z., 2012. An experimental study on short-time particle resuspension from inner surfaces of straight ventilation ducts. Build. Environ. 53, 119–127.

https://doi.org/10.1016/j.buildenv.2012.01.005

Wang, Y., Li, J., Jing, H., Zhang, Q., Jiang, J., Biswas, P., 2015. Laboratory Evaluation and Calibration of Three Low-Cost Particle Sensors for Particulate Matter Measurement. Aerosol Sci. Technol. 49, 1063–1077. https://doi.org/10.1080/02786826.2015.1100710

Weber, M.J., 1986. Handbook of laser science and technology, 4th ed. CRC Press, Boca Raton.

Weekly, K., Rim, D., Zhang, L., Bayen, A.M., Nazaroff, W.W., Spanos, C.J., 2013. Low-cost coarse airborne particulate matter sensing for indoor occupancy detection, in: 2013 IEEE International Conference on Automation Science and Engineering (CASE). IEEE, pp. 32–37. https://doi.org/10.1109/CoASE.2013.6653970

Yan, L.-Q., Tseng, C.-W., Jensen, H.W., Ramamoorthi, R., 2015. Physically-accurate fur reflectance. ACM Trans. Graph. 34, 1–13. https://doi.org/10.1145/2816795.2818080

Yanosky, J.D., Williams, P.L., MacIntosh, D.L., 2002. A comparison of two direct-reading aerosol monitors with the federal reference method for PM2.5 in indoor air. Atmos. Environ. 36, 107–113. https://doi.org/10.1016/S1352-2310(01)00422-8

Zikova, N., Hopke, P.K., Ferro, A.R., 2017. Evaluation of new low-cost particle monitors for PM2.5 concentrations measurements. J. Aerosol Sci. 105, 24–34. https://doi.org/10.1016/j.jaerosci.2016.11.010

VITA

Parichehr Salimifard

EDUCATION

- **Ph.D**. in **Architectural Engineering** – **Mechanical Option**, *2014-2018*
  Pennsylvania State University, University Park, PA
- **Master of Science** in **Architectural Engineering – Mechanical Option**, *2012-2014*
  with **Minor** in **Computational Science,**
  Pennsylvania State University, University Park, PA
- **Bachelor of Science** in **Mechanical Engineering**, *2007-2011*
  Persian Gulf University, Bushehr, Iran
- Studied the first year of **Architectural Engineering**, *2006-2007*
  Persian Gulf University, Bushehr, Iran

HONORS & AWARDS

- American Association for Aerosol Research (AAAR) Travel Grant, 2017
- College of Engineering Travel Grant-in-Aid, 2015, 2016, and 2017
- Penn State College of Engineering Distinguished Teaching Fellowship, 2017
- American Society of Heating, Refrigeration, and Air-Conditioning Engineers (ASHRAE) Graduate Grant-in-Aid Fellowship, 2016-2017
- Engineering Diversity Travel Scholarship, 2013, 2015, and 2016
- Sloan Foundation Travel Fellowship, 2015 Healthy Buildings America Conference
- ASHRAE/IBPSA-USA Building Simulation Conference Student Scholarship, 2014
- Laraine and Jack Beiter Excellence in Architectural Engineering Fellowship, 2012

SELECTED PUBLICATIONS & CONFERENCE PRESENTATIONS

- ***Salimifard, P.***, *Rim, D., and Freihaut, J.D.* "Evaluating Performance of Low-Cost Optical Particle Counters in Sensing Bioaerosols; an Experimental Chamber Study." *10th International Aerosol Conference. September 2- 7, 2018. St. Louis, MO.*
- ***Salimifard, P.***, *Rim, D., and Freihaut, J.D.* "Low-cost particle sensors: performance evaluation for indoor bioaerosols." Indoor Air 2018. *July 22- 27, 2018. Philadelphia, PA.*
- ***Salimifard, P.***, *Rim, D., and Freihaut, J.D.* "An experimental comparison of aerodynamic and optical particle sensing for indoor aerosols." *36th American Association for Aerosol Research Annual Conference. October 16- 20, 2017. Raleigh, NC.*
- ***Salimifard, P.***, *Rim, D., Gomes, C., Kremer, P., and Freihaut, J.D. "*Resuspension of biological particles from indoor surfaces: Effects of humidity and air swirl.*" Science of The Total Environment, 583, 241-247, 2017.*
- ***Salimifard, P.***, *Rim, D., and Freihaut, J.D.* "Effect of Relative Humidity on Resuspension of Indoor Allergen Particles." *35th American Association for Aerosol Research Annual Conference. October 17- 21, 2016. Portland, OR.*
- ***Salimifard, P.***, *Kremer, P., Rim, D., and Freihaut, J.D.* "Resuspension of Bacterial Spore Particles from Duct Surfaces." *Healthy Buildings 2015. July 19- 22, 2015. Boulder, CO.*
- ***Salimifard, P.***, *Delgoshaei, P., Xu, K., and Freihaut, J.D.* "Comparison of Actual Supply Air Fan Performance Data to ASHRAE 90.1 Standard-2010 and DOE Commercial Reference Buildings Part Load Fan Energy Use Formula." *2014 ASHRAE/IBPSA-USA Building Simulation Conference. September 10-12, 2014. Atlanta, GA.*